

# Quantum spin-liquid behavior in the spin-1/2 random Heisenberg antiferromagnet on the triangular lattice

HIKARU KAWAMURA and KEN WATANABE

*Faculty of Science, Osaka University  
Toyonaka, 560-0043*

Experimental quest for the hypothetical “quantum spin liquid” state has recently met a few promising candidate materials including organic salts  $\kappa$ -(ET)<sub>2</sub>Cu<sub>2</sub>(CN)<sub>3</sub> and EtMe<sub>3</sub>Sb[Pd(dmit)<sub>2</sub>]<sub>2</sub>,  $S = 1/2$  triangular-lattice Heisenberg antiferromagnets consisting of molecular dimers. These compounds exhibit no magnetic ordering nor the spin freezing down to very low temperature, while various physical quantities exhibit gapless behaviors. Recent dielectric measurements revealed the glassy dielectric response suggesting the random freezing of the electric polarization degrees of freedom. Inspired by this observation, we propose as a minimal model of the observed quantum spin-liquid behavior the  $S = 1/2$  antiferromagnetic Heisenberg on the triangular lattice with a quenched randomness in the exchange interaction. We study both zero- and finite-temperature properties of the model by an exact diagonalization method.

We consider the AF bond-random  $S = 1/2$  quantum Heisenberg model on the triangular lattice whose Hamiltonian is given by

$$\mathcal{H} = \sum_{\langle ij \rangle} J_{ij} \vec{S}_i \cdot \vec{S}_j - H \sum_i S_i^z, \quad (1)$$

where  $\vec{S}_i = (S_i^x, S_i^y, S_i^z)$  is a spin-1/2 operator at the  $i$ -th site on the triangular lattice,  $H$  is the magnetic-field intensity, and  $J_{ij} > 0$  is the random nearest-neighbor AF coupling obeying the bond-independent uniform distribution between  $[(1 - \Delta)J, (1 + \Delta)J]$ , with the mean  $J$ . The parameter  $\Delta$  represents the extent of the randomness:  $\Delta = 0$  corresponds to the regular system and  $\Delta = 1$  to the maximally random system.

This modelling is motivated by the recent experimental observation

on  $\kappa$ -(ET)<sub>2</sub>Cu<sub>2</sub>(CN)<sub>3</sub> that the dielectric degrees of freedom actually exist on each molecular dimer which might be slowed down and tend to be frozen at lower temperatures. The spatially random locations of spin-1/2 carrying electrons from dimer to dimer might give rise to the effective randomness for the exchange interaction between dimers: see Fig.1.

By means of an exact diagonalization method, both the zero- and finite-temperature properties of the model are computed for finite lattices. The total number of spins  $N$  is  $N = 9, 12, 15, 18, 21, 24, 27, 30$  for  $T = 0$ , and  $N = 9, 12, 15, 18$  for  $T > 0$ , periodic boundary conditions being employed. Sample average is taken over 500 ( $N = 9, 12, 15$ ), 250 ( $N = 18, 21$ ), 160 ( $N = 24$ ), 80 ( $N = 27$ ) and 24 ( $N = 30$ ) independent bond realizations in the  $T = 0$  calculation, while 500 ( $N = 9, 12$ ), 80 ( $N = 15$ ) and 40 ( $N = 18$ ) in the  $T > 0$  calculation.

Our  $T = 0$  data indicate that the system with strong randomness of  $\Delta \geq 0.6$  does not possess the antiferromagnetic long-range order nor the spin-glass-type random order. In that sense, the system is in the randomness-induced quantum spin-liquid state.

In Fig.2(a), we show the temperature dependence of the specific heat per spin  $C$  (in units of Boltzmann constant) for the random cases of  $\Delta = 0.7$  and 1.0. At lower temperatures  $T \lesssim 0.1$ , the specific heat exhibits a  $T$ -linear behavior  $C \simeq \gamma T$ , quite different from the behavior of the non-random model. Hence, the spin-liquid phase at  $\Delta > \Delta_c$  is characterized by the  $T$ -linear specific heat, with the  $\gamma$ -value estimated to be  $\gamma \simeq 0.57$  for  $\Delta = 0.7$ . If we use the experimentally estimated  $J$ -value

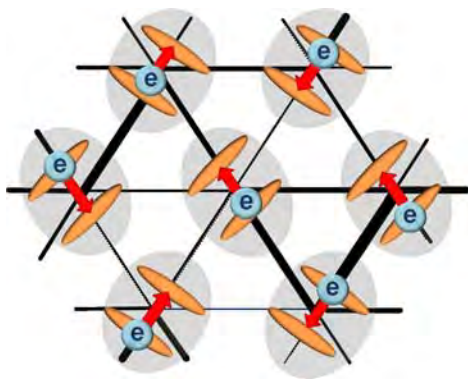


Figure 1: Illustration of the random freezing of the electric polarization at each dimer molecule. The glassy dielectric response experimentally observed in some organic salts suggests the biased position of the spin-carrying electron in a molecular dimer occurring at macroscopic time scales. The electric polarization appears at each dimer molecule in a spatially random manner, as indicated by arrows. This might result in the random modification of the exchange couplings acting between two  $S = 1/2$  spins on neighboring dimer molecules, spanning from a weaker  $J$  (thin bond) to a stronger  $J$  (thick bond).

of  $\kappa$ -(ET) $_2$ Cu $_2$ (CN) $_3$  to be  $J \sim 250\text{K}$ , we get  $\gamma \simeq 19\text{mJK}^{-2}\text{mol}^{-1}$  which is not far from the value determined from the specific-heat measurements on the ET salt  $\gamma \simeq 12\text{mJK}^{-2}\text{mol}^{-1}$ . As shown in the inset, the specific heat turns out to be insensitive to applied fields without any appreciable field dependence up to a field of  $0.1J$ .

In Fig.2(b), we show the temperature dependence of the magnetic susceptibility per spin  $\chi$  for several values of  $\Delta$ . For smaller  $\Delta$ , the susceptibility goes to zero in the  $T \rightarrow 0$  limit with a finite gap. At  $\Delta = 0.7$ , it tends to a finite value, while at  $\Delta = 1.0$  it tends to diverge toward  $T = 0$  obeying the Curie law  $\propto 1/T$ . The Curie-like diverging component arises only when a considerable amount of randomness  $\Delta > 0.7$  is introduced. The existence of a weak Curie-like component suggests that, in strongly random systems, a small fraction of free spins ( $\sim 2\%$ ) are generated at low tem-

peratures.

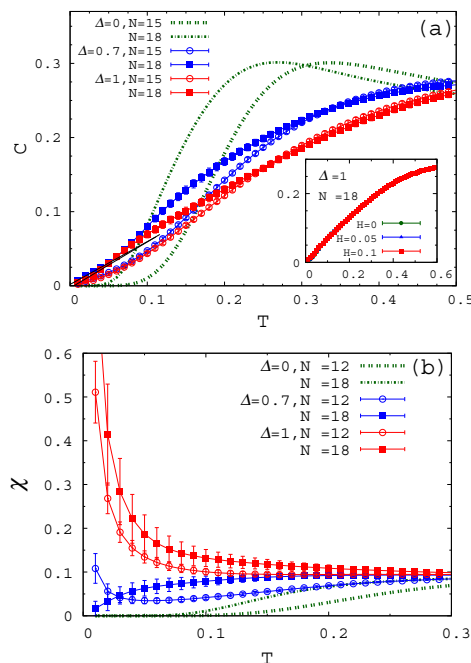


Figure 2: (a) The temperature dependence of the specific heat per spin  $C$  for the randomness  $\Delta = 0, 0.7$  and  $1.0$ , and for sizes  $N = 15$  and  $18$ . The lines are linear fits of the low-temperature data. The inset represents the corresponding data under magnetic fields for the randomness  $\Delta = 1.0$  and for the size  $N = 18$ . (b) The temperature dependence of the uniform susceptibility per spin  $\chi$  for the randomness  $\Delta = 0, 0.7$  and  $1.0$ , and for the sizes  $N = 12$  and  $18$ .

Thus, the  $S = 1/2$  random AF Heisenberg model with a moderately strong randomness exhibits a spin-liquid ground state, *i.e.*, a state without the conventional Néel ordering nor the spin freezing. This randomness-induced quantum spin-liquid state exhibits gapless behaviors including the temperature-linear specific heat. The results provide a consistent explanation of the recent experimental observations on organic salts.

#### References

- [1] K. Watanabe, H. Kawamura, H. Nakano and T. Sakai, J. Phys. Soc. Jpn. 83, 034714 (2014).

# Numerical simulation of the statistical model of earthquakes

HIKARU KAWAMURA and YUSHI UEDA

*Faculty of Science, Osaka University*

*Toyonaka, 560-0043*

An earthquake is a stick-slip dynamical instability of a pre-existing fault driven by the motion of a tectonic plate [1]. There is a widespread expectation that a large earthquake might be preceded by a precursory nucleation process which occurs prior to the high-speed rupture of a mainshock. Nucleation process is localized to a compact “seed” area with its rupture velocity orders of magnitude smaller than the seismic wave velocity.

In this year’s project, nucleation process of the one-dimensional Burridge-Knopoff model of earthquakes obeying the rate- and state-dependent friction (RSF) law is studied both analytically and numerically [1,2]. The properties of the nucleation dynamics, the nucleation lengths and the duration times are examined together with their continuum limits.

The one-dimensional (1D) BK model consists of a 1D array of identical blocks which are mutually connected with the two neighboring blocks via the elastic springs of the spring stiffness  $k_c$ , and are connected to the moving plate via the springs of the spring stiffness  $k_p$  [1]. The dimensionless equation of motion can be written as

$$d^2 u_i / dt^2 = \nu t - u_i + l^2 (u_{i+1} - 2u_i + u_{i-1}) - \phi, \quad (1)$$

where  $l \equiv (k_c/k_p)^{1/2}$ . The RSF force  $\phi$  reads as  $\phi = c + a \log(1 + \frac{v_i}{v^*}) + b \log \theta_i$ , where  $v^*$  is the dimensionless crossover velocity, and the dimensionless state variable  $\theta_i$  obeys the aging law,  $d\theta_i/dt = 1 - v_i \theta_i$ .

We observe that the model exhibits qualitatively different behaviors depending on whether the frictional instability is either “weak” or “strong”. A slow and long-lasting nucleation process, the quasi-static ini-

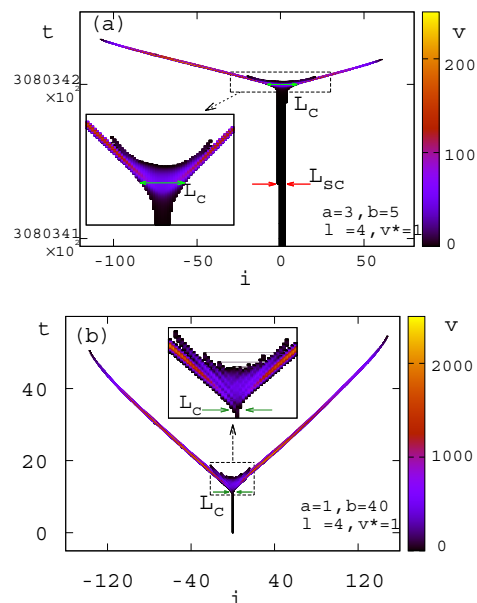


Figure 1: Color plots of typical earthquake nucleation processes depicted in the block-number (position) versus the time plane.

tial phase, is realized in the former case only. We illustrate in fig.1 typical examples of seismic events realized in the stationary state of the model for each case of (a) the weak, and (b) the strong frictional instability. The model possesses a borderline value of  $b$  determined solely by the stiffness parameter  $l$ ,  $b_c(l) = 2l^2 + 1$ , which discriminates the strong/weak instability behaviors.

- 1) H. Kawamura, T. Hatano, N. Kato, S. Biswas and B.K. Chakrabarti, *Rev. Mod. Phys.* 84, 839 (2012).
- 2) Y. Ueda, S. Morimoto, S. Kakui, T. Yamamoto and H. Kawamura, arXiv:1401.3247.

# Numerical Study on Spin Liquid in Frustrated Systems

Tôru SAKAI<sup>1,2</sup>, Hiroki NAKANO<sup>2</sup>, Tokuro SHIMOKAWA<sup>3</sup>,  
and Makoto ISODA<sup>4</sup>

<sup>1</sup>*Quantum Beam Science Directorate, Japan Atomic Energy Agency  
SPring-8, Kouto, Sayo, Hyogo 679-5148, Japan*

<sup>2</sup>*Department of Material Science, University of Hyogo,  
Kouto, Kamigori, Hyogo 678-1297, Japan*

<sup>3</sup>*Osaka University, Toyonaka, Osaka 560-0043, Japan*

<sup>4</sup>*Faculty of Education, Kagawa University,  
Takamatsu, Kagawa 760-8522, Japan*

## 1 Novel Spin Liquid Behavior at 1/3 of the Saturation Magnetization in the S=1/2 Kagome-Lattice Antiferromagnet

The magnetization processes of the S=1/2 isotropic Heisenberg quantum antiferromagnets on the kagome and triangular lattices are studied. Data from numerical-diagonalization method up to 39-spin systems, are reexamined from the viewpoint of the derivative of the magnetization with respect to the magnetic field. We find that for the kagome-lattice antiferromagnet, the behavior of the derivative around the 1/3 height of the magnetization saturation is quite different from the cases of typical magnetization plateaux. This new phenomenon is called the “magnetization ramp”[1]. We also compare it with the 1/3 magnetization plateau of the triangular antiferromagnet. The critical exponent analysis indicates a clear difference between the magnetization plateau and ramp[2]. In order to clarify the difference more, we study a generalized anisotropic triangular-lattice model including the regular-triangular- and the kagome-lattice

antiferromagnets in the parameter space. It revealed a quantum phase transition between the triangular- and kagome-lattices at 1/3 of the saturation magnetization[3].

## 2 Exotic Quantum Spin Liquid Behavior of the Spin Nanotubes

Recently some quantum spin systems on tube lattices, so called spin nanotubes, have been synthesized. They are expected to be interesting low-dimensional systems like the carbon nanotubes. As the first step of theoretical study on the spin nanotube, we investigate the S=1/2 three-leg spin tube, which is the simplest one, using the density matrix renormalization group (DMRG) and the numerical exact diagonalization (ED), combined with a precise finite-size scaling analysis named level spectroscopy[4]. The spin gap, which is one of the most interesting macroscopic quantum effects, was revealed to be open for any finite rung exchange couplings, in contrast to the three-leg spin ladder system which is gapless. It is consistent with the previous effective Hamiltonian approach. We also found a new

quantum phase transition caused by an asymmetric rung interaction. When one of the three rung coupling constants is changed, the spin gap would vanish. In addition we theoretically predict some new field-induced quantum phase transitions. A chirality-mediated novel superconductivity mechanism is also proposed[5, 6, 7, 8].

These results were obtained by the numerical exact diagonalization of the  $S = 1/2$  spin tube with 30 spins, using the system A with 8 nodes.

## References

- [1] H. Nakano and T. Sakai: J. Phys. Soc. Jpn. 79 (2010) 053707.
- [2] T. Sakai and H. Nakano: Phys. Rev. B 83 (2011) 100405(R).
- [3] T. Saka and H. Nakano: physica status solidi B 250 (2013) 579.
- [4] T. Sakai, M. Sato, K. Okunishi, Y. Otsuka, K. Okamoto and C. Itoi: Phys. Rev. B 78 (2008) 184415.
- [5] T. Sakai, M. Sato, K. Okamoto, K. Okunishi and C. Itoi: J. Phys.: Condens. Matter 22 (2010) 403201.
- [6] K. Okunishi, M. Sato, T. Sakai, K. Okamoto and C. Itoi: Phys. Rev. B 85 (2012) 054416.
- [7] T. Sakai and K. Okamoto: JPS Conf. Proc. 2 (2013) 010208.
- [8] T. Sakai and K. Okamoto: JPS Conf. Proc. 1 (2013) 012025.

# Novel Spin Flop Transition in Low-Dimensional Quantum Spin Systems

Tôru SAKAI<sup>1,2</sup>, Hiroki NAKANO<sup>2</sup>, Tokuro SHIMOKAWA<sup>3</sup>,  
and Makoto ISODA<sup>4</sup>

<sup>1</sup>*Quantum Beam Science Directorate, Japan Atomic Energy Agency  
SPring-8, Kouto, Sayo, Hyogo 679-5148, Japan*

<sup>2</sup>*Department of Material Science, University of Hyogo,  
Kouto, Kamigori, Hyogo 678-1297, Japan*

<sup>3</sup>*Osaka University, Toyonaka, Osaka 560-0043, Japan*

<sup>4</sup>*Faculty of Education, Kagawa University,  
Takamatsu, Kagawa 760-8522, Japan*

## 1 Novel Spin Flop Phenomenon in the S=1/2 Square Kagome Lattice Antiferromagnet

Using the large-scale numerical exact diagonalization, we investigated the S=1/2 Heisenberg antiferromagnet on a two-dimensional lattice composed of vertex-sharing triangles called the square kagome lattice. The lattice is similar to the kagome lattice but different from it. We examine the ground-state properties and the magnetization process of this model. We find that a magnetization jump appears at the higher-field-side edge of the magnetization plateau at the one-third height of the saturation. A spin-flop phenomenon is clearly observed at the jump even when the system is isotropic in the spin space[1]

## 2 Quantum Phase Transition of the S=1/2 Cairo Pentagon Lattice Antiferromagnets

The magnetization process of the S=1/2 Cairo Pentagon Lattice is investigated using the large-scale numerical exact diagonalization up to the 36-spin clusters. As a result, we found an interesting quantum phase transition, with respect to the ratio of the two inequivalent antiferromagnetic bonds, between two different magnetization curves around 1/3 of the saturation magnetization. Namely, the magnetization curve with a jump before the 1/3 magnetization plateau changes to the one with a jump after the plateau[2].

These results were obtained by the numerical exact diagonalization of the  $S = 1/2$  square-kagome lattice, using the system B.

## References

- [1] H. Nakano and T. Sakai: J. Phys. Soc. Jpn. 82 (2013) 083709.
- [2] H. Nakano, M. Isoda and T. Sakai: to appear in J. Phys. Soc. Jpn.

# Slow Dynamical Processes in Nonequilibrium Metastable States

Kazuhiro Fuchizaki, Yuta Asano, and Kazuki Hatsumura  
*Department of Physics, Ehime University, Matsuyama 790-8577*

In FY 2013, we continued pursuing thermodynamic identity of the modified Lennard-Jones (mLJ) system, whose phase diagram has been already reported [1,2]. A shortcut to understanding or predicting thermodynamic outcomes, including the phase behavior, is to establish the equation of state (EOS). To this end, we tried two approaches. One was to construct an approximate EOS using the EOS of the Lennard-Jones (LJ) system as the reference EOS. The procedure and the consequence [3] is briefly outlined below. The other was to set up an EOS as accurate as possible. To realize this latter option, we employed the modified Benedict–Webb–Rubin (mBWR) form, which was created on a phenomenological basis but is known to be able to reproduce the thermodynamic properties of the LJ fluid within a wide temperature ( $T$ )–pressure ( $p$ )–density ( $\rho$ ) range. We confirmed that the mBWR EOS can successfully capture mLJ fluid’s behavior as well [4]. The way of constructing the EOS is summarized in the following. It should be emphasized that our mBWR EOS was constructed so as to ensure the temperature dependence of the third virial coefficient  $B_3$ . The reflection of  $B_3$  on the EOS becomes crucially important when the system approaches the critical point. This aspect, which was not mentioned in our paper [4], is briefly touched on.

Predicting the thermodynamic properties of the mLJ fluid from the LJ EOS [3]

The properties of the mLJ fluid were treated as perturbations of the LJ fluid case, and the discrepancies were expressed as density series expansions. Here, two methods were examined to obtain the series expansions. The first

one is rather heuristic; the pressure of the mLJ fluid was expressed by a relationship, which is approximately correct up to  $\mathcal{O}(\rho^2)$ , by paying attention to the fact that the difference from LJ fluid’s pressure is ascribable only to the tail of the LJ potential omitted in the mLJ potential. The second one is systematic; based on a functional derivative of the free energy, we could obtain the expression for mLJ fluid’s free energy that is correct up to  $\mathcal{O}(\rho)$ . A proper approximation was introduced to make the coefficient of the correction term (proportional to  $\rho$ ) relatively tractable for actual computations. The two methods work equally well. The second virial coefficient of the mLJ fluid was well reproduced by these methods. Reproduction of the liquid–vapor coexisting envelope was also satisfactory, except in the vicinity of the critical point.

mBWR EOS for the mLJ Fluid [4]

Some features of the mLJ fluid behavior were well rationalized by the perturbative treatment mentioned above. Furthermore, we tried to describe the thermodynamic states of the mLJ fluid using the mBWR EOS.

The mBWR EOS contains 32 linear parameters and one nonlinear parameter. Therefore, the major task for us was to find the appropriate values for the parameters with which to capture the thermodynamic behavior of the mLJ fluid over as wide a range as possible. Ten parameters were primarily determined in such a manner that the temperature dependence of  $B_3$  as well as  $B_2$  is reproducible. The remaining parameters were determined so that the resultant EOS became compatible with the extensive set of data for the internal energy and  $p$  at given  $T$  and  $\rho$ . These data, con-

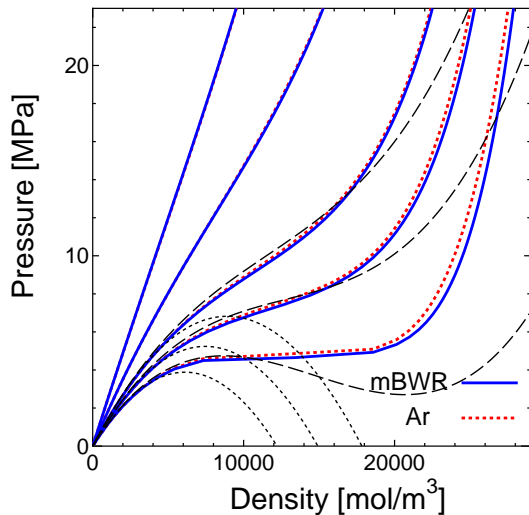


Figure 1: Isotherms of fluid argon near the critical point.

sisting of as many as 677  $T$ - $p$  data points, were prepared by conducting molecular dynamics (MD) simulations over such a wide region,  $0.7 \leq T \leq 20$  and  $0.001 \leq \rho \leq 1.15$ . The mBWR EOS thus constructed satisfactorily reproduces the liquid-gas coexistence envelope, which has been established from the Gibbs ensemble simulation [1].

Recalling that the dominant form of the mLJ potential is basically the same as that of the LJ potential, the substances, whose thermodynamic states are well deducible from the LJ potential, are expected to be describable using the mLJ potential. This expectation was confirmed by finding the mLJ parameters,  $\epsilon$  and  $\sigma$ , that fit the fluid in question. For example, fluid argon is well described by choosing  $\epsilon = 139.8k_B$  J and  $\sigma = 3.389$  Å, where  $k_B$  is Boltzmann's constant. As an example, the pressure variations against density observed for argon along several isotherms are compared with the corresponding variations predicted from the present EOS in Fig. 1. The isotherms delineated by thin dotted and dashed lines are those obtained from the virial expansions up to the terms with  $B_2$  and  $B_3$ , respectively. Unless including the effect of  $B_3$ , the isotherms no longer show the van der Waals loop behavior. It is thus essential to take the temperature dependence of  $B_3$  into consideration upon construction of the EOS.

Table 1: The updated set of the parameters involved in the mBWR EOS.

$i$	$x_i$	$i$	$x_i$
1	0.8269(8)	17	162.415(2)
2	3.187(5)	18	-67086.7(7)
3	-7.684(9)	19	33975.3(3)
4	0.409(7)	20	-243048(2)
5	-0.901(3)	21	-18.71(4)
6	0.898(2)	22	-549873(6)
7	5.00(2)	23	36.86(4)
8	-18.85(9)	24	-591544(6)
9	243083(2)	25	-146.839(1)
10	0.311926(3)	26	-366949(4)
11	3.10032(3)	27	-146.453(1)
12	-23.1883(2)	28	-157374(2)
13	20.0562(2)	29	588.307(6)
14	166.922(2)	30	-45105.1(5)
15	-6971.64(7)	31	-1443.50(1)
16	-357.638(4)	32	414.447(4)
		$\gamma$	2.2650

Updating the parameters in the mBWR EOS

Although the construction of the EOS for the mLJ fluid is said to be successful, it is still not fully satisfied in that the thermodynamic quantities in the low-temperature and low-density region, which were also employed for determination of the parameters, obtained through the MD simulation were not well equilibrated (as mentioned in Ref. [4]). This insufficiency was covered; the quantities in the region in question were reevaluated after a sufficient equilibration was performed. The 33 parameters were recalculated, using the same procedure as outlined above, but referring to the new set of pressures and internal energies. The values of the parameters thus updated are listed in Table table1. The set of the parameters must be the most refined version to date.

## References

- [1] Y. Asano and K. Fuchizaki: J. Chem. Phys. **137** (2012) 174502.
- [2] K. Fuchizaki and Y. Asano: J. Phys. Soc. Jpn. **82** (2013) 033001.
- [3] K. Fuchizaki and Y. Asano: J. Phys. Soc. Jpn. **82** (2013) 124001.
- [4] Y. Asano and K. Fuchizaki: J. Phys. Soc. Jpn. **83** (2014) 034601.

# Simulation of Cold Atoms with Parallelized Worm Algorithm \*

Naoki KAWASHIMA

*Institute for Solid State Physics, University of Tokyo  
Kashiwa-no-ha, Kashiwa, Chiba 277-8581*

The world-line quantum Monte Carlo (QMC) simulation with worm update is very effective for a broad range of the lattice boson/spin problems in condensed matter physics. In particular, recent developments in the experimental technology that made possible to cool atoms down to sub-micro Kelvin temperatures demand more accurate and larger-scale simulations in various setups. While the worm-update QMC is arguably the only method for dealing with systems that are directly comparable to experiments in size, it has been impossible to run it on parallel machines for an obvious reason — the update of the whole system is realized through only one moving object that cannot be split into pieces. In the present project, we aim at developing a new algorithm that can be parallelized and demonstrating its efficiency by applying it to Bose-Hubbard model in 2+1 dimensions.

Here we present a parallelized multiple-worm algorithm (PMWA) for QMC simulations.[1] A PMWA is a generalization of the worm algorithm and it removes the intrinsic drawback due to the serial-operation nature by introducing a large number of worms. With many worms distributed over the system, it is possible to decompose the whole space-time into many domains, each being assigned to a processor. The neighboring processors send and receive updated

configurations on their boundaries, once in every few Monte Carlo (MC) steps. Therefore, the time required for communication can be negligible for sufficiently large systems. Moreover, with a PMWA we can measure an arbitrary n-point Green function which is difficult in conventional worm-type algorithms when  $n > 4$ . The algorithm is based on the directed-loop implementation of the worm algorithm (DLA) that samples from the distribution

$$W(\{\psi_k\}) \equiv \prod_{k=1}^{N_\tau} \langle \psi_{k+1} | 1 - \Delta H_\eta | \psi_k \rangle$$

where  $\Delta\tau \equiv \beta/N_\tau$ ,  $\psi_k$  is a basis vector in some complete orthonormal basis set, and  $H_\eta \equiv H - \eta Q$  is the Hamiltonian with a fictitious source term  $\eta Q$  that generates discontinuities of worldlines, namely “worms.” A configuration in DLA is characterized by a graph, edges and vertices, and state variables defined on edges in the graph.

The update procedure of the conventional DLA consists of two phases; the worm phase in which the motion of the worm causes changes in the state variables, and the vertex phase in which vertices are redistributed. While the vertex phase in the new algorithm is just the same as the conventional DLA, the worm phase must be modified. In contrast to the conventional DLA, we let the worms proliferate or decrease freely according to the weight controlled by the parameter  $\eta$ . In conventional DLA, therefore, we “wait” for the worms disappear to measure the observables. In the

---

\*This report is based on the collaboration with A. Masaki-Kato, T. Suzuki, K. Harada, and S. Todo published as [1]

present algorithm, we estimate them instead by extrapolation to the  $\eta \rightarrow 0$ . Corresponding to this modification, the worm update is modified in two ways: worms are created and annihilated at many places at the same time, and we introduce a special update procedure for the region near the boundaries. As a result, the worm phase in the new algorithm consists of three steps: worm creation and annihilation, worm scattering, and a domain-boundary update. The last step is necessary only for parallelization, and is not used when the program runs on a serial machine.

The essential difference between the new algorithm and the conventional worm algorithm or DLA is that we regard the parity of the local number of worms as an intermediate representation of the state. To be more specific, for updating a local configuration around a vertex, we simply let a worm scatter at the vertex in the conventional algorithm. In the new algorithm, instead we assign a single-bit variable to each leg of the vertex. If we have even (odd) number of worms on the leg, we assign 0 (1) to it. Then we forget about the specific worm configuration on each leg and consider a stochastic process in terms of these new variables. Once a new configuration (in terms of the parity variables) is selected, we restore a specific worm configuration according to a weight with restriction imposed by the parity variables. This parity representation is especially useful in handling boundaries, since by it we can avoid a cumbersome “time” ordering of the scattering events that would be necessary to keep the detailed balance condition in the conventional representation.

In order to recover the results in the zero-worm density (or  $\eta \rightarrow 0$  limit), we have to numerically extrapolate a few sets of finite- $\eta$  results. In principle, we can do that by using quadratic fitting function. If the system is in the superfluid phase, however, due to the influence of the spontaneous  $U(1)$  symmetry breaking that would take place in the thermo-

dynamic limit, there is relatively broad region of  $\eta$  in which the term linear in  $\eta$  is dominating even in finite systems. In such cases, by a linear fitting we can obtain a good approximate value of the thermodynamic limit.

One of the advantage of the present method is that we can directly measure the order parameter  $\langle b \rangle$ . Moreover, we can measure arbitrary multipoint Green’s function simply measuring the product of the local worm densities at the points appearing in the argument of Green’s function. For the demonstration of the efficiency of the present algorithm, we carried out a simulation of the systems ranging from  $L = 8$  upto  $L = 10240$  at fixed  $\beta t = 16$ . This is much larger than a single processor’s memory can accommodate. We successfully equilibrate the whole system and extrapolate to the zero  $\eta$  limit. While this is already something that cannot be done by the conventional method, our code based on the present method showed a reasonably good scaling of the computational time. For an example, in the range between 8 processors to 1024 processors, the estimated statistical error in the energy with fixed system size and the wall time was approximately proportional to  $N_p^{-0.41}$  with  $N_p$  being the number of processors, when the system is deep in the superfluid phase, whereas  $N_p^{-0.5}$  is ideal.

## References

- [1] Akiko Masaki-Kato, Takafumi Suzuki, Kenji Harada, Synge Todo, Naoki Kawashima: Physical Review Letters **112**, 140603 (2014).

# Signatures of 1+continuous replica symmetry breaking around the jamming point

Hajime YOSHINO

*School of Science, Osaka University*

*Machikaneyama 1-1, Toyonaka, Osaka 560-0043*

The fate of the super-cooled liquid state at low temperatures or high densities is an important open question in physics. Very recently a notable progress on the theoretical side has been made through the construction of the exact replica mean-field theory (replicated van der waals theory) in the large-dimensional limit [1, 3]. An important new prediction of the theory is that the replica symmetry breaking (RSB) is not limited to the usual 1 step RSB assumed in conventional view points but is extended to 1+ continuous RSB at high densities around the jamming point.

In the present work we performed extensive MD simulations of the out-of equilibrium dynamics of a densely packed three-dimensional emulsion system (see our previous work [2] for the details) focusing on the fluctuation-dissipation relation (FDR). The purpose of the present work is to clarify if the 1+ continuous structure, which is suggested by the 1+ continuous RSB scenario, appear in FDR in the realistic three-dimensional system.

We measured the shear-stress relaxation taking care of the aging effects. The system is quenched from the liquid state to the working temperature  $T$ . After some waiting time  $t_w$ , the shear-strain of small amplitude  $\gamma$  is put to the system via affine transformation. Then relaxation of the shear-stress  $\sigma(t)$  is measured as the function of the elapsed time  $t$  after the switch-on of the perturbation. We also measured the shear stress auto-correlation function  $C(t, t_w) \equiv \langle \sigma(t)\sigma(t_w) \rangle$ . In equilibrium,

the response  $\mu(t, t_w) = \langle \sigma(t) \rangle / \gamma$  and  $C(t, t_w)$  are related by the fluctuation dissipation theorem (FDT). In Fig. 1, we show the two data set in a parametric plot which clearly indicated the anticipated 1+continuous FDR.

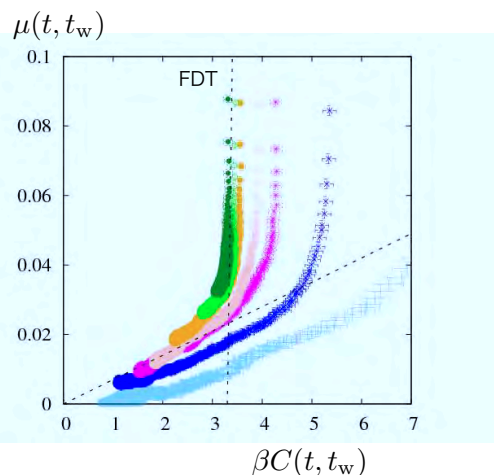


Figure 1: Parametric plot of the response and correlation functions associated with shear at volume fraction  $\phi = 0.67$  and  $k_B T / \epsilon = 10^{-5}$ . The waiting times  $t_w$  as varied as  $t_w = 10^2, 10^3, 3 \cdot 10^3, 10^4, 3 \cdot 10^4, 5 \cdot 10^4, 10^5$  from the bottom to the top. The two dotted straight lines are the equilibrium FDT line  $\mu(t, t_w) = \beta C(t, t_w)$  and the 1-step extended one  $\mu(t, t_w) = x \beta C(t, t_w)$  with  $x = 0.007$ . It can be seen that a curved, continuously varying regime exists between the two asymptotic regimes.

## References

- [1] P. Charbonneau, J. Kurchan, G. Parisi, P. Urbani, F. Zamponi, Nature Communications 5, 3725 (2014).
- [2] S. Okamura and H. Yoshino, arXiv:1306.2777.
- [3] H. Yoshino and F. Zamponi, arXiv:1403.6967.

# Simulation studies of near-field hydrodynamic effects in model active suspensions

Akira Furukawa

*Institute of Industrial Science, University of Tokyo  
Komaba 4-6-1, Meguro-ku, Tokyo 153-8505*

Using a fluid-particle dynamics approach [1], which is a hybrid simulation method for the dynamics of complex colloidal suspensions, we numerically studied the effects of hydrodynamic interactions on the collective dynamics of active suspensions within a simple model for bacterial motility: each microorganism is modeled as a stroke-averaged dumb-bell swimmer with prescribed dipolar force pairs. The present study illustrates that hydrodynamic interactions not only affect kinetic pathways in active suspensions, but also cause major changes in their steady state properties.

Simulations of the following issues (i) and (ii) were partially and fully performed at the ISSP Supercomputer Center, respectively. The programs are parallelized with a combination of OpenMP and MPI techniques.

(i) Using both simulations and qualitative arguments, we revealed the following [2]. When the separation between swimmers is comparable to their size, the swimmers' motions are strongly affected by activity-induced hydrodynamic forces. To further understand these effects, we investigated semi-dilute suspensions of swimmers in the presence of thermal fluctuations. A direct comparison between simulations with and without hydrodynamic interactions shows these to enhance the dynamic clustering at a relatively small volume fraction; with our chosen model the key ingredient for this clustering behavior is hydrodynamic

trapping of one swimmer by another, induced by the active forces. Furthermore, the density dependence of the motility (of both the translational and rotational motions) exhibits distinctly different behaviors with and without hydrodynamic interactions; we argue that this is linked to the clustering tendency.

(ii) In recent experiments on *E. coli* in the presence of additional attractive forces (created via a depletion potential due to polymer additives) it was shown experimentally and by simulation that activity produces a significant shift of the phase boundary compared to that of a passivated system with the same attractions [3]. However the configurations favored by such an attraction need not coincide with those stabilized by the activity-induced hydrodynamic interactions. Moreover, one very recent study suggests a mechanism whereby the equilibrium phase separation caused by attractions is interrupted by activity-induced cluster breakup [4]. We are currently addressing this problem by simulation [5].

## References

- [1] H. Tanaka and T. Araki, Phys. Rev. Lett. **85**, 1338 (2000).
- [2] A. Furukawa, D. Marenduzzo, and M.E. Cates, submitted to Phys.Rev.E.

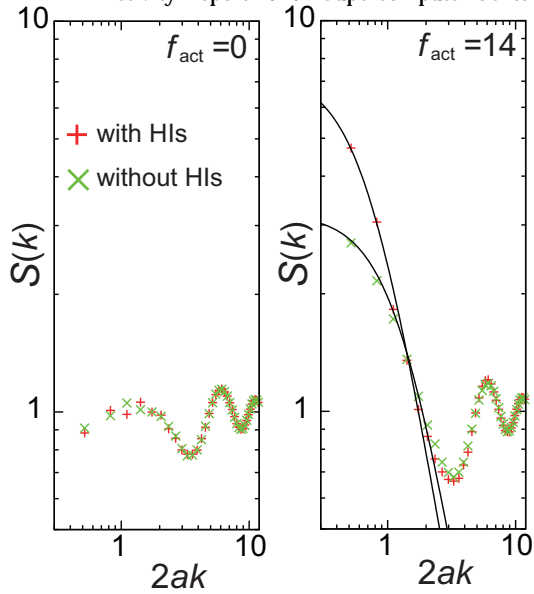


Figure 1: The structure factor  $S(k)$  for passive (left panel) and active (right panel) suspensions. In active suspensions, the clustering is evident; the structure factor for  $2ak < 1$ , where  $2a$  is roughly the swimmer size, can be described by the Ornstein-Zernike form, which is represented by the black solid curves in the cases with and without hydrodynamic interactions, respectively. The overall clustering tendency is significantly enhanced by the addition of hydrodynamic interactions.

- [3] J. Schwarz-Linek, C. Valeriani, A. Cacciuto, M.E. Cates, D. Marenduzzo, A.N. Morozov, and W.C.K. Poon, PNAS **109**, 4052 (2012).
- [4] B. M. Mognetti, A. Šarić, S. Angioletti-Uberti, A. Cacciuto, C. Valeriani and D. Frenkel, Phys. Rev. Lett. **111**, 245702 (2013).
- [5] in preparation

## Edge state in 2d quantum spin and bosonic systems

Takafumi SUZUKI

*Research center for Nano-micro Structure Science and Engineering,  
University of Hyogo, Shosha, Himeji, Hyogo 671-2280*

In this project, we studied (A) edge state of two-dimensional bosonic lattice systems in trapped potentials, (B) edge state of multi-boxes SU(N) Heisenberg model on a square lattice, and (C) magnetic excitations of the Heisenberg-Kitaev model on a honeycomb lattice. The digests of them are shown as follows.

### **A. Edge state of two-dimensional bosonic lattice systems in confinement potentials**

In condensed matter physics, edge state of topological insulators (TIs) has been studied extensively [A1]. The fundamental properties of TIs are that the bulk with an energy gap is characterized by non-local order parameters and a stable metallic state against perturbations breaking specific symmetries appears at the edge of bulk. In quantum spin systems, the Haldane state in the S=1 antiferromagnetic Heisenberg chain [A2] shows the similar properties; a finite spin gap, hidden  $Z_2$  symmetry breaking and free edge spins. Recently, edge/surface states of gapped states in the higher dimensional spin/bosonic systems have been much attracted. To study the higher dimensional spin/bosonic systems, a cold atomic system in optical lattice is one of ideal candidates, because it provides a good controllability for model parameters. However, the presence of confinement potential seems to be an unavoidable problem in experiments, and the effect of confinement potentials (i.e. non-uniformity of systems) on the edge states has not been well studied yet.

In this study, we focused on the effect of the confinement potential in 2D bosonic lattice systems and discussed the edge states of bosonic Mott insulating regions. In order to study it, we treated the rectangular lattice systems, where the chemical potential only changes along a uni-axial (x-axial) direction and open (periodic) boundary condition along the x (y)-axis direction were applied. From the quantum Monte Carlo (QMC) calculations, we discussed the temperature dependence of local

helicity modulus and off-diagonal correlation functions by changing the curvature of confinement potential. Since there exists the uni-axial potential, there are three regions in the ground state:  $\rho=1$  bosonic Mott insulating region,  $\rho \neq 0$  fluid (IC) region, and vacuum region. Here  $\rho$  is particle density per site. When width (W) of IC region surrounding the  $\rho=0$  (Mott insulating) region, is narrow ( $W < 10$  sites), off-diagonal correlation shows an exponential decay at a finite temperature. However, when the width W is enough large ( $W \sim 20$  sites), we found that the correlation function at edges clearly shows power-law decay below an offset temperature, where the local helicity modulus satisfies the same equation at the KT fixed point of the 2D uniform XY model.

### **B. Edge state of multi-boxes SU(N) Heisenberg model on a square lattice**

The ground state phase diagram of the multibox SU(N) Heisenberg model on a square lattice has been predicted by Read and Sachdev [B1]. This mode is the higher symmetry version of the conventional Heisenberg model for SU(2) spin. For the model with the Young tableaux with m rows and n columns, it was predicted that the N-n phase diagram does not depend on the value m, and has a single line that separates the Neel phase and valence bond solid (VBS) phases. The VBS phases can be also classified into three phases depending on the value of n. The ground state is a nematic VBS order with 180-degree rotational symmetry breakings of lattice for  $n=2 \pmod{4}$ , whereas a columnar order with translational and 90-degree rotational symmetry breakings of lattice is stabilized for  $n=1$  or  $3 \pmod{4}$ . If n is a multiple of 4, there is no spontaneous breaking of lattice symmetry. Based on the VBS picture, the  $n=4$  state is regarded as the 2D version of the 1D Haldane state.

In this study, we calculated the edge spin correlation of the multibox SU(N) Heisenberg model by QMC method based on the loop algorithm. In Figure 1, the results for the

SU(N=20) and  $n=2$  are shown. We found that, even in the nematic ground state case, the correlation of the edge spins is power-law decay in contrast to an exponential decay of the correlation perpendicular to the edge.

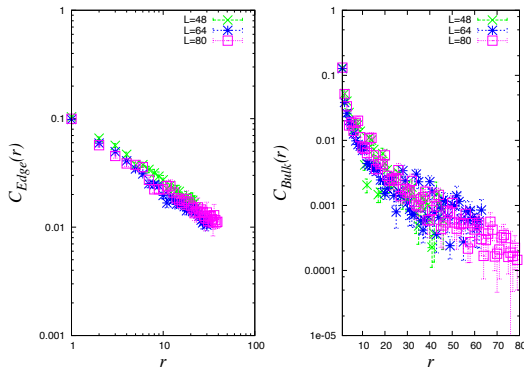


Fig. 1: Spin-spin correlation on the edge for SU(N=20) and  $(m,n)=(1,2)$  at the inverse temperature  $\beta=32L$ . Left (Right) hand side is the results on edge sites and Right one is the correlation perpendicular to the edge direction.

### C. Magnetic excitations of the Heisenberg-Kitaev model on a honeycomb lattice

In recent years, effects of spin-orbit couplings have much attracted in strongly correlated electron systems. In 5d-transition metal oxides, coulomb repulsion is relatively small against a kinetic energy. This allows us to expect that they show a metallic feature. However, it was reported experimentally that several Iridium oxides, such as  $\text{Sr}_2\text{IrO}_4$  and  $\text{A}_2\text{IrO}_3$  ( $A=\text{Na}$  or  $\text{Li}$ ), show an insulator nature. Theoretically, it was pointed that the presence of the strong spin-orbit coupling is a key to understand the insulating property of those compounds [C3]. For example,  $\text{Na}_2\text{IrO}_3$  has the small gap 0.35 [eV] [C1] and shows the phase transition to the magnetic ordered state (zigzag order) under  $T \sim 20[\text{K}]$ [C2]. The magnetic moments of  $\text{Na}_2\text{IrO}_3$  are carried by Ir ions locating at the center of edge-shared  $\text{IrO}_6$  octahedrons, and construct the layered honeycomb lattice. The interesting point of this compound is that the interactions between magnetic moments on Ir ions include the Kitaev-type anisotropy in addition to the conventional Heisenberg type interactions because the Ir-O-Ir bond on the interaction path takes almost 90 degree [C3]. In the phase diagram for the Heisenberg-Kitaev model on the honeycomb lattice, three magnetic ordered

phases appear by tuning the coupling ratio of the Kitaev and Heisenberg term; the Neel, stripy and spin liquid phase. Several authors have discussed the origin of zigzag order observed in  $\text{Na}_2\text{IrO}_3$  and proposed the parameter set that can explain experimental observations [C2,C4].

In order to discuss the suitability of proposed parameters, we calculated the spin-wave excitations and dynamical structure factor by the numerical exact-diagonalization method. Via comparisons with inelastic neutron scattering measurements, we discussed the several parameter sets proposed in previous papers [C2,C4].

In this project, we parallelized the Lanczos code to calculate the dynamic structure factors. In Figure 2, we show a bench march results of our code.

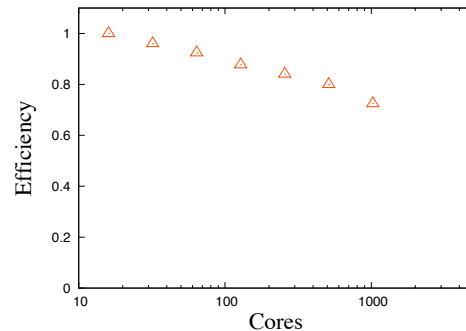


Fig. 2: Strong-scaling results for parallelized Lanczos code. The horizontal axis is the efficiency and the value is scaled by the results for 16 cores. In the ideal case, “efficiency” should keep constant at one. The sampling was performed for the N=32 Heisenberg-Kitaev model on the honeycomb lattice when OpenMP threads were fixed at four, where N is the system size.

### References

- [A1] M. Z. Hasan and C. L. Kane, Rev. Mod. Phys. **82**, 3045 (2010), X. L. Qi and S. C. Zhang, Rev. Mod. Phys. **83**, 1057 (2011).
- [A2] F. D. M. Haldane, Phys. Lett. A **93**, 464 (1983); Phys. Rev. Lett. **50**, 1153 (1983).
- [B1] Nucl. Phys. B 316, 609 (1989).
- [C1] R. Comin, et al., Phys. Rev. Lett. **109**, 266406 (2012).
- [C2] S. K. Choi, et al., Phys. Rev. Lett. **108**, 127204 (2012); F. Ye, et al., Phys. Rev. B **85**, 180403(R) (2012).
- [C3] J. Chaloupka, G. Jackeili and G. Khaliullin, Phys. Rev. Lett. **105**, 027204 (2010).
- [C4] Y. Yamaji, et al., arXiv:1402.1030.

# Calculation of dispersion surfaces and rocking curves for X-ray ‘In-plane $n$ -beam’ cases

Kouhei OKITSU

*Institute of Engineering Innovation, University of Tokyo*

*2-11-16 Yayoi, Bunkyo-ku, Tokyo 113-8656*

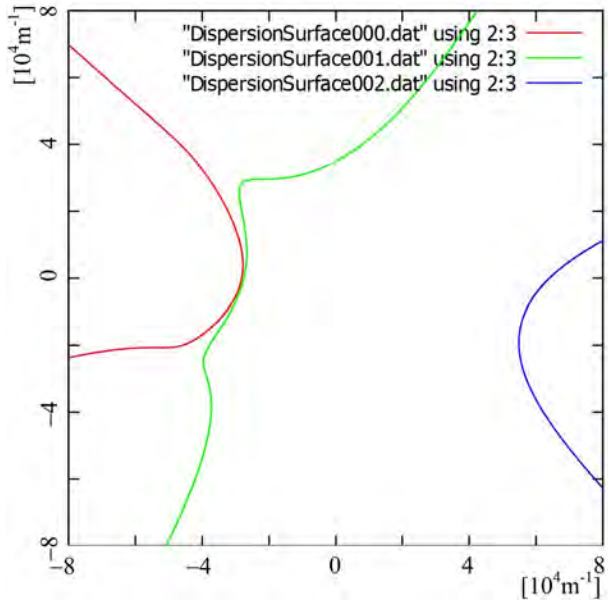


Figure 1: Dispersion surfaces calculated for 0 0 0- (forward-diffracted), 5 1 1- and  $3 \bar{1} \bar{3}$ - ‘in-plane’ three-beam case of silicon crystal.

A computer program with which dispersion surfaces and X-ray reflection intensities for ‘in-plane’  $n$ -beam cases has been developed, in which  $n$  X-ray beams whose planes of incidence are coplanar are simultaneously strong in the crystal. This case was studied several decades ago before numerical solutions for general  $n$ -beam cases were given with Ewald-Laue (E-L) formulation by Colella [1] and with Takagi-Taupin (T-T) formulation by the present author [2-5] since the polarization coupling effect does not have to be considered.

Incidentally, the method to fix the wavelength of the synchrotron X-rays with a mono-

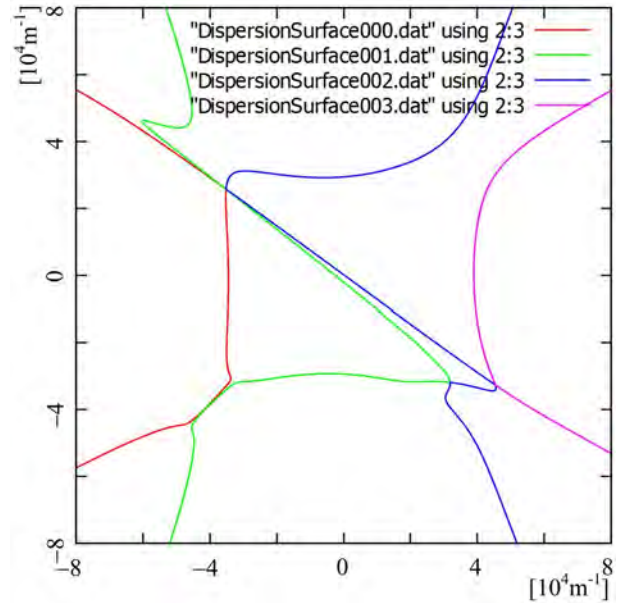


Figure 2: Dispersion surfaces for 0 0 0- (forward-diffracted), 2 2 0-,  $4 \bar{2} \bar{2}$ - and 0 6  $\bar{2}$ - ‘in-plane’ X-ray four-beam case of silicon crystal.

lithic silicon crystal giving two-bounced  $\mathbf{h}_1$  and  $\mathbf{h}_2$  reflections, is widely used. In this case,  $\mathbf{h}_3 (= \mathbf{h}_1 + \mathbf{h}_2)$  reflection occurs necessarily. Here, scattering vectors  $\mathbf{h}_1$ ,  $\mathbf{h}_2$  and  $\mathbf{h}_3$  are coplanar. However, this case was discussed just using the two-beam approximation and the interference effect due to X-rays reflected by  $\mathbf{h}_3$  has completely been neglected for many years. The present work is intended precisely to deal with this effect.

Figure 1 shows dispersion surfaces calculated in this work under an assumption that

$\mathbf{h}_1, 5\ 1\ 1$ - and  $\mathbf{h}_3, 3\ \bar{1}\ \bar{3}$ - ‘in-plane’ three-beam condition is satisfied. The abscissa and ordinate are positions in the reciprocal space in the directions parallel and perpendicular to the crystal surface, respectively. The three curves are loci of initial point of wave vectors of Bloch waves. When selecting  $\mathbf{h}_1, 5\ 1\ 1$  reflection as the first reflection and  $\mathbf{h}_2, 2\ \bar{2}\ \bar{4}$ -reflection as the second one to fix the wavelength of the synchrotron X-rays,  $\mathbf{h}_3, 3\ \bar{1}\ \bar{3}$ -reflection occurs necessarily, which was neglected completely for several decades.

The program has been coded such that other reflections that simultaneously occurs are searched automatically after the first and second reflection indices are input. Figure 2 shows four dispersion surfaces for a four-beam case by inputting  $2\ 2\ 0$  and  $\bar{4}\ 2\ 2$  as the first and second indices. Here,  $0\ 6\ \bar{2}$  has been automatically found as the third reflection. Very complex-shaped dispersion surfaces are found in this figure.

Furthermore, third or more reflection indices are not necessarily coplanar. It has been found with this program that as many as 48 reciprocal lattice nodes can be on the surface of the Ewald sphere, which revealed the importance of consideration on  $n$ -beam cases whereas almost all discussions on X-ray diffraction phenomena have been limited to the two-beam cases. Considerations on this situation is important not only for X-ray crystal optical devices designed based on the dynamical diffraction theory but also for crystal structure analysis based on the ‘two-beam’ kinematical theory almost for a hundred years.

Since the equivalence between the E-L and T-T formulations described with Fourier transform has been explicitly clarified in reference [5], both of them should be properly used for purpose when describing X-ray  $n$ -beam cases that is apparently difficult to discuss. The reason why only the two-beam approximation has been used in both dynamical and kinematical theories for a hundred years, is that it was just

easy to discuss in spite that there are many problems that should be discussed based on the  $n$ -beam approximation.

## References

- [1] R. Colella: *Acta Cryst. A* **30** (1974) 413-423.
- [2] K. Okitsu: *Acta Cryst A* **59** (2003) 235-244.
- [3] K. Okitsu, Y. Yoda, Y. Imai, Y. Ueji, Y. Urano and X.-W. Zhang: *Acta Cryst A* **62** (2006) 237-247.
- [4] K. Okitsu, Y. Yoda, Y. Imai and Y. Ueji: *Acta Cryst A* **67** (2011) 550-556.
- [5] K. Okitsu, Y. Imai and Y. Yoda: *In-Tech Recent Advances in Crystallography* (2012) 67-86.

# Equilibrium-state calculation in spin-glass models

Koji HUKUSHIMA

*Department of Basic Science, University of Tokyo  
3-8-1 Komaba, Meguro-ku, Tokyo 153-8902*

Mean-field theory of spin glasses has provided a number of novel concepts for understanding of a phase transition in disordered glassy systems. In particular, replica-symmetry breaking (RSB) plays an essential role in describing complex free-energy structure. It turns out that the pattern of RSB is clarified into two distinct classes, full RSB and one-step RSB. Since the mean-field theory has been established, one of the main issues is whether such concepts survive in short-ranged spin-glass models in finite dimensions. Most of the effort has been devoted to examining the issue in an Ising spin glass model in three dimensions, whose corresponding mean field model, i.e., the Sherrington-Kirkpatrick model, exhibits the full RSB. Despite extensive studies including large scale numerical simulations, a definite conclusion has not yet been drawn.

Some mean-field spin-glass models with the one-step RSB have attracted much attention of many researchers in recent years. For instance,  $p$ -state Potts glass with  $p \geq 3$  belongs to this class. These models are regarded as a prototype of a phenomenological picture of structural glass transition, called random first-order transition (RFOT), which is characterized by a thermodynamic transition with a discontinuous order parameter without latent heat. The advisability of the RSB picture in finite dimensional spin glass models comes to an issue again in the context of the structural glass transition. While the existence of the spin-glass transition of the Potts glass in three dimensions is clarified for  $p \leq 6$ [1,2], no feature predicted by RFOT based on the one-step RSB is found in numerical simulations and the nature of low temperature phase is not fully understood.

Our purpose is hopefully to detect some evidence of RFOT in a three dimensional Potts glass model by using Monte Carlo simulations.

Recently, the fragility of the RFOT feature against finite dimensional fluctuation is discussed in Ref.[3]. According to the argument, if RFOT in finite dimensions is a possibility, the model should take a sufficient large number of states  $p$  in high dimensions, say  $d \geq 9$  with  $d$  being spatial dimension. Instead, our strategy is to take a large number of connectivity up to third neighbor couplings with keeping dimensions three.

We have performed a large scale Monte Carlo simulations based on extended ensemble method for the 7-state Potts glass model in three dimensions with third neighbor couplings. Our findings are as follows[4]: (1) The model exhibits a thermodynamic spin-glass transition at finite temperature  $T_c$ , that is in contrast with the fact that the 7-state Potts glass with nearest neighbor couplings has no glassy phase at up to very low temperature. (2) The value of the critical exponent for the correlation length is very close to  $2/d$  derived by a heuristic scaling argument based on RFOT. (3) It is strongly suggested that the spin-glass order parameter appears discontinuously at  $T_c$  and no latent heat exists. (4) The order-parameter distribution below  $T_c$  has double peaks at zero and a finite value corresponding to the self-overlap state. These are fully compatible with those expected from the RFOT picture based on the one-step RSB. Presumably, this is the first numerical evidence showing (one-step) RSB in three dimensional spin-glass models and this also gives the first explicit statistical-mechanical model with RFOT features in three dimensions.

The present work has been done in collaboration with Takashi Takahashi.

- [1] L. W. Lee, et al: Phys. Rev. B**74** (2007) 0104416.
- [2] A. Cruz, et al: Phys. Rev. B**79** (2009) 184408.
- [3] C. Cammarota, et al: Phys. Rev. B**87** (2013) 064202.
- [4] T. Takahashi and KH: in preparation.

# Clarification of magnon turbulence in nano-contacts.

Katsuyoshi Matsushita  
 Cybermedia center, Osaka university  
 Toyonaka, Osaka 560-0043

The response phenomena of magnets have been investigated in order to clarify their potential in the industrial applications. Especially, the instability problem of the microscopic magnetic structure under the electronic current is an important issue related to the availability of the magnetic devices. For example, in the case of the communication device using voltage signals, the instability frequently results in a noisy signal and limits the efficiency of the devices. The further physical understanding the instability is needed to give keys to solve the issue.

In the present work, we shed light on the current induced turbulence in magnetic system as a possible instability in the magnetic system[1]. We have showed that a nanoscopic magnetic system confining a domain wall under current exhibits a transition from a steady state to a turbulence. In the study we conjectured that the critical parameters, namely the critical twist angle of the magnetic system  $\Theta_c$  and the critical applied current  $j_c$ , of the transition only depends on the characteristic length, which depends only on the applied current and the exchange stiffness. To confirm this conjecture, we should determine the main factors of the transition. As a first step of the determination, we concentrate on the effect of the Gilbert damping.

We carried out the numerical simulation of the nanoscopic magnetic wire system under the current where the turbulence appears and evaluate the critical twist angle of the magnetic system. Figure 1 shows the time average magnetization  $S$ . The abrupt change of the order

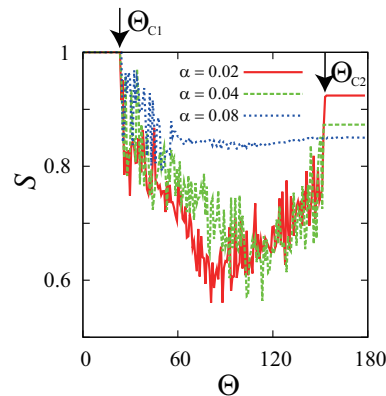


Figure 1: Order parameter as a function of twist angle of magnetic structure (See Ref.1) for  $\alpha = 0.02, 0.04$  and  $0.08$  at around  $j \simeq 1.5j_c$ .  $\Theta_{c1}$  and  $\Theta_{c2}$

parameter reflects the transition between the steady state (not fluctuating  $S$ ) and the turbulence (fluctuating  $S$ ). The small change in the Gilbert damping constant  $\alpha$  does not change the transition twist angles  $\Theta_{c1}$  and  $\Theta_{c2}$  for  $\alpha$  of realistic small values (0.02 and 0.04). This indicates that the effect of the Gilbert damping is not a main factor for determining the transition points as conjectured previously in the realistic system. However for unrealistically large  $\alpha$  (0.08), the turbulence fluctuation is suppressed because of strong damping and thereby  $\Theta_{c2}$  can not be determined from the simulation.

## References

- [1] K. Matsushita *et al.*, J. Phys. Soc. Jpn **82** (2013) 033801.

# Novel ordering in frustrated spin systems

Tsuyoshi Okubo

*Institute for Solid State Physics, University of Tokyo  
Kashiwa-no-ha, Kashiwa, Chiba 277-8581*

Frustrated spin systems have attracted recent interests. Typical examples of such frustrated systems in two dimension are Heisenberg antiferromagnets on the kagome lattice and the triangular lattice. Recently a new type of frustrated lattice interconnecting the triangular lattice and the kagome lattice has been found in  $\text{NaBa}_2\text{Mn}_3\text{F}_{11}$  [1]. In this *kagome-triangular* lattice, a kagome lattice deforms so as to generate the next-nearest (NN) neighbor interactions between three of six NN neighbors on the regular kagome lattice.

The Hamiltonian of the kagome-triangular lattice Heisenberg model is given by

$$\mathcal{H} = J_1 \sum_{\langle i,j \rangle_1} \vec{S}_i \cdot \vec{S}_j + J_2 \sum_{\langle i,j \rangle_2} \vec{S}_i \cdot \vec{S}_j, \quad (1)$$

where  $\vec{S}_i$  is a unit vector with three components, and  $\langle i,j \rangle_1$  ( $\langle i,j \rangle_2$ ) represents the sum over the nearest neighbor (NN neighbor) pairs on the kagome-triangular lattice.

Based on an analysis of the Fourier transform of the exchange interactions, we found that typical  $q = 0$  state and  $\sqrt{3} \times \sqrt{3}$  state appear for antiferromagnetic  $J_1$  with antiferromagnetic  $J_2$  and ferromagnetic  $J_2$ , respectively. In contrast, for the case of ferromagnetic  $J_1$  and antiferromagnetic  $J_2$  the wavevector which minimizes the energy appears along the line connecting  $q = 0$  and the M point, indicating a possible novel ordered structure.

In order to investigate the ordering of the kagome-triangular lattice Heisenberg model, we performed extensive Monte Carlo simulations. The Monte Carlo simulations were performed based on the standard heat-bath

method combined with the over-relaxation method. The lattice is a  $L \times L$  kagome-triangular lattice with  $24 \leq L \leq 96$  with periodic boundary conditions.

For ferromagnetic  $J_1$  and antiferromagnetic  $J_2$  with  $J_2/|J_1| \gtrsim 1$ , the ground state is a non-coplaner multiple- $q$  state which is a superposition of three independent wavevectors at the M points. Based on the analysis of snapshots obtained from Monte Carlo simulations, we conclude that this multiple- $q$  state is identical to the 12 sublattices cuboctahedral order found in the conventional  $J_1$ - $J_2$  kagome lattice Heisenberg model[2, 3]. In addition to this cuboctahedral phase, we found a novel incommensurate non-coplaner phase, which did not appear in the conventional kagome lattice  $J_1$ - $J_2$  Heisenberg model, for  $1/2 \lesssim J_2/|J_1| \lesssim 1$ . Details of this incommensurate phase will be investigated in future works.

## References

- [1] H. Ishikawa, T. Okubo, Y. Okamoto, and Z. Hiroi: J. Phys. Soc. Jpn. **83** (2014) 043703.
- [2] J. C. Domenge, P. Sindzingre, C. Lhuillier, and L. Pierre: Phys. Rev. B **72** (2005) 024433.
- [3] J. C. Domenge, C. Lhuillier, L. Messio, L. Pierre and P. Viot: Phys. Rev. B **77** (2008) 172413.

# Nonequilibrium phase transitions in Strongly Correlated Electron Systems

Takashi OKA

*Department of Applied Physics,*

*The University of Tokyo, Hongo, Bunkyo-ku, Tokyo 133-8656*

Owing to recent developments in experimental techniques such as pump-probe measurements and nonlinear transport, the research of nonequilibrium properties of strongly correlated electron systems is becoming more and more important. From the theory side, the bottleneck of progress is the lack of reliable numerical methods which can be used to study phase transitions that takes place dynamically. Most previous methods such as QMC were developed to study equilibrium time-independent problems. Recently, the dynamical mean field theory (DMFT), a very standard method in correlated electron theory, was extended to nonequilibrium dynamics using the Keldysh green's function method. This method can be applied to models of strongly correlated systems such as the Hubbard model. In collaboration with H. Aoki, N. Tsuji, M. Eckstein, M. Kollar, and P. Werner, I wrote a review article on this topic, which will be published in Review of Modern Physics [1]. The essence of this method is to take into account the local correlation, which is important to describe the Mott physics, by starting from a impurity model represented by

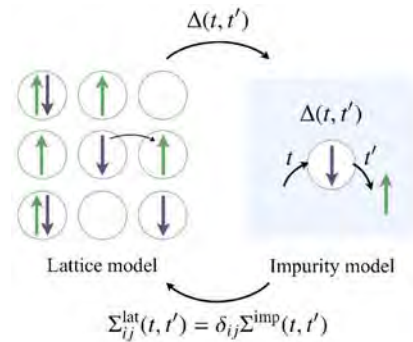


Fig.1 A schematic representation of the algorithm of dynamical mean field theory.

the Anderson model, and incorporate the band effect by performing a self-consistent loop on the green's function (Fig.1). Nonequilibrium DMFT has been applied to several problems such as the photo-induced metallization, dielectric breakdown problem, as well as quantum quench. In the project with the supercomputer in ISSP, I am trying to extend nonequilibrium DMFT to study unconventional superconductivity in cuprates [2]. At present, we have developed the calculation scheme and algorithm and implemented a test program. I expect to report further progress shortly.

## References

- [1] H. Aoki, N. Tsuji, M. Eckstein, M. Kollar, T. Oka, and P. Werner, "Nonequilibrium

dynamical mean-field theory and its applications”, *to appear in Rev. Mod. Phys.* [2] T. Oka, M. Babadi, and V. Pietila, *in progress.*

# The Scaling Law of the Systems with Long-Range Interactions

HYUGA Masahiko

*Department of Basic Science, University of Tokyo*

*3-8-1 Komaba, Meguro, Tokyo 153-8902, Japan*

30 April 2014

The systems with long-range interactions are known to exhibit an odd behaviour, such as ensemble inequivalence<sup>1</sup>, negative specific heat, and explicit shape- and size-dependency of thermodynamic relations.

Since we should concern all interaction forces of every particle pairs for long-range systems, numerical analysis is more difficult compared to short-range systems. Thus, numerical calculation of long-range systems should be done on super computers.

In this research, we have studied the scaling law of the systems with both long- and short-range interactions. For systems only with a single long-range interactions which scales as  $\sim 1/r^\alpha$ , the scaling law is conjectured by Tsallis[2] and confirmed later by many numerical simulations [3]. In this theory, thermodynamic quantities scale as  $E \sim NN^*\mathcal{E}^*$ ,  $T \sim N^*T^*$ ,  $V \sim N\mathcal{V}$  where  $d$  is a spacial dimension and  $N^*$  is given by  $N^* = N^{1-\alpha/d}$ .

However, for systems with both short- and long-range interactions,  $N^*$  should be mod-

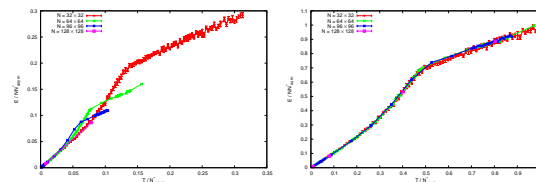


Fig. 1: Left: the relation between energy and temperature for  $N^* = N^{1-\alpha/d}$  (previously conjectured formula), and right: our new formula of  $N^*$ . You can see four lines lap over each other for bottom figure, which means the scaling factor  $N^*$  is correct.

ified for small system size. We conjectured what formula of  $N^*$  should be suited for such systems and confirmed this formula by numerical simulations.

In order to confirm our new formula of  $N^*$ , we have numerically simulated a classic lattice system with two potentials whose decaying speed is different each other. This computation requires a lot of computational power, so the super computer was much helpful for this simulation.

The result obtained by our simulation is plotted in Fig.1. Four different lines does not lap over each other for  $N^*$  of previous work [left figure], but for newly suggested  $N^*$  those lines lap over each other [right figure].

<sup>1</sup>For short-range systems, all the thermodynamic relations calculated from the microcanonical ensemble and the canonical ensemble agrees each other. This property is called the *ensemble equivalence*. However, this property does not hold for some systems with long-range interactions [1].

## 参考文献

- [1] A.Campa, A.Giansanti, D.Mukamel, and S.Ruffo, *Physica A* **365** (2006) 120–127
- [2] C.Tsallis, *Fractals* **3** (1995) 541–547
- [3] See, for example, L.Sampaio, M.Albuquerque, and F. Menezes, *Phys. Rev. B* **55** (1997) 5611–5614

# Molecular Dynamics Simulation Study of Nucleation Mechanism of Calcium Carbonate Crystal in the Presence of Impurities

Hiroki NADA

*National Institute of Advanced Industrial Science and Technology (AIST)  
Onogawa16-1, Tsukuba, Ibaraki 305-8569*

The polymorphism of calcium carbonate ( $\text{CaCO}_3$ ) has attracted great interest from long ago. The most thermodynamically stable  $\text{CaCO}_3$  crystal is calcite. However, the nucleation of metastable vaterite occurs instead of calcite. The nucleation of metastable aragonite or metastable hydrated  $\text{CaCO}_3$  crystals also occurs in the presence of impurities, such as  $\text{Mg}^{2+}$  ions. The  $\text{CaCO}_3$  polymorphism indicates that the nucleation of metastable  $\text{CaCO}_3$  crystals can be kinetically favored over the nucleation of calcite. However, the cause of the polymorphism remained unclear, because it was difficult to observe the initial stage of nucleation at the atomic scale in solution.

Recently, several experimental studies have reported the nucleation of  $\text{CaCO}_3$  crystals from amorphous  $\text{CaCO}_3$  (ACC) particles formed in solution. Therefore, the structure of ACC may be particularly relevant to  $\text{CaCO}_3$  polymorphism. In this project, we investigated the effects of  $\text{Mg}^{2+}$  ions and  $\text{H}_2\text{O}$  molecules on the atomic-scale structure of ACC by means of molecular dynamics (MD) simulation [1, 2].

The simulation was performed for bulk ACC. The system for ACC was a cubic consisting of 840 particles, which was the sum of the number of  $\text{Ca}^{2+}$  ions,  $\text{Mg}^{2+}$  ions,  $\text{CO}_3^{2-}$  ions and  $\text{H}_2\text{O}$  molecules. Three-dimensional periodic boundary conditions were imposed on the system. The fraction of  $\text{Mg}^{2+}$  in the system was 0, 0.25, 0.5, 0.75 and 1.0, and the fraction of  $\text{H}_2\text{O}$  molecules in the system was 0, 0.25,

0.5, 0.75. The  $\text{CaCO}_3$  potential model proposed by Raiteri et al. was used to estimate the  $\text{CaCO}_3$  interactions in ACC [3].  $\text{Mg}^{2+}$  potential parameters were developed in this project [1]. The interaction for the  $\text{H}_2\text{O}$  molecules was estimated using the TIP4P-Ew model [4]. Temperature and pressure were maintained at 300 K and 1 atm, respectively.

The simulation performed using NEC SX-9 in ISSP provided us the following new findings: The structure of pure ACC resembled that of vaterite rather than those of calcite and aragonite. However,  $\text{Mg}^{2+}$  ions hindered the formation of a vaterite-like structure in ACC. When the fraction of  $\text{H}_2\text{O}$  molecules was high and  $\text{Mg}^{2+}$  ions were present, the formation of monohydrocalcite-like structure was promoted.

## References

- [1] H. Tomono et al., *J. Phys. Chem. B*, **117** (2013) 14849.
- [2] F. Zhu et al., *Chem. Asian J.*, **8** (2013) 3002.
- [3] P. Raiteri et al., *J. Phys. Chem. C*, **114** (2010) 5997.
- [4] H. W. Horn et al., *J. Chem. Phys.*, **120** (2004) 9665.

# Numerical study of quantum liquid phase using tensor network variational method

Kenji HARADA

Graduate School of Informatics, Kyoto University, Kyoto 606-8501, Japan

In the past decade, the disordered behaviors of materials on a layer have been attracting attention. In particular, the possibility of a quantum spin liquid state has been studied. In general, the order of a quantum spin liquid state can be regarded as a topological one which cannot be transformed to a trivial state. However, except for special theoretical models, the evidence of topological order on effective models of materials is poor.

The antiferromagnetic Heisenberg model on a Shastry-Sutherland lattice is an effective model of  $\text{SrCu}_2(\text{BO}_3)_2$ . We have an interest in the possibility of intermediate disordered phase between a plaquette valence-bond-solid (VBS) phase and an antiferromagnetic phase on this model. We studied the ground states by using MERA tensor network methods. In our results, the plaquette VBS order is very weak near the antiferromagnetic phase. Thus, the existence of intermediate disorder phase is not clear yet. We continue to improve the numerical precision by applying a new algorithm of tensor networks.

In some cases, to protect the topological state against a trivial state, we need symmetry on models. Then, it is called *symmetry-protected topological order*. The hidden order of quantum spin model on a chain is a striking example of the symmetry-protected topological order[1]. We found the generalized Jordan-Wigner transformation[2] to disentangle the topological order of  $S=1$  bilinear-biquadratic (BLBQ) models on a chain[3]. We successfully extended it to  $\text{SO}(N)$  BLBQ models[4]. Using this non-local transformation, we can map an  $\text{SO}(N)$  BLBQ model to a  $N$ -color bosonic model. In particular, a symmetry-protected topological order can be transformed to a Landau symmetry-broken order analytically. We can study a symmetry-protected topological state as a conventional symmetry-broken state. In addition, the negative-sign problem of quantum Monte Carlo (QMC) calculation[5] perfectly disappears. Thus, we can study the topological ordered state by QMC with high precision. Using a worm algorithm on the ISSP super computer system B, we observed the rapid growth of entropy (See Fig. 1) and finite temperature behaviors of topological order parameter (See Fig. 2). The conventional approach cannot calculate these quantities with high precision.

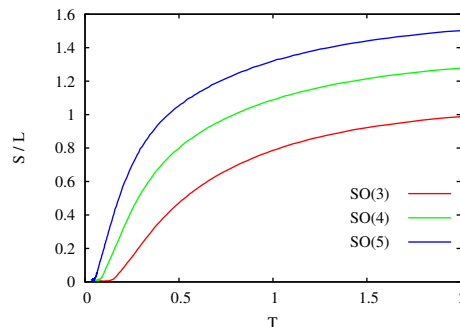


FIG. 1. Entropy per site of  $\text{SO}(3)$ ,  $\text{SO}(4)$ , and  $\text{SO}(5)$  BLBQ models on a chain at the generalized VBS points. The chain length  $L$  is 256.

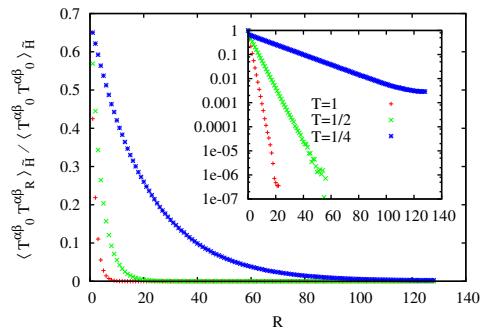


FIG. 2. Two point correlation function of topological order parameter at the AKLT[6] point of  $S=1$  BLBQ model on a chain. The chain length  $L$  is 256. The inset is a semi log plot.

- [1] F. Pollmann, A. M. Turner, E. Berg, and M. Oshikawa, Phys. Rev. B **81**, 064439 (2010); F. Pollmann, E. Berg, A. M. Turner, and M. Oshikawa, Phys. Rev. B **85**, 075125 (2012).
- [2] L. Messio and F. Mila, Phys. Rev. Lett. **109**, 205306 (2012).
- [3] K. Okunishi and K. Harada, Phys. Rev. B **89**, 134422 (2014).
- [4] H.-H. Tu, G.-M. Zhang and T. Xiang, Phys. Rev. B **78**, 094404 (2008).
- [5] K. Harada and N. Kawashima, J. Phys. Soc. Jpn. **70**, 13 (2001).
- [6] I. Affleck, T. Kennedy, E. H. Lieb, and H. Tasaki, Phys. Rev. Lett. **59**, 799 (1987).

# Numerical study on low-energy states of quantum spin systems

Hiroki NAKANO

*Graduate School of Material Science, University of Hyogo  
3-2-1 Kouto, Kamigori-cho, Ako-gun, Hyogo 678-1297, Japan*

Presice estimation of physical quantities of a quantum spin system is often difficult because the system is a typical many-body problem. Under circumstances, importance of numerical approaches, especially, methods beyond any approximations, becomes higher and higher. Computational studies have contributed much for our deep understanding of various quantum spin systems. However, it is still difficult to treat frustrated quantum spin systems in spatial dimensions larger than one. The reason of this difficulty is that such systems cannot be treated by the density matrix renormalization group (DMRG) calculations and the quantum Monte Carlo simulations. The numerical diagonalization method based on the Lanczos algorithm is an almost unique way as a valid method for such frustrated quantum spin systems. In this method, unfortunately, only very small system sizes can be treated. To overcome this disadvantage, we have successfully developed a hybrid-type parallelized code of Lanczos diagonalization[1]. Using this Lanczos-diagonalization calculation as a primary approach, we investigate quantum spin systems. We also employ other numerical methods as supplementary ones; we examine quantum spin systems from various points of view.

The primary study of this year in the present project is the magnetization jump in the  $S = 1/2$  Heisenberg antiferromagnet on the square-kagome lattice[2]. We find that the system shows a magnetization plateau at the one-third height of the saturation in its magnetization process; the plateau is accompanied by a magnetization jump at the higher-field edge. In order to clarify the mechanism of the occur-

rence of the jump, we observe the local magnetization, capturing the behavior of the spin-flop phenomenon in spite of the fact that the system is isotropic in spin space, where the spin-flop phenomenon is widely known to be a phenomenon that occurs when the system includes some anisotropy. The same behavior is observed in the Heisenberg antiferromagnet on the Cairo-pentagon lattice[3].

Properties of other frustrated Heisenberg antiferromagnet were studied by numerical-diagonalization method [4, 5, 6, 7]. Randomness effect in a frustrated system was also investigated[8]. Our numerical results and theoretical arguments contribute to analyze experiments of various magnetic compounds[9, 10, 11]. Our studies of quantum spin systems by several numerical approaches including parallelized calculations of Lanczos diagonalization contribute to our understandings of these systems.

## References

- [1] H. Nakano and A. Terai: J. Phys. Soc. Jpn. **78** (2009) 014003.
- [2] H. Nakano and T. Sakai: J. Phys. Soc. Jpn. **82** (2013) 083709.
- [3] H. Nakano, M. Isoda, and T. Sakai: J. Phys. Soc. Jpn. **83** (2014) 053702.
- [4] H. Nakano and T. Sakai: to be published in JPS Conf. Proc.
- [5] T. Shimokawa and H. Nakano: J. Kor. Phys. Soc. **63** (2013) 591.

- [6] Toru Sakai and H. Nakano: J. Kor. Phys. Soc. **63** (2013) 601.
- [7] H. Nakano, Synge Todo, and Toru Sakai: J. Phys. Soc. Jpn. **82** (2013) 043715.
- [8] K. Watanabe, H. Kawamura, H. Nakano and T. Sakai: J. Phys. Soc. Jpn. **83** (2014) 034714.
- [9] K. Iwase, H. Yamaguchi, T. Ono, T. Shimokawa, H. Nakano, A. Matsuo, K. Kindo, H. Nojiri, and Y. Hosokoshi: J. Phys. Soc. Jpn. **82** (2013) 074719.
- [10] H. Yamaguchi, S. Nagata, M. Tada, K. Iwase, T. Ono, S. Nishihara, Y. Hosokoshi, T. Shimokawa, H. Nakano, H. Nojiri, A. Matsuo and K. Kindo, and T. Kawakami: Phys. Rev. B **87** (2013) 125120.
- [11] H. Yamaguchi, K. Iwase, T. Ono, T. Shimokawa, H. Nakano, Y. Shimura, N. Kase, S. Kittaka, T. Sakakibara, T. Kawakami, and Y. Hosokoshi: Phys. Rev. Lett. **110** (2013) 157205.

# Dynamical scaling analysis on the low-temperature phase for the $RP^2$ model in two dimensions

Y. Ozeki<sup>1</sup>, A. Matsuda<sup>1</sup>, Y. Echinaka<sup>1</sup> and Y. Tomita<sup>2</sup>

<sup>1</sup>Graduate School of Informatics and Engineering, The University of Electro-Communications

<sup>2</sup>College of Engineering, Shibaura Institute of Technology

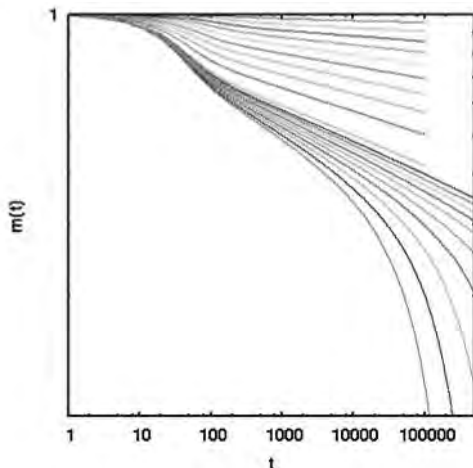


Figure 1: Calculations are made with  $\Delta T = 0.05$  for  $0.050 \leq T \leq 0.500$ , and with  $\Delta T = 0.005$  for  $0.510 \leq T \leq 0.555$ .

We investigate the nature of the phase transition which has been reported to appear in the low-temperature regime for the  $RP^2$  model in two dimensions. [1, 2] They suggested that there exist a topological phase transition like the Kosterlitz-Thouless (KT) one, while, recently, a possibility of no transition has been claimed [3, 4]. We apply the nonequilibrium relaxation (NER) method and examine the improved dynamical scaling analysis [5, 6] for the KT transition by the use of the Bayesian inference and the kernel method, and the relaxation of fluctuations to discuss the critical exponents  $\eta$  and  $z$  inside the KT phase.

The Hamiltonian for the  $RP^2$  model is

$$\mathcal{H} = -J \sum_{\langle ij \rangle} \cos^2(\theta_i - \theta_j). \quad (1)$$

We perform Monte Carlo simulation with Metropolis dynamics. First, we estimate the relaxation of the order parameter  $m(t) = \langle \sum_i \cos \theta_i \rangle_t / N$  from the all-aligned state, where  $\langle \cdots \rangle_t$  represents the dynamical average at  $t$  Monte Carlo steps

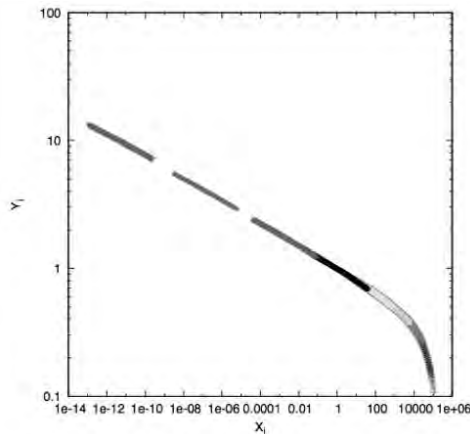


Figure 2: Scaling plot.

(MCS). Calculations are performed on lattices up to  $15001 \times 1500$  with skew boundary condition. The averaging is made for 1024 independently chosen samples. The result is shown in Fig. 1; note the unit of temperature is  $2J/3k_B$  which is used in the Lebwohl-Lasher model.

In the NER analysis of KT transition, it has been an efficient tool due to the finite-time scaling ,

$$m(t, T) = \tau^{-\lambda} \Psi(t/\tau), \quad (2)$$

where  $m(t, T)$  is a relaxation of magnetization from the all aligned state.  $\tau(T)$  is the relaxation time, which is expected to diverge as

$$\tau(T) \sim \exp(c/\sqrt{T - T_{KT}}) \quad (3)$$

in  $T > T_{KT}$ . To estimate  $T_{KT}$ , we fit the data to the above formula using the improved method applying the Bayes inference and the kernel method. [6] In Fig. 2, we show the resulting scaling plot for  $X = t/\tau$  vs.  $Y = \tau^\lambda m(t)$ . Furthermore, we apply the algebraic form  $\tau(T) \sim |T - T_c|^{-z\nu}$  instead of eq.(3), and compare the results. This provides the indication of the KT transition at  $T = 0.508$  in the present model.

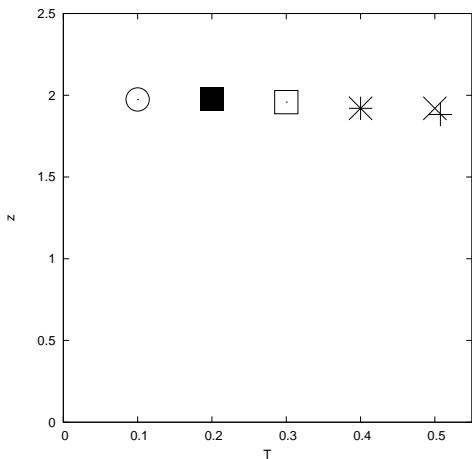


Figure 3: Temperature dependence of the exponent  $z$  inside the KT phase.

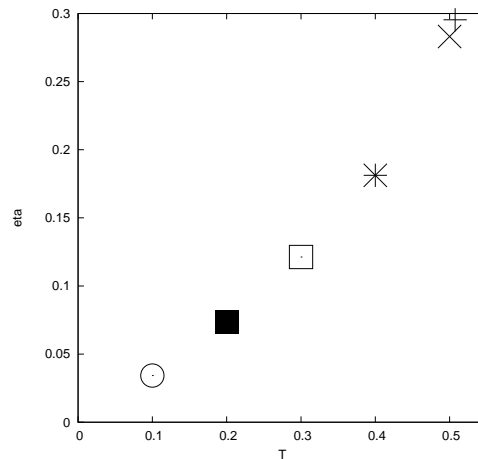


Figure 4: Temperature dependence of the exponent  $\eta$  inside the KT phase.

Next we examine critical exponents at and below the estimated KT transition temperature. We calculate  $m(t)$  and

$$f_{mm}(t) \equiv N \left( \frac{\langle m^2 \rangle_t}{\langle m \rangle_t^2} - 1 \right) \quad (4)$$

to estimate these exponents. Calculations are performed on  $401 \times 400$  lattice. The averaging is made for  $4^5$  independently chosen samples. From the dynamical scaling argument, the asymptotic forms of these quantities are expected as [5]

$$m(t) \sim t^{-\eta/2z}, \quad (5)$$

$$f_{mm}(t) \sim t^{2/z}. \quad (6)$$

Thus we estimate  $z$  and  $\eta$  for several values of temperatures. The results are shown in Figs. 3 and 4. For the dynamical exponent  $z$ , which seems to be located around 2 irrespective of temperature. For the static exponent  $\eta$ , which is decreasing linearly in the limit of  $T \rightarrow 0$ . These behaviors are quite similar with the XY model in two dimensions [7] in which the existence of the KT transition has been believed.

The present numerical study indicates that there exists a KT transition in the  $RP^2$  model in two dimensions. In the NER analysis, we observe and analyze relaxations up to an MCS where no size dependence clearly appears. Thus, one may recognize that the observed behavior is that in the thermodynamic limit.

## References

- [1] H. Kunz and G. Zumbach, Phys. Rev. B **46** 662 (1992).
- [2] E. Mondal and S. K. Roy, Phys. Lett. A **312** 397 (2003).
- [3] R. Paredes V. *et al*, Phys. Rev. E **78** 051706 (2008).
- [4] A. I. Fariñas Sánchez *et al*, Cond. Matter Phys. **13** 13601 (2010).
- [5] Y. Ozeki, K. Ogawa and N. Ito, Phys. Rev. E **67** 026702 (2003), Y. Ozeki and N. Ito, J. Phys. A: Math. Theor. **40** R149 (2007);
- [6] Y. Ozeki and Y. Echinaka, Activity Report 2012 (Supercomputer Center, ISSP, 2013)
- [7] Y. Ozeki, S. Yotsuyanagi, T. Sakai and Y. Echinaka, Phys. Rev. E **89** 022122 (2014).

# Novel ordered phase and dynamical response under driving field

Seiji MIYASHITA

*Department of Physics, University of Tokyo  
7-3-1 Hongo, Bunkyo-ku, Tokyo 113-0033, Tokyo*

## 1 Quantum dynamics under time-dependent external field

### 1.1 Phase transitions in a cavity driven by an external alternate field

We have studied what kinds of cooperative phenomena take place in systems driven by an external alternate field. In particular, we investigated a cavity system in which a single cavity photon mode couples with many discrete energy systems which we call ‘spin’ hereafter.[1] The spins are independent of each other but they couple with each other by effective interaction due to the cavity mode. The cavity mode is excited by a resonant external field. The coupling between spin and cavity mode composes a hybrid system where the energy spectrum exhibits an avoided level structure, which has been attracted from a view point of information transfer between photon system and condensed matter.[2] It is known that the coupling causes the so-called Dicke transition where the spontaneous excitation appears even in the ground state, and also that the coupling causes a non-equilibrium phase transition which is called ‘optical bistability’ as a function of strength of external field.

The system is modeled by the Dicke model or the model with rotation-field approximation (Tavis-Cummings model).

$$\mathcal{H} = \hbar\omega_0 a^\dagger a + \hbar\omega_A \sum_{i=1}^N S_i^z,$$

$$+ \hbar\hat{g} \sum_{i=1}^N (S_i^+ + S_i^-)(a^\dagger + a) + \hat{\xi}(a^\dagger + a) \cos(\omega_{\text{ext}}t). \quad (1)$$

where  $\omega_0$  is a frequency of the cavity photon, and  $\omega_A$  denotes the excitation energy of the spin, and  $g$  is the strength of the coupling. The last term is the external AC field whose strength is  $\xi$ . We study the model with a quantum master equation where we take into account the external driving field and dissipative effect due to a coupling to the thermal bath.

First we drove a quantum master equation in which effects of the interaction in the system is taken into account. This adjustment is necessary to reproduce the spontaneous symmetry breaking phenomena correctly. We also pointed out that the mean-field approximation holds in a proper scaling limits  $\hat{g} = g/\sqrt{N}$  and  $\hat{\xi} = \sqrt{N}\xi$ , and studied cooperative phenomena in the region of strong coupling ( $g$ ) and the strong driving  $\xi$ . We found a new type of symmetry broken state, the region of which is depicted by dots in the phase diagram (Fig. 1).

The mechanism of the new symmetry broken state is given from the view point of the Coherent Destruction of Tunneling (CDT). The lines denote the position where the spin system is expected to show the CDT.

### 1.2 Landau-Zener dynamics in uniaxial quantum spins

We have studied the Landau-Zener mechanism in isotropic spin systems, where the dynamics is independent of the total spin  $S$ . In the case of classical spin in uniaxial spin systems, the so-called Stoner-Wohlfarth mechanism takes place, and the spin dynamics has a

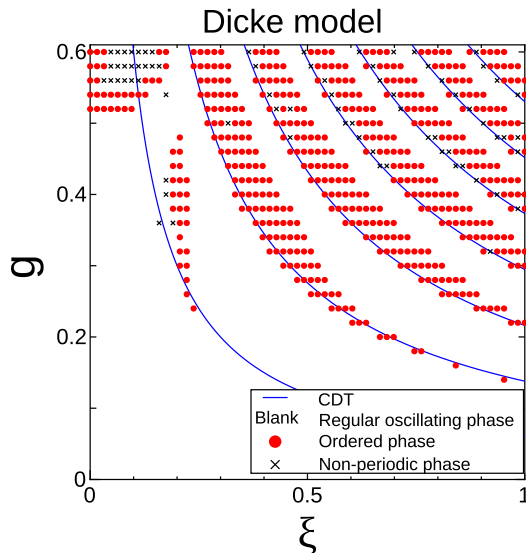


Figure 1: Phase diagram of the driven Dicked model (cited from [1])

threshold phenomenon at which the magnetization jumps. In quantum system similar phenomena takes place, which can be regarded as a first order phase transition in quantum system. We studied the nature of the metastable state associated with the first order phase transition in quantum systems.

## 2 Other topics

### 2.1 Phase transitions of systems with bistable states which have different local lattice structures

We have pointed out the effects of long range interaction due to elastic interaction of lattice distortion which is brought by the different local lattice structures of bistable states. This mechanism is relevant in many systems, such as the spin-crossover, Jahn-Teller system, and martensite systems. We studied the effect of long range interaction on the system with short range antiferromagnetic model and obtained full phase diagram for ferro- and antiferromagnetic short range interactions in the elastic model.[3]. We also studied the nature of the domain wall in such system where we found that the width of the domain wall depends on the time scale of spin dynamics[3].

In such systems with long range interaction causes peculiar properties. We found the

present model holds the extensivity, but not the additivity[5].

### 2.2 Phase transition between Mott insulator and Itinerant ferromagnetism

We also studied quantum phase transition of an itinerant ferromagnetism motivated by the Nagaoka ferromagnetism. In the system the electron density is controlled by the chemical potential. The change of the total spin as a function of the chemical potential is obtained by an exact diagonalization and also DMRG method. Various properties, such as magnetization process, the spin-correlation function, and also entanglement entropy was studied[6].

## References

- [1] T Shirai, T Mori and S Miyashita, Novel symmetry-broken phase in a driven cavity system in the thermodynamic limit, *J. Phys. B: At. Mol. Opt. Phys.* **47** (2014) 025501 (9pp).
- [2] S. Miyashita, T. Shirai, T. Mori, H. De Raedt, S. Bertaina, and I. Chiorescu, Photon and spin dependence of the resonance lines shape in the strong coupling regime, *J. Phys. B: At. Mol. Opt. Phys.* **45**, 124010(10pp) (2012).
- [3] Masamichi Nishino, and Seiji Miyashita, Effect of the short-range interaction on critical phenomena in elastic interaction systems, *Phys. Rev. B* **88**, 014108 (2013).
- [4] Masamichi Nishino, Taro Nakada, Cristian Enachescu, Kamel Boukheddaden, and Seiji Miyashita, Crossover of the roughness exponent for interface growth in systems with long-range interactions due to lattice distortion, *Phys. Rev. B* **88**, 094303 (2013).
- [5] T Mori, Nonadditivity in Quasiequilibrium States of Spin Systems with Lattice Distortion, *Phys. Rev. Lett.* **111**, 020601 (2013).
- [6] H. Onishi and S. Miyashita, "Doping Control of Realization of an Extended-Nagaoka Ferromagnetic State from the Mott state", in preparation.

# Transport phenomena in disordered topological insulators

TOMI OHTSUKI<sup>1</sup>  
 TOHRU KAWARABAYASHI<sup>2</sup>  
 KEITH SLEVIN<sup>3</sup>  
 KOJI KOBAYASHI<sup>1</sup>

1) Dept. Phys., Sophia University, Chiyoda-ku, Tokyo 102-8554, Japan

2) Dept. Phys., Toho University, Miyama 2-2-1, Funabashi 274-8510, Japan

3) Dept. Phys., Osaka University, Toyonaka, Osaka 560-0043, Japan

Recent discoveries of two-dimensional quantum spin Hall states and three-dimensional topological insulators (TIs) have inspired extensive research for these novel materials. In the impurity free systems where the translational invariance exists, the topological insulator is characterized by the non-zero topological numbers, which are defined via integral over Brillouin zone. This definition is no longer valid once the translational invariance is broken due to disorder. In this case, we usually use edge/surface states to characterize TIs.

Here we study the bulk properties of the disordered three-dimensional topological insulators numerically, and show how to distinguish TI from ordinary insulators by investigating the transport properties of bulk states. We first calculate bulk conductance via transfer matrix method, from which we draw the phase diagram for disordered TI [1]. Along the phase boundary between different TI phases, we show that the Dirac semimetal emerges even in the presence of disorder. With increase of disorder, the Dirac semimetal undergoes semimetal to metal transition. We propose that the density of states exhibits novel single parameter scaling behavior near the Dirac semimetal to metal transition.

To confirm the scaling behavior, we have performed large scale numerical calculation of the density of states via kernel polynomial method. We consider  $200 \times 200 \times 200$  cubic systems described by Wilson-Dirac Hamiltonian, which are large enough to discuss approxi-

mately the thermodynamic limit. We then estimate the critical exponent  $\nu$  for the length scale to be  $\approx 0.9$ , and the dynamical exponent  $z$  to be  $\approx 1.5$ , significantly different from those of the Anderson transition (in which we obtain  $\nu = 1.38 \pm 0.01$  and  $z = 3$  [2]). Scaling relations of vanishing density of states, diverging diffusion constant, vanishing conductivity as well as vanishing Dirac electron velocity are derived [3].

## References

1. K. Kobayashi, T. Ohtsuki, K.-I. Imura: PRL **110**, 236803 (2013)
2. K. Slevin, T. Ohtsuki: New J. Phys. **16**, 015012 (2014)
3. K. Kobayashi, T. Ohtsuki, K.-I. Imura, I. Herbut: PRL **112**, 016402 (2014)

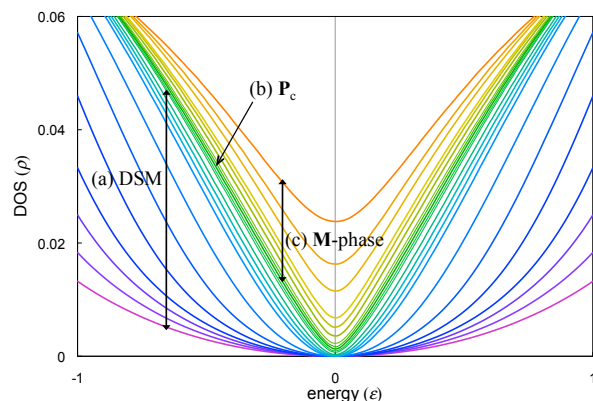


Figure 1: Density of states calculated in different phases: (a) on the boundary, (b) at the tricritical point, and (c) in the metal phase.

# Transport phenomena in disordered topological insulators

TOMI OHTSUKI<sup>1</sup>KEITH SLEVIN<sup>2</sup>YOSUKE HARASHIMA<sup>2</sup>1) *Dept. Phys., Sophia University, Chiyoda-ku, Tokyo 102-8554, Japan*2) *Dept. Phys., Osaka University, Toyonaka, Osaka 560-0043, Japan*

In heavily doped semiconductors, a zero temperature metal-insulator transition (MIT) is observed as a function of doping concentration  $N_d$ . For samples with doping concentrations below a critical concentration  $N_c$ , the conductivity extrapolated to zero temperature  $\sigma(T = 0)$  is found to be zero, while for samples with concentrations exceeding this critical concentration,  $\sigma(T = 0)$  is finite.

The object of this study is to understand the MIT in doped semiconductors by determining how the Coulomb interaction affects the critical behaviour of the Anderson transition. We do this by simulating a model of a doped semiconductor that treats on an equal footing both the disorder due to the random spatial distribution of the dopants and the Coulomb interaction between the carriers.

To study a phase transition, we need to consider a reasonably large number of electrons, so exact diagonalization is impractical. Instead we use the Kohn-Sham formulation of density functional theory. The local density approximation (LDA) is adopted. We then observe a localisation-delocalisation transition of the highest occupied Kohn-Sham eigenfunction as a function of donor concentration. Simulations were performed for system sizes in the range  $L = 229 \sim 400 \text{ \AA}$  and donor concentrations of  $N_d = N/L^3 = 0.4 \sim 1.3 \times 10^{18} \text{ cm}^{-3}$ , which corresponds to  $5 \sim 85$  electrons. We set the finite difference grid spacing to 18 Bohr, which is about half of the effective Bohr radius for Si. The donors were randomly distributed on a simple cubic lattice with spacing 36 Bohr. This avoids the situation that two donors are

unphysically close. The number of samples for each system size and donor concentration varies between 1500 and 3000.

Applying a multi-fractal finite size scaling method [1], we find that the model exhibits a localization-delocalization transition at approximately the right carrier concentration (see Figure 1) [2]. Moreover, we find that the critical exponent  $\nu \approx 1.3$ , which is different from that for the standard Anderson transition.

## References

1. A. Rodriguez, L. J. Vasquez, K. Slevin, and R. A. Romer: *Phys. Rev. Lett.* **105** (2010) 046403, *Phys. Rev. B* **84** (2011) 134209.
2. Y. Harashima, K. Slevin: arXiv:1308.1191

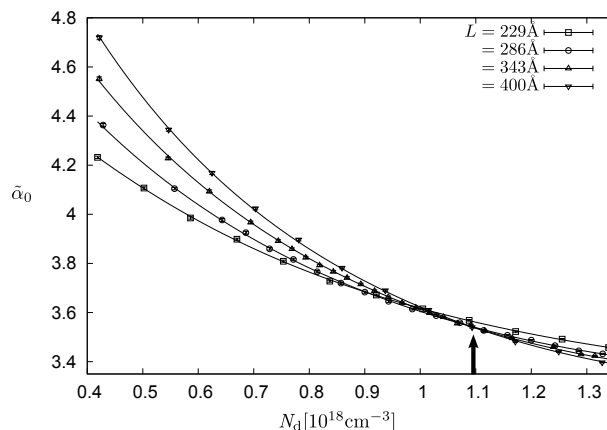


Figure 1: The generalized multi-fractal exponent  $\alpha_0$  as a function of donor concentration for several system sizes. The solid lines are a finite size scaling fit to the data. The critical concentration is indicated by an arrow.

# Study on Statistical Physics Based on Quantum Information Theory

Shu TANAKA

*Department of Chemistry, The University of Tokyo*

*7-3-1 Hongo, Bunkyo-ku, Tokyo 113-0033*

*Yukawa Institute for Theoretical Physics, Kyoto University*

*Kitashirakawa-Oiwakecho, Sakyo-Ku, Kyoto 606-8502*

As a next-generation information technology, quantum information technology has been attracted attention in science. In addition, quantum information science opens a new window on a wide area of physics, *e.g.*, quantum statistical physics. We studied the following two topics in this project[1, 2, 3, 4].

## (a) Quantum Annealing for Clustering Problem[1, 2]

In general, it is hard to obtain the best solution of optimization problems. Optimization problems are widespread in science and technology and efficient algorithms have been proposed. Most of combinatorial optimization problems can be mapped onto random Ising model and its generalized model. Thus, development of such algorithms have been done in statistical physics.

In 1998, Kadowaki and Nishimori proposed a versatile algorithm called quantum annealing to obtain the best solution by gradually decreasing quantum fluctuation[5]. The quantum annealing is an alternative to the simulated annealing [6] in which the temperature (*i.e.*, thermal fluctuation) gradually decreases. The efficiency of quantum annealing has been considered for a long time using simple models. In addition, very recently, actual equipment of quantum annealing has been developed[7].

To examine the performance of quantum annealing, we considered quantum annealing to solve a clustering problem which is a typ-

ical applicable optimization problem[1]. In our quantum annealing, not only the quantum fluctuation but also the thermal fluctuation are simultaneously controlled. As a result, the efficiency of quantum annealing is better than that of simulated annealing although computational costs of both methods are comparable. In this study, we performed the Monte Carlo simulation based on parallel computation.

The performance of quantum annealing is not good for systems in which phase transition occurs. This fact is known as difficulty in the quantum annealing. In order to avoid the difficulty, we also considered another type of fluctuation to add the Hamiltonian which represents optimization problems[2].

The above studies were done in collaboration with Kenichi Kurihara (Google Inc.), Seiji Miyashita (The University of Tokyo), Hiroshi Nakagawa (The University of Tokyo), Issei Sato (The University of Tokyo), and Ryo Tamura (National Institute for Materials Science).

## (b) Entanglement Properties of Two-dimensional Quantum Systems[3, 4]

Entanglement properties have been considered in not only quantum information science but also various fields of physics such as quantum statistical physics. Some beautiful relations between entanglement properties and strongly correlated quantum systems have been found. We have considered entan-

glement properties of two-dimensional quantum systems[3, 4]. A part of this study is now in progress. The obtained results in this study will be reported elsewhere.

The above study was done in collaboration with Hosho Katsura (Gakushuin University, The University of Tokyo) and Ryo Tamura (National Institute for Materials Science).

## References

- [1] I. Sato, S. Tanaka, K. Kurihara, S. Miyashita, and H. Nakagawa: Neurocomputing **121** (2013) 523.
- [2] R. Tamura and S. Tanaka: Kinki University Series on Quantum Computing – Vol. 9, “Physics, Mathematics, and All That Quantum Jazz” (World Scientific), in press.
- [3] S. Tanaka: Interdisciplinary Information Sciences **19** (2013) 101.
- [4] S. Tanaka, R. Tamura, and H. Katsura: Kinki University Series on Quantum Computing – Vol. 9, “Physics, Mathematics, and All That Quantum Jazz” (World Scientific), in press.
- [5] T. Kadowaki and H. Nishimori: Phys. Rev. E **58** (1998) 5355.
- [6] S. Kirkpatrick, C. D. Gelatt, and M. P. Vecchi: Science **220** (1983) 671.
- [7] <http://www.dwavesys.com/>

# Control of Phase Transition Behavior in Lattice Models

Shu TANAKA

*Department of Chemistry, The University of Tokyo*

*7-3-1 Hongo, Bunkyo-ku, Tokyo 113-0033*

*Yukawa Institute for Theoretical Physics, Kyoto University*

*Kitashirakawa-Oiwakecho, Sakyo-Ku, Kyoto 606-8502*

Investigation of relation between underlying properties in considered models and phase transition behavior is an important topic in statistical physics. In addition, how to control phase transition nature is also an interesting issue. We considered the following two topics in this project[1, 2].

## **(a) Network growth rule dependence of fractal dimension**[1]

It is well-known that conventional percolation transition in static models is continuous phase transition. The critical exponents depending on spatial dimension were investigated. However, there are new type of percolation transitions in dynamical network model. In 2009, Achlioptas et al. proposed a new type of network growth rule and considered percolation transition behavior[3]. They concluded that a discontinuous phase transition occurs using their network growth rule while a continuous phase transition occurs under conventional network growth rules. We constructed a rule that includes the conventional rule and the Achlioptas rule. In our rule, a parameter  $q$  which expresses network growth rule is introduced. The relation between the parameter  $q$  and geometric properties at the percolation point was investigated using Monte Carlo simulations. In particular, we focused on the fractal dimension of the percolated cluster at the percolation point. As a result, the fractal dimension increases as the network growth rule

approaches the Achlioptas rule.

This work was done in collaboration with Ryo Tamura (National Institute for Materials Science).

## **(b) Relation between the Potts model with invisible states and frustrated spin systems**[2]

Recently, frustrated systems where the order parameter is described by the direct product between two groups have been studied. In these systems, unconventional phase transition often occurs. Tamura and Kawashima found that a first-order phase transition with  $C_3$  symmetry breaking occurs in two-dimensional frustrated systems where the order parameter space is  $SO(3) \times C_3$ [4, 5]. To explain the phase transition nature qualitatively, the Potts model with invisible states was introduced[6, 7]. By introducing a local parameter in frustrated systems, we considered the relation between the Potts model with invisible states and frustrated spin systems using Monte Carlo simulations. We also estimated the effective interaction of the Potts model with invisible states in frustrated systems using the Curie-Weiss type analysis. This study is closely related to other unconventional phase transition observed in other frustrated systems[8, 9].

This work was done in collaboration with Naoki Kawashima (Institute for Solid State Physics, The University of Tokyo) and Ryo Tamura (National Institute for Materials Sci-

## References

- [1] S. Tanaka and R. Tamura: J. Phys. Soc. Jpn. **82** (2013) 053002.
- [2] R. Tamura, S. Tanaka, and N. Kawashima: JPS Conf. Proc. **1** (2014) 012125.
- [3] D. Achlioptas, R. M. D'Souza, and J. Spencer: Science **323** (2009) 1453.
- [4] R. Tamura and N. Kawashima: J. Phys. Soc. Jpn. **77** (2008) 103002.
- [5] R. Tamura and N. Kawashima: J. Phys. Soc. Jpn. **80** (2011) 074008.
- [6] R. Tamura, S. Tanaka, and N. Kawashima: Prog. Theor. Phys. **124** (2010) 381.
- [7] R. Tamura and S. Tanaka: Kinki University Series on Quantum Computing – Vol. 9, “Physics, Mathematics, and All That Quantum Jazz” (World Scientific), in press.
- [8] R. Tamura, S. Tanaka, and N. Kawashima: Phys. Rev. B **87** (2013) 214401.
- [9] R. Tamura and S. Tanaka: Phys. Rev. E **88** (2013) 052138.

# Analysis of Quantum Phase Transitions with Large Finite-Size Effect

Syngé Todo

*Department of Physics, University of Tokyo, Tokyo 113-0033, Japan*

Quantum phase transitions are phase transitions between two different ground states that are triggered by quantum fluctuations at absolute zero temperature. We develop various novel and powerful techniques to tackle various exotic quantum critical phenomena observed in quantum spin systems and performed large-scale and high-precision simulations on the ISSP supercomputer system.

## Quantum Monte Carlo simulation with dynamic control of anisotropy [1]

In systems with strong spatial anisotropy, it is often difficult to carry out the conventional finite-size-scaling analysis due to large corrections to scaling. To overcome this difficulty, we develop a novel algorithm where the aspect ratio of the system is optimized dynamically during the Monte Carlo update so that the isotropy is recovered virtually. The optimization is done by the Robbins-Monro machine-learning algorithm. Using this method we can determine the quantum critical points precisely as well as the critical exponents of several physical quantities. We establish that the staggered and columnar dimer models both belong to the conventional  $O(3)$  universality class but the optimal aspect ratio of the former model shows the non-monotonic behavior, which comes from the weakly irrelevant cubic term. We also extend our scheme to the quantum critical point with  $z > 1$ .

## Quantum Monte Carlo measurement of local $Z_2$ Berry phase [2]

We develop a loop cluster algorithm Monte Carlo method for calculating the local  $Z_2$  Berry phase of the quantum spin models. The

Berry connection, which is given as the inner product of two ground states with different local twist angles, is expressed as a Monte Carlo average on the worldlines with fixed spin configurations at the imaginary-time boundaries. The “complex weight problem” caused by the local twist is solved by adopting the meron cluster algorithm. We also propose that the gauge-fixed local Berry connection can be an effective tool to estimate precisely the quantum critical point. In addition, we extend the present technique to  $SU(N)$  spin models, where  $N$  topologically different phases can be distinguished successfully by the local  $Z_N$  Berry phase.

## BCL: Balance Condition Library [3]

We have introduced a novel geometric approach that breaks the detailed balance of the Markov chain explicitly (while keeping the (total) balance satisfied) and minimizes (often eliminates) rejection rate. We are now developing the open-source library, BCL (Balance Condition Library), which provides a C++ reference implementation of our algorithm together with the Metropolis-Hasting and Gibbs sampler in Markov Chain Monte Carlo, as well as the API for C, Fortran, Python, etc.

## References

- [1] S. Yasuda and S. Todo: Phys. Rev. E **88** (2013) 061301(R).
- [2] Y. Motoyama and S. Todo: Phys. Rev. E **87** (2013) 021301(R).
- [3] <http://github.com/cmsi/bcl>.

# Development and application of a new quantum Monte Carlo Algorithm for lattice bosons

Akiko Masaki

*Institute for Solid State Physics,*

*The University of Tokyo, Kashiwa-no-ha, Kashiwa, Chiba 277-8581*

Large-scale computations have the possibility of solving many important remaining problems in quantum many-body physics. Recently high-performance computers, e.g. K-computer, have gained its FLOPS using many cores. Namely the parallelization of algorithms is an effective way to solve these remaining problems. The worm algorithm [1, 2] which has the broad range of applicability is a most efficient global-update algorithm for the world-line quantum Monte Carlo method. However the parallelization of the worm is not straightforward because of the event-driven motions of a worm that is a single-point object in the configuration space.

Based on the directed-loop algorithm [2] we investigated the parallelizable multi-worm algorithm (PMWA) where multiple worms are introduced by an artificial source field  $\eta$  and the configuration space decompose into domains [3]. We estimate physical observables by extrapolation to  $\eta = 0$  imit. Introducing multiple-worms requires the different procedure from the conventional worm algorithm so as to satisfy the detailed balance condition. Our algorithm satisfies it. In

addition, the propagation of worms between domains and the update of states on domain boundaries are effectively carried out by communications between domains so that the ergodicity is recovered. PMWA is applicable to the soft-core Boson model and the quantum spin model without the negative-sign problem as with the conventional worm algorithm.

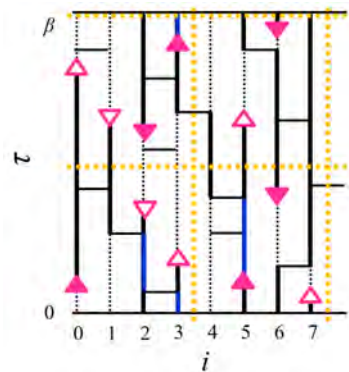


Figure 1: The configuration space of PMWA.

We applied PMWA to the extended Hardcore Bose-Hubbard model on square lattice defined by

$$\mathcal{H} = -t \sum_{\langle i,j \rangle} b_i^\dagger b_j + V \sum_i n_i n_j - \mu \sum_i (n_i + n_j),$$

where  $b_i$  ( $b_i^\dagger$ ) is the annihilation (creation) operator at  $i$  th site,  $t$  is the hopping energy,  $V$

is the nearest-neighbor interaction and  $\mu$  denotes the chemical potential respectively. Firstly we derived the extrapolation rule to obtain physical quantities at  $\eta = 0$ . Then we confirmed that extrapolated PMWA result shows the agreement with DLA results.

We accomplished simulations of up to the size of  $L \times L \times \beta = 10,240 \times 10,240 \times 16$  using 3,200 processing cores, where  $L$  is the number of the lattice site per spatial direction and  $\beta$  is the inverse of temperature. This size is extremely larger than the workable size of the conventional worm algorithm with single processor. We measured the standard error as a function of the number of domains  $N$  to estimate the performance of the algorithm.

As a result, we found a weak effect of  $N$  for the relaxation time by the simulation with fixed number of the Monte Carlo steps. Moreover, when we compare with the DLA results, PMWA results is more accurate than DLA in fixed wall-clock time with  $N > 8$ .

## References

- [1] N. Prokofev, B. Svistunov and I. Tupitsyn, Sov. Phys. JETP **87**, 310 (1998).
- [2] O. F. Syljuasen and A. W. Sandvik, Phys. Rev. E **66**, 046701 (2012).
- [3] Akiko Masaki-Kato, Takafumi Suzuki, Kenji Harada, Synge Todo, Naoki Kawashima, Phys. Rev. Lett. **112**, 140603 (2014).

# Morphology of Lipid Vesicles: effects of confinement and genus

Ai Sakashita and Hiroshi Noguchi  
*Institute for Solid State Physics, University of Tokyo*  
*Kashiwa-no-ha, Kashiwa, Chiba 277-8581*

Cell organelles such as Golgi apparatus, endoplasmic reticulum, and mitochondria have very complicated shapes; Among these organelles, mitochondria have a specific feature, *i.e.*, it consists of two bilayer membranes. The nuclear membrane and endoplasmic reticulum are connected and together form complicated shapes. The nucleus is wrapped by two bilayer membranes connected by many lipidic pores. Thus, its shape is considered as a stomatocyte of a high-genus vesicle connected with a tubular network. We focus on geometrical constraints and investigated a vesicle confined in a spherical vesicle [1] and non-zero genus vesicles [2] using the dynamically triangulated surface model.

Figure 1 shows examples of vesicle shapes confined in a sphere [1]. Reduced volume  $v_r$ , area difference  $\Delta a$ , and the volume ratio  $v_{\text{con}}$  of the inner vesicle to the outer sphere are three parameters to determine the vesicle shape. Under a strong confinement, an additional bud is formed in a stomatocyte in order to fill the volume between the vesicles. In the limit  $v_r \rightarrow 1$ , this double stomatocyte is the most stable shape. At  $v_r \simeq 0.9$ , other novel shapes can be found in equilibrium. As  $\Delta a$  increases, a stomatocyte transforms into a vesicle with a planar slit and subsequently forms a doublet. As negative values of  $\Delta a$ , the inner bud forms a tubular or discocyte shape. This discocyte bud resembles the crista structures in mitochondria.

For genus-1 toroidal vesicles, we obtained the free-energy profiles using a generalized ensemble Monte Carlo method [2]. At large  $v_r$ , obtained vesicle shapes agree with the previous theoretical results for axisymmetric shapes:

double-necked stomatocyte, discoidal toroid, and circular toroid. However, for small  $v_r$ , it is found that a non-axisymmetric discoidal toroid and handled discocyte exist in thermal equilibrium in the parameter range, in which the previous theory predicts axisymmetric shapes. The entropy caused by shape fluctuations slightly modifies the stability of the vesicle shapes.

We have also observed a liposome confined in a spherical liposome and genus-1 and 2 liposomes using a fast confocal laser microscopy. Our simulation results reproduce shape transformations observed in our experiments well.

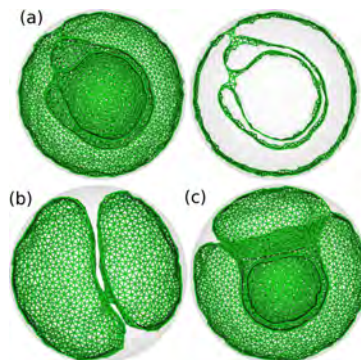


Figure 1: Snapshots of a vesicle confined in a sphere. (a) Double stomatocyte. (b) Doublet. (c) Triplet.

## References

- [1] A. Sakashita, M. Imai and H. Noguchi: Phys. Rev. E **89** (2014) 040701(R).
- [2] A. Sakashita, M. Imai and H. Noguchi: arXiv:1405.3076 [cond-mat.soft].

## Efficient sampling simulation of the soft modes significantly contribute to protein properties

Akio KITAO

*Institute of Molecular and Cellular Biosciences, University of Tokyo*

Biological processes are often associated with significant conformational changes of biomolecules, which are relevant to their functions. The free energy landscape (FEL) along appropriate reaction coordinates provides us essential information to characterize the mechanism of conformational changes and functions. In this sense, efficient and accurate sampling of the conformational space to calculate the FEL is a major topic for molecular dynamics (MD). Let  $\boldsymbol{\theta}(\mathbf{x})$  be collective variables (CVs) defined as functions of  $\mathbf{x}$ , where  $\mathbf{x}$  is the Cartesian coordinate of atom. Supposing that  $\mathbf{z}$  is a particular realization of these CVs, the FEL  $F(\mathbf{z})$  is defined as:

$$F(\mathbf{z}) = -\frac{1}{\beta} \ln \left\{ Q^{-1} \int e^{-\beta V(\mathbf{x})} \prod_{l=1}^L \delta(\theta_l(\mathbf{x}) - z_l) d\mathbf{x} \right\}, \quad (1)$$

where  $Q = \int e^{-\beta V(\mathbf{x})} d\mathbf{x}$ ,  $L$  is the number of CVs,  $V(\mathbf{x})$  is the potential energy,  $\delta$  is Dirac's delta function, and  $\beta = 1/k_B T$ , where  $k_B$  is the Boltzmann constant and  $T$  is the temperature. If  $\boldsymbol{\theta}(\mathbf{x})$  can be regarded as appropriate reaction coordinate, the goal is to calculate  $F(\mathbf{z})$ .

However, sampling of large conformational space within a limited simulation time is still a challenging problem, because of complexity of FEL and the large gap between simulation time step and

time scale of biological process. In order to tackle the difficulty, we proposed a new efficient conformational sampling method, Multi-scale Sampling using Temperature Accelerated and Replica-exchange MD (MuSTAR MD) [1].

MuSTAR MD is an extension of temperature accelerated MD (TAMD) and can also be considered as a variation of replica-exchange MD (REMD). In the MuSTAR MD simulation, each replica contains an all-atom model, at least one coarse-grained model, and a CVs that interacts with the other models through coupling terms. The coarse-grained model is introduced to drive efficient sampling of large conformational space and the all-atom model can serve to conduct accurate conformational sampling. Equations of motion for MuSTAR MD consists of Cartesian spaces and CV space,

$$m_i^\alpha \ddot{\mathbf{x}}_i^\alpha = -\frac{\partial V^\alpha(\mathbf{x}^\alpha)}{\partial \mathbf{x}_i^\alpha} - \frac{\partial W^\alpha(\mathbf{x}^\alpha, \mathbf{z})}{\partial \mathbf{x}_i^\alpha} + (thr, \beta^\alpha) = -\frac{\partial U^\alpha(\mathbf{x}^\alpha, \mathbf{z})}{\partial \mathbf{x}_i^\alpha} + (thr, \beta^\alpha), \quad (2)$$

$$m^z \ddot{z}_l = -\sum_{\alpha} \frac{\partial W^\alpha(\mathbf{x}^\alpha, \mathbf{z})}{\partial z_l} + (thr, \beta^z). \quad (3)$$

where  $\mathbf{x}_i^\alpha$  and  $V^\alpha(\mathbf{x}^\alpha)$  are the position vector in Cartesian coordinate for the  $i$ -th atom of model  $\alpha$  and potential energy functions in each model, respectively, and  $W^\alpha(\mathbf{x}^\alpha, \mathbf{z})$  is the coupling terms

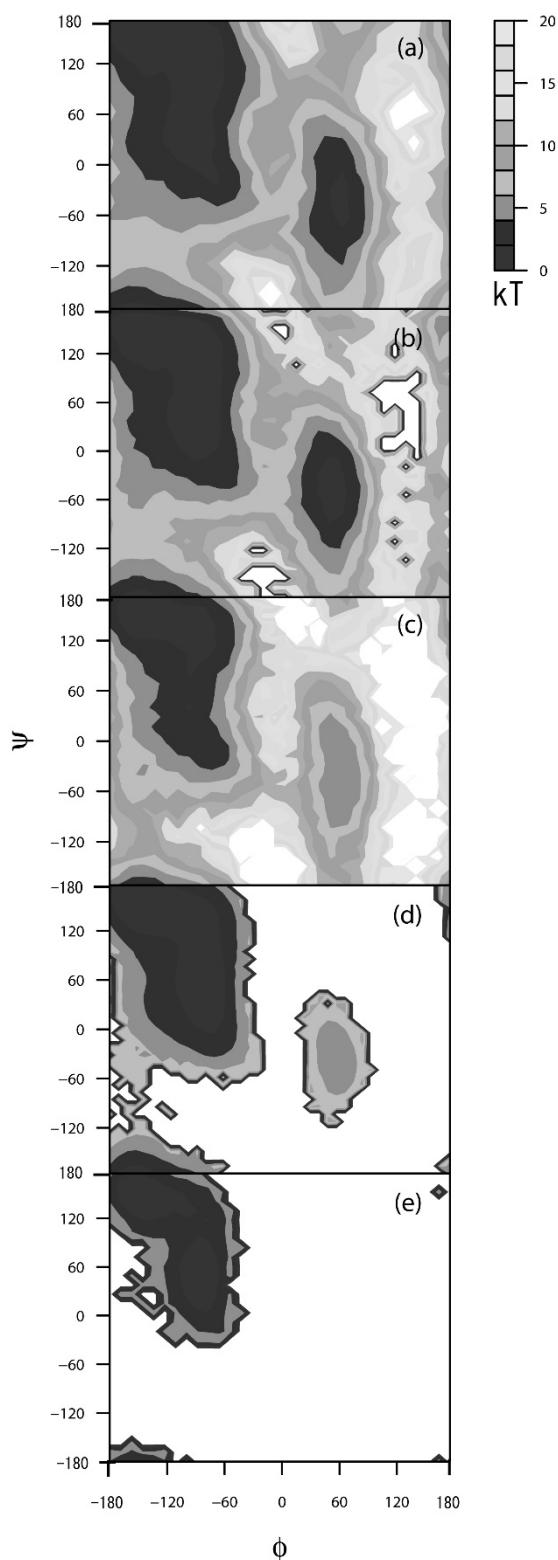


**Figure** FEL of Ala-dipeptide in vacuum using the AMBER force field parm99SB with respect to backbone dihedral angles  $\phi$  and  $\psi$ . The results from (a) MuSTAR MD (10 ns $\times$ 8 replicas), (b) TAMD (80ns), (c) REMD (10 ns $\times$ 8 replicas), (d) REUS (5ns $\times$ 16), (e) CMD (80 ns).

between model  $\alpha$  and the CV system.  $\alpha$  can represent

either fine-grained or coarse-grained model. The thermostat parameters are related to temperatures as  $\beta^\alpha = 1/k_B T^\alpha$  and  $\beta^z = 1/k_B T^z$ . The coupling terms are defined as:

$$W^\alpha(\mathbf{x}^\alpha, \mathbf{z}) = \frac{K^\alpha}{2} \sum_{l=1}^L (\theta_l(\mathbf{x}^\alpha) - z_l)^2, \quad (4)$$

$$U^\alpha(\mathbf{x}^\alpha, \mathbf{z}) = V^\alpha(\mathbf{x}^\alpha) + W^\alpha(\mathbf{x}^\alpha, \mathbf{z}), \quad (5)$$

where  $K^\alpha$  is the coupling-strength between model  $\alpha$  and the CV system. The parameters are exchanged between neighboring replicas in some interval obeying the Metropolis method.

We applied MuSTAR MD for typical test cases, Ala-dipeptide in vacuum. Figures (a)-(e) are FELs at 300 K calculated from the results of MuSTAR MD, TAMD, REMD, replica-exchange umbrella sampling (REUS) and conventional MD (CMD), respectively. The sampled conformational space obtained from same simulation time is broader in the order of MuSTAR MD>TAMD>REMD>REUS>CMD. In addition, among five methods examined, MuSTAR MD showed the closest results to that obtained from long-time umbrella sampling simulation.

MuSTAR MD shows the high performance in sampling efficiency and accuracy compared to established enhanced sampling methods. The advantageous features of MuSTAR MD are: 1) High temperature of the CV system enhances conformational sampling. 2) Multiple coarse-grained models can be introduced to guide the system to move to multiple structures. 3) Applications to larger system are expected to be relatively easy. The proposed methods are expected to be applied to the further computational studies of biological phenomena including large conformational change, such as allosteric transition.

## References

- [1] Y. Yamamori and A. Kitao, *J. Chem. Phys.*, **139**, 145105(2014).

# Data Analyses and Visualization of Bubbles

Hiroshi WATANABE

*Institute for Solid State Physics, University of Tokyo  
Kashiwa-no-ha, Kashiwa, Chiba 277-8581*

A rapid increase in computational power allows us to simulate huge scale systems. However, as the size of simulation increases, the amount of data also increases and becomes quite huge which is difficult to process for further analysis. Therefore, some device is required to process such huge data. Visualization of data is also important. Appropriate visualization not only allows us to understand physical phenomena in an intuitive way, but may serve as a trigger of new discoveries. However, there is no general guide of visualization and we have to appropriate method according to problems. In this manuscript, we report on some devices to process huge data and their visualization.

We perform molecular dynamics simulations of multi-bubble nuclei involving up to 730 million particles on K-computer. If we store all data of position of particles, it requires 17GB per frame. Since one run involves about 1000 frames, the total amount of data could be 17TB per run, which is not impossible but unrealistic. Therefore, some kinds of compression are compression to store data for further analysis. While it is preferable to reduce the total amount of data, the important information should not be lost. We therefore divide the system into small subcells and count the number of particles in each subcell and store it as an integer (data type `unsigned char` in C language) instead of storing the local density with floating-point variables. The size of the subcells are determined so that the number of particles will not exceed 255, which is the maximum value of `unsigned char`. The num-

ber of subcells of the largest run is 32768000, *i.e.*, 32.7MB per frame. Therefore, we have succeeded to compress the data by 500 times. Additionally, we do not have to care about the byte order, since we use `unsigned char` which is free from the byte-order problem.



The picture is a visualization of bubbles using our data format. We define a subcell to be in the *gas state* when its density is less than some threshold, and identify the bubbles using the site-percolation criterion on the simple cubic lattice [1]. After identifying bubbles, we compute a center of inertia and volume of each bubble and draw bubble as sphere. From the information of the spheres, the image is produced by POV-Ray [2]

## References

- [1] H. Watanabe, M. Suzuki, and N. Ito: *Comput. Phys. Commun.* **184** (2013) 2775.
- [2] (<http://www.povray.org>)

# Theoretical Study on Magnetic Refrigeration using Ising Model

Ryo TAMURA

*International Center for Young Scientists, National Institute for Materials Science  
1-2-1, Sengen, Tsukuba-city, Ibaraki, 305-0047*

Magnetic refrigeration is a cooling technology which has attracted attention in energy science as an alternative to gas refrigeration. Magnetic refrigeration uses magnetocaloric effect which is a cross correlated phenomenon between the heat and the magnetic degree of freedom. In most experimental studies, magnetic refrigeration efficiency was estimated by the entropy change when the magnetic field is changed from 0 to finite  $H$  in isothermal process. Magnetic materials with large entropy change are regarded as a good material since these absorb large amount of heat. From this point, ferromagnets near the Curie temperature is a good magnetic refrigeration material. Experimental studies on magnetic refrigeration have been aggressively done throughout the world.

Our purpose is to propose a method that utilizes the underlying magnetic refrigeration effect in magnetic materials including nonferromagnets. We considered the Ising model on a cubic lattice:

$$\mathcal{H} = -J_{ab} \sum_{\langle i,j \rangle_{ab}} s_i s_j - J_c \sum_{\langle i,j \rangle_c} s_i s_j - H \sum_i s_i,$$

$$s_i = \pm \frac{1}{2},$$

where the first and second terms represent nearest-neighbor interactions on  $ab$ -plane and along  $c$ -axis, respectively, and the third term denotes the Zeeman term.

We considered four types of signs of interactions: (a)  $J_{ab} > 0, J_c > 0$ ; (b)  $J_{ab} < 0, J_c > 0$ ; (c)  $J_{ab} > 0, J_c < 0$ ; (d)  $J_{ab} < 0, J_c < 0$ . The

ground states of each case are (a) Ferromagnetic state (the corresponding wave vector is  $(000)$ ), (b) A-type antiferromagnetic state (the corresponding wave vector is  $(\pi\pi 0)$ ), (c) C-type antiferromagnetic state (the corresponding wave vector is  $(00\pi)$ ), and (d) G-type antiferromagnetic state (the corresponding wave vector is  $(\pi\pi\pi)$ ). We calculated the magnetic entropy as a function of temperature and magnetic field of this model whose linear dimension is up to  $L = 16$  using the Wang-Landau method[2]. The Wang-Landau method can directly calculate the density of states and the absolute value of magnetic entropy without integrating the specific heat. In ferromagnetic phase and paramagnetic phase, the magnetic entropy decreases as the magnetic field increases at fixed temperature. However, the magnetic entropy as a function of magnetic field at fixed temperature  $T$  has a peak at finite magnetic field  $H_{\max}(T)$  in antiferromagnetic phases. From the obtained results, we proposed a new protocol to obtain the maximum magnetic refrigeration efficiency in the isothermal process: *The magnetic field should be changed from  $H_{\max}(T)$  to  $H$ .* This method can be applied not only antiferromagnets but also general types of magnetic materials. Furthermore, the proposed protocol is the same as the conventional one for ferromagnets and paramagnets.

This work was done in collaboration with Takahisa Ohno (NIMS) and Hideaki Kitazawa (NIMS).

## References

- [1] R. Tamura, T. Ohno, and H. Kitazawa:  
Appl. Phys. Lett. **104** (2014) 052415.  
[This topic was reported in Press  
Release in NIMS (March 10, 2014),  
MyNavi News (March 12, 2014),  
The Chemical Daily (March 19,  
2014), The Science News (March 28,  
2014).]
  
- [2] F. Wang and D. P. Landau: Phys. Rev.  
Lett. **86** (2001) 2050.

# Investigation of Phase Transitions and Their Microscopic Mechanisms in Frustrated Spin Systems

Ryo TAMURA

*International Center for Young Scientists, National Institute for Materials Science  
1-2-1, Sengen, Tsukuba-city, Ibaraki, 305-0047*

Geometrically frustrated spin systems often exhibit unconventional phase transitions and dynamic behaviors, which are not observed in unfrustrated spin systems. We investigated phase transition nature in two geometrically frustrated spin systems[1, 2].

– **Simultaneous occurrence of  $Z_2$  vortex dissociation and second-order phase transition**[1]

We considered the Heisenberg model with the nearest-neighbor and the third nearest-neighbor interactions on a distorted triangular lattice. We focused on the case that the order parameter space is described by  $SO(3) \times Z_2$ .  $SO(3)$  and  $Z_2$  correspond to global rotation symmetry of spins and lattice rotation symmetry, respectively. The long-range order of spins at finite temperatures is prohibited by the Mermin-Wagner theorem[3]. Instead, the  $Z_2$  vortex dissociation related to  $SO(3)$  symmetry occurs at finite temperature, which was first pointed out by Kawamura and Miyashita[4]. We considered finite-temperature properties of the model using Monte Carlo simulations. A second-order phase transition with  $Z_2$  symmetry breaking was observed. In addition, it was found that  $Z_2$  vortex dissociation occurs at the second-order phase transition point. By the finite-size scaling, we concluded that the second-order phase transition belongs to the two-dimensional Ising universality class, which suggests that the  $Z_2$  vortex dissociation does not affect the critical phenomena. To our knowledge, this is the first example to exhibit

$Z_2$  vortex dissociation at the critical point.

This work was done collaboration with Shu Tanaka (The University of Tokyo, Kyoto University) and Naoki Kawashima (Institute for Solid State Physics, The University of Tokyo).

– **Strange behavior of latent heat in a geometrically frustrated spin system**[2]

We studied phase transition behavior of the Heisenberg model with the nearest-neighbor and the third nearest-neighbor interactions on a stacked triangular lattice. This is three-dimensional version of the studies in Refs.[5, 6, 7]. We focused on the case that the order parameter space is represented by  $SO(3) \times C_3$ .  $SO(3)$  and  $C_3$  correspond to global rotation symmetry of spins and lattice rotation symmetry, respectively, which is similar with two-dimensional case as described before. Temperature dependence of each order parameter was obtained by Monte Carlo simulations, which indicates that the first-order phase transition with  $SO(3) \times C_3$  symmetry breaking occurs at finite temperature. We also considered inter-layer interaction dependence of transition temperature and latent heat. As the interlayer interaction increases, the transition temperature increases but the latent heat decreases. The latter behavior is not observed in usual unfrustrated spin systems such as the ferromagnetic Potts model.

This work was done collaboration with Shu Tanaka (The University of Tokyo, Kyoto University).

## References

- [1] R. Tamura, S. Tanaka, and N. Kawashima: Phys. Rev. B **87** (2013) 214401. [**Selected as Physical Review B Kaleidoscope**]
- [2] R. Tamura and S. Tanaka: Phys. Rev. E **88** (2013) 052138.
- [3] N. D. Mermin and H. Wagner: Phys. Rev. Lett. **17** (1966) 1133.
- [4] H. Kawamura and S. Miyashita: J. Phys. Soc. Jpn. **53** (1984) 9, *ibid.* **53** (1984) 4138.
- [5] R. Tamura and N. Kawashima: J. Phys. Soc. Jpn. **77** (2008) 103002.
- [6] R. Tamura and N. Kawashima: J. Phys. Soc. Jpn. **80** (2011) 074008.
- [7] R. Tamura, S. Tanaka, and N. Kawashima: JPS Conf. Proc. **1** (2014) 012125.

## Multiscale Simulation for Soft Matter: Sol-Gel Transition in Wormlike Micellar Solution during Flow

Takahiro Murashima

*Department of Physics, Tohoku University,  
Aramaki-Aza-Aoba, Aoba-Ward, Sendai, Miyagi 980-8578*

Surfactant is an important material for our daily life. Surfactants spontaneously aggregate in a solvent because it consists of a hydrophilic head group and a hydrophobic tail group and shows a variety of complex structure: sphere, cylinder, lamellar, cubic and sponge structures. Self-assembled surfactants in a solvent make a curved membrane with a hydrophilic and hydrophobic layer. According to the concentration of surfactants, the size of the membrane changes, and the structure of micelle is selected in order to minimize the elastic curvature energy. A particle-field hybrid method implementing the kinetic Monte-Carlo method taking account of the Helfrich's bending energy of a membrane with Langevin thermostat [1] has succeeded in describing the sol-gel phase diagram of dilute micellar solution in equilibrium and a shear-induced instability which is found as a negative slope in shear stress. This instability comes from the breakup process of micellar branches and will lead to shear banding [1]. However, it is tough to simulate a macroscopic flow behavior such as shear banding in a particle-field hybrid method because a quite large number of

degrees of freedom are needed to simulate a fluid dynamic behavior.

We have developed multi-scale simulation technique bridging the macroscopic fluid dynamics and microscopic (mesoscopic) molecular dynamics to simulate a fluid dynamic behavior of entangled polymer melt [2, 3]. Applying this method to the particle-field hybrid method, we can simulate a fluid dynamic behavior of the micellar solution [4, 5]. In the multi-scale simulation, the microscopic simulator is used as a constitutive equation in general fluid dynamic simulation. Applying a shear to the microscopic simulator, the stress tensor is obtained according to the structure of micelles. The updated stress tensor drives the flow to balance the stress tensors among the fluid elements. The multi-scale simulation alternately updates macroscopic flow field and microscopic micellar structure.

We have investigated a channel flow of the micellar solution. The macroscopic fluid system is divided into  $N_e$  fluid elements and each fluid element has  $N_s$  simulators. The total number of the microscopic simulators in this system is  $N_t = N_e \times N_s$ . When the number of

CPUs is equal to  $Nt$  or the integral multiple of  $Nt$ , the multi-scale simulation is most efficient. On System B (SGI Altix ICE 8400EX) with 1024 cores, the weak scaling parallel efficiency of our multi-scale simulation is almost 100 % as shown in Fig 1 because the microscopic simulators are independent of the others during a time-interval of a fluid dynamic simulation and the time of communication is negligibly small in a total computation time.

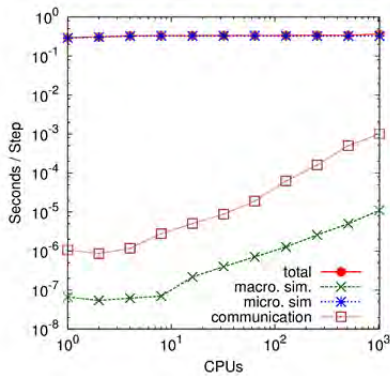


Fig:1 Weak scaling parallel efficiency

To decrease the noise coming from the low number of static samples (the number of molecules in a simulation box), we need more than 100 simulation box per one fluid element. To resolve the macroscopic fluid dynamics in a channel, we need to divide a channel into more than 20 fluid elements. Thus, we select  $Ne = 24$  and  $Ns = 128$ , namely  $Nt = 3,072$ . Each simulation box has 3,000 particles which represent spherical micelles and then each fluid element is described by using 384,000 particles. On System B with 1024 cores, this simulation takes 0.75 sec per unit time interval. The noise in stress tensor is sufficiently small and we can

investigate the time evolution of the multiscale simulation of micellar solution. Initial condition of the micellar solution is sol state where the spherical micelles are randomly distributed. The micelles spontaneously aggregate and make wormlike micelles during a flow in a channel. The growth of wormlike micelles results in a gel state. This situation mimics a real process where micellar solution starts to flow immediately after surfactants are put into water. Even if we apply high pressure difference between upstream and downstream, this initial transition from sol to gel is observed. The velocity gradient increases near the wall. The state of micellar solution near the wall changes from gel to sol under the high velocity gradient field. The sol region develops from the vicinity of the wall to the bulk. The transition from gel to sol in the vicinity of the wall is clearly observed as increasing the pressure difference between upstream and downstream.

## References

- [1] M. Toda, T. Kawakatsu, AIP Conf. Proc. **1518**, (2013) 419-423.
- [2] T. Murashima, T. Taniguchi, EPL, **96** (2011) 18002.
- [3] T. Murashima, S. Yasuda, T. Taniguchi, R. Yamamoto, JPSJ, **82** (2013) 012001.
- [4] T. Murashima, M. Toda, T. Kawakatsu, AIP Conf. Proc. **1518**, (2013) 436-439.
- [5] T. Murashima, M. Toda, T. Kawakatsu, NIC Series, **46** (2013) 187-192.

# Numerical Study of Coulomb Glass

Takamichi TERAO

*Department of Electrical, Electronic and Computer Engineering,  
Gifu University, Yanagido 1-1, Gifu 501-1193*

Electronic states in Coulomb glass, in which the disorder and many-body electron-electron interaction are incorporated, have been extensively studied during the last few decades. The properties of compensated doped semiconductors, ultrathin films, and granular metals are well described by these Coulomb-glass models. Most of the past numerical studies have been devoted to examining the properties of Coulomb glasses in equilibrium, and they have shown the existence of a Coulomb gap at the Fermi level. Recent experiments have demonstrated the non-equilibrium nature of Coulomb glasses, such as logarithmic relation, aging, and memory effects below some critical temperature.

In this study, kinetic Monte Carlo simulations of disordered thin films, in which strongly interacting electrons hopping between randomly distributed sites that correspond to the localization centers of the single-electron wave functions, have been performed [1,2]. At first, the two-time autocorrelation function  $C(t, t_w)$  has been calculated to clarify the non-equilibrium nature of interacting electrons in disordered thin films. The waiting time  $t_w$  is the time elapsed since the quenching from an infinite temperature. The function  $C(t, t_w)$  is the overlap of the charge configurations at times  $t + t_w$  and  $t_w$ . We have confirmed aging phenomena in the autocorrelation function

$C(t, t_w)$  (Figure 1).

In addition, the temperature dependence of the mean square displacement (MSD) of electrons has been investigated to clarify the microscopic dynamics of electrons, and a crossover from diffusive to subdiffusive behavior has been observed. These results imply that there is a characteristic temperature  $T_c$  in this system, and the dynamical behavior such as the relaxation and diffusive motion of electrons changes at  $T \approx T_c$ , which reflects the glassy behavior of this system with lower temperature regime.

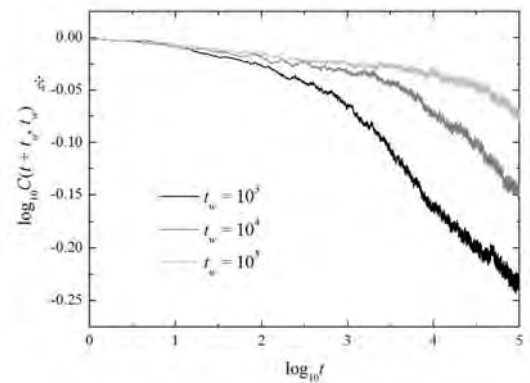


Fig. 1: Two-time autocorrelation function

$$C(t, t_w)$$

## References

- [1] T. Terao, A. Kono, and W. Takahashi: AIP conference proceedings **1518**, (2013) 320.
- [2] T. Terao: Philos. Mag. **89**, (2009) 405.

# Physical properties of low-dimensional electron systems created on solid surfaces and their control

Takeshi INAOKA

*Department of Physics and Earth Sciences, Faculty of Science,  
University of the Ryukyus, 1 Senbaru, Nishihara, Okinawa 903-0213*

This academic year, we investigated collective excitations of two-dimensional electron systems with ultralow density and the strain effect on the band structure of bulk silicon (Si) and germanium (Ge). The latter investigation of the strain effect forms a basis to understand the strain effect on subbands formed at surfaces or interfaces.

## (1) Exchange-correlation and temperature effects on plasmons in strongly-correlated two-dimensional electron systems [1]

In two-dimensional (2D) electron systems with ultralow density, electrons are strongly correlated, which has striking exchange-correlation (XC) effects on the 2D plasmons (PLs) in these systems. By means of the finite-temperature local-field correction, we examined the 2DPLs in a density-parameter range of  $9.1 \leq r_s \leq 21.8$  and a temperature range of  $0.5 \leq T/T_F \leq 8.4$  (normalized by Fermi temperature  $T_F$ ). We analyzed the PL dispersions that were observed from single quantum wells by Raman spectroscopy. With increasing wave number  $q$ , the XC effects start to operate to lower the PL energy strikingly. This operation is more remarkable at lower electron densities. Even in our strongly correlated and extremely nondegenerate 2D electron systems, the size of the XC holes can be well normalized by inverse Fermi wave number  $k_F^{-1}$ . From comparison with the experiment, the finite-temperature local-field correction (Singwi-Tosi-Land-Sjölander approximation) is expected to describe the PLs quantitatively in a smaller  $q$  range of  $q \lesssim k_F$ , but in a larger  $q$  range of  $q \gtrsim k_F$ , this correction begins to overestimate

the XC effect. With an increase in temperature, the PL dispersion curve goes up strikingly in a larger  $q$  range. This remarkable  $T$  dependence can be ascribed largely to the  $T$  dependence of the constituent electronic transitions of the PLs through the Fermi-Dirac distribution function. We performed the above calculation on the system A.

## (2) Internal-strain effect on the valence band of strained Si [2]

Now that performance enhancement of Si devices due to downsizing begins to show its limitations, one promising solution is to change the band structure by applying strain in order to realize higher mobility. By means of the local density-functional method including the spin-orbit interaction, we examined the effect of internal strain, namely, relative atom displacement of two atoms in the crystal unit cell on the valence band of strained Si. We analyzed the [111] ([110]) band dispersion for [111] ([110]) uniaxial compression and (111) ((110)) biaxial tensility, because the hole effective mass  $m^*$  becomes conspicuously small in the [111] ([110]) direction for these strain types [3]. Under the practical condition of no normal stress, uniaxial compression (biaxial tensility) entails additional normal tensility (compression) and internal strain. We achieved the total-energy minimum with a change in both normal and internal strain. The above uniaxial compression or biaxial tensility lifts degeneracy of the upper two valence bands at the  $\Gamma$  point, and the band with a conspicuously small  $m^*$  value projects above the other two around the  $\Gamma$  point. With increasing internal strain, the energy separation between the

highest and second-highest bands,  $E_1 - E_2$ , becomes dramatically larger, and the band with the effective-mass ratio  $m^*/m_e = 0.10 - 0.11$  extends remarkably down to a lower energy region, until it crosses or gets admixed with the second-highest band. This holds true to all the strain types and strain orientations considered here. We found that this band variation due to internal strain is strongly correlated with the change in the specific bond angles in the tetrahedral unit cell. Some angles are closely related to the highest valence band which includes stronger coupling in the [111] or [110] direction, namely, which has stronger dispersion in this direction, while other angles are strongly correlated with the second-highest valence band which involves stronger coupling in the (111) or (110) plane, namely, which has weaker dispersion in the [111] or [110] direction. The change in these two types of bond angles due to internal strain can reasonably explain the conspicuous growth in  $E_1 - E_2$ . Details are given in [2]. To do the above calculation, we used the program package 'ABINIT' [4,5] on the system B.

### (3) Indirect-to-direct band gap transition of Ge induced by tensile strain [6]

Tensile strain is reported to induce an indirect-to-direct band gap transition of Ge where the conduction-band bottom shifts from the L point to the  $\Gamma$  point. This transition producing the direct gap enhances photoabsorption intensity in a lower energy region, and this strained Ge becomes a good candidate for solar-cell materials. According to first-principles calculations, uniaxial tensility in the [111] direction induces the transition at 4.2% strain [7], and biaxial tensility in the (001) plane does at 2.0% strain [8]. In [8], they evaluated the decreasing rate of the Land  $\Gamma$ -point energies with small strain coefficient for uniaxial and biaxial tensility with various orientations, predicted that biaxial tensility in the (001) plane induces the transition at the smallest strain, and estimated the critical strain as 2.0% for this strain type. These two studies take no account of internal strain. We employed a hybrid density-functional method (HSE06) where

exchange terms due to the Hartree-Fock approximation are incorporated into those in the local density approximation (LDA) and which remarkably improves underestimation of the band gap in the LDA. Taking the internal strain into consideration, we analyzed the transition for uniaxial and biaxial tensility with various orientations. According to our evaluation for room temperature, uniaxial tensility in the [001] and [111] directions gives rise to the transition at 4.2% and 3.7% strain, respectively. Biaxial tensility in the (001) and (110) planes causes the transition at 1.5% and 2.3% strain, respectively. No transition occurs for uniaxial tensility in the [110] direction and biaxial tensility in the (111) plane. Corresponding to [8], biaxial tensility in the (001) plane induces the transition at the smallest strain, though our critical strain coefficient is somewhat smaller than that in [8]. To carry out the above calculation, we used the program package 'Vienna Ab initio Simulation Package' (VASP) [9,10] on the system B.

## References

- [1] T. Inaoka, Y. Sugiyama, and K. Sato: Phys. Status Solidi B (2014) published online, Doi: 10.1002/pssb.201350147. (11 pages).
- [2] T. Inaoka, S. Yanagisawa, and Y. Kadekawa: J. Appl. Phys. **115** (2014) 063702 (14 pages).
- [3] T. Inaoka, Y. Kinjyo, S. Yanagisawa, and K. Tomori: J. Appl. Phys. **113** (2013) 183718 (13 pages).
- [4] X. Gonze et al., Z. Kristallogr. **220** (2005) 558-562.
- [5] X. Gonze et al., Comput. Phys. Commun. **180** (2009) 2582-2615.
- [6] T. Inaoka, T. Furukawa, R. Toma, and S. Yanagisawa: in preparation.
- [7] F. Zhang, V. H. Crespi, and P. Zhang, Phys. Rev. Lett. **102** (2009) 156401 (4 pages).
- [8] Y. Hoshina, K. Iwasaki, A. Yamada, and M. Konagai: Jpn. J. Appl. Phys. **48** (2009) 04C125 (6 pages).
- [9] G. Kresse and J. Hafner. Phys. Rev. B **47** (1993) 558-561.
- [10] G. Kresse and J. Furthmüller. Comput. Mat. Sci. **6** (1996) 15-50.

# Ground-State Phase Diagram of a Spin-1/2 Anisotropic Rung-Alternating Ladder

Takashi Tonegawa

*Professor Emeritus, Kobe University*

With the help of some physical considerations, we [1] have numerically investigated the ground-state phase diagram of a spin-1/2 anisotropic rung-alternating ladder, which is described by the Hamiltonian,

$$\begin{aligned} \mathcal{H} = & J_1 \sum_{l=1}^L \{ \vec{S}_{l,a} \cdot \vec{S}_{l+1,a} + \vec{S}_{l,b} \cdot \vec{S}_{l+1,b} \} \\ & + J_r \sum_{l=1}^{L/2} [ \vec{S}_{2l-1,a}, \vec{S}_{2l-1,b} ]_{\delta} \\ & + J'_r \sum_{l=1}^{L/2} [ \vec{S}_{2l,a}, \vec{S}_{2l,b} ]_{\delta} \end{aligned} \quad (1)$$

with

$$\begin{aligned} [ \vec{S}_{l,a}, \vec{S}_{l,b} ]_{\delta} \\ \equiv \delta_r^{xy} (S_{l,a}^x S_{l,b}^x + S_{l,a}^y S_{l,b}^y) + \delta_r^z S_{l,a}^z S_{l,b}^z. \end{aligned} \quad (2)$$

Here,  $\vec{S}_{l,\lambda}$  ( $\lambda = a$  or  $b$ ) is the spin-1/2 operator at the  $l$ -th site of the  $\lambda$  leg;  $L$  is the number of spins in each leg, being assumed to be even;  $J_1$  is the magnitude of the isotropic leg interaction;  $J_r$  and  $J'_r$  are those of the two kinds of anisotropic rung interactions which are alternating;  $\delta_r^{xy}$  and  $\delta_r^z$  are the  $XXZ$ -type anisotropy parameters of the rung interactions. This system has a frustration when  $J_r J'_r < 0$  irrespective of the sign of  $J_1$ . In Fig.1 the present spin-1/2 rung-alternating ladder is schematically sketched. For simplicity, we study in this report only the case where  $J_1 = 0.2$ ,  $J_r = -1$  and  $|J'_r| \leq 1$ . As regards the anisotropy of the rung interactions, however, we treat both the case where it is of the Ising-type ( $\delta_r^z = 1$  and  $0 \leq \delta_r^{x,y} \leq 1$ ) and the case where it is of the  $XY$ -type ( $\delta_r^{x,y} = 1$  and  $0 \leq \delta_r^z \leq 1$ ).

When  $J'_r = -1$ , by performing the degenerate perturbation calculations, we can map the present spin-1/2 ladder onto the one-dimensional spin-1 chain governed by the effective Hamiltonian,

$$\mathcal{H}_{\text{eff},1} = \frac{J_1}{2} \left\{ \sum_{l=1}^L \vec{T}_l \cdot \vec{T}_{l+1} + D \sum_{l=1}^L (T_l^z)^2 \right\} \quad (3)$$

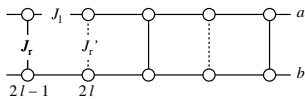


Figure 1: Sketch of the present spin-1/2 rung-alternating ladder.

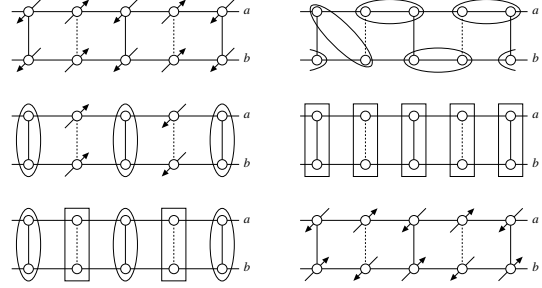


Figure 2: Schematic representations of various phases appearing in the ground-state phase diagrams of the present spin-1/2 rung-alternating ladder; the antiferromagnetic stripe Néel (top left), Haldane (top right), 'ferromagnetic'-singlet dimer' (central left), triplet dimer (central right), 'triplet dimer'-singlet dimer' (bottom left) and Néel (bottom right) phases. Ellipses show the singlet dimer pairs and rectangles the triplet dimer pairs.

with

$$D = (\delta_r^{xy} - \delta_r^z) / J_1, \quad (4)$$

where  $\vec{T}_l$  is the pseudo  $S=1$  operator at the  $l$ -th site. Chen *et al.* [2] have already determined the ground-state phase diagram of this spin-1 chain, and showed that as the value of  $D$  increases, the phase transition from the Néel phase to the Haldane phase takes place at  $D \sim -0.4$  and that from the Haldane phase to the large- $D$  phase at  $D \sim 1.0$ . From these results, we may conclude that in our spin-1/2 ladder with  $J'_r = -1$ , the phase transition from the antiferromagnetic stripe Néel (ASN) phase (see the top left of Fig.2) to the Haldane phase (the top right of Fig.2) occurs at  $\delta_r^{xy} \sim 0.9$  when  $\delta_r^z = 1$  and that from the Haldane to the triplet dimer (TD) phase (the central right of Fig.2) at  $\delta_r^z \sim 0.8$  when  $\delta_r^{x,y} = 1$ . It is noted that the Néel and large- $D$  phases in the spin-1 chain correspond, respectively, to the ASN and TD phases in the spin-1/2 rung-alternating ladder.

When  $J'_r = 1$ , on the other hand, it is naturally expected that a pair of  $S=1/2$  spins at the  $(2l)$ -th site of the  $a$  and  $b$  legs is in the singlet dimer state  $\frac{1}{\sqrt{2}}(|\uparrow_a \downarrow_b\rangle - |\downarrow_a \uparrow_b\rangle)$ , while a pair of  $S=1/2$

spins at the  $(2l-1)$ -th site of the  $a$  and  $b$  legs is in one of the ferromagnetic states  $|\uparrow_a \uparrow_b\rangle$  and  $|\downarrow_a \downarrow_b\rangle$  or in the triplet dimer state  $\frac{1}{\sqrt{2}}(|\uparrow_a \downarrow_b\rangle + |\downarrow_a \uparrow_b\rangle)$  depending upon whether the anisotropy of the rung interactions is of the Ising-type or of the  $XY$  type. We have carried out a third-order perturbation calculation to obtain the effective interaction between two ferromagnetic states in a neighboring pair of spins at the  $(2l-1)$ -th and  $(2l+1)$ -th sites; the result shows that it is antiferromagnetic when  $J_1 > 0$ . Thus, the ground state in the case of Ising-type rung interactions is the ‘ferromagnetic’-‘singlet dimer’ (F-SD) state (the central left of Fig.2), and that in the case of  $XY$ -type rung interactions is the ‘triplet dimer’-‘singlet dimer’ (TD-SD) state (the bottom left of Fig.2).

We show in Fig.3 our results for the ground-phase diagrams; the left one is that on the  $\delta_r^{xy}$ - $J_r'$  plane in the case of Ising-type rung interactions where  $\delta_r^z = 1$ , and the right one is that on the  $\delta_r^z$ - $J_r'$  plane in the case of  $XY$ -type rung interactions where  $\delta_r^{xy} = 1$ . We first discuss the former phase diagram. By examining the  $J_r'$ -dependence of the finite- $L$  (up to  $L=14$ ) excitation spin gap within the  $M=0$  subspace,  $M$  being the total magnetization, calculated by the exact diagonalization (ED) method for a given value of  $\delta_r^{xy}$  as well as the  $l$ -dependence of the finite- $L$  site magnetization  $m_{l,\lambda}(L)$  (up to  $L=192$ ), calculated by the density-matrix renormalization-group (DMRG) method [3] for a given set of  $J_r'$  and  $\delta_r^{xy}$ , we have reached the conclusion that the Haldane phase appears in the frustrated region where  $0 < J_r' < 1$ . The appearance of the Haldane phase in the case of Ising-type interactions is contrary to the ordinary situation [2], and this is called the inversion phenomenon concerning the interaction anisotropy [4]. Examining the Fourier transform of  $m_{l,\lambda}(L)$ , we have also shown that the incommensurate state becomes the ground state within the region of the Haldane phase. The solid lines are the second-order (2D Ising) phase boundary lines, which is determined by the phenomenological renormalization group analysis [5]. The dotted lines separate the commensurate and incommensurate regions; the region between these lines is the incommensurate one.

Let us move to the discussions on the latter phase diagram. Similarly to the above case, we have confirmed that the Néel phase (the bottom right of Fig.2) appears in the frustrated region. The appearance of the Néel phase in the case of  $XY$ -type interactions is also the inversion phenomenon concerning the interaction anisotropy [4]. The results of our DMRG calculations show that jump anomalies from zero to a finite value occur in the  $m_{l,\lambda}(L)$  versus  $J_r'$  curve for a given value of  $\delta_r^{xy}$ . From

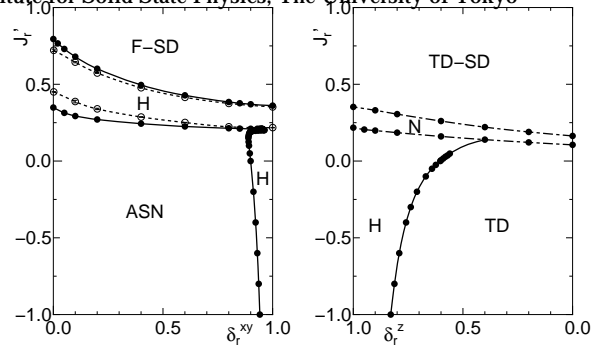


Figure 3: Ground-state phase diagram in the case of Ising-type rung interactions (left) and that in the case of  $XY$ -type rung interactions (right). In the left phase diagram, the ‘ferromagnetic’-‘singlet dimer’ (F-SD), Haldane (H) and antiferromagnetic stripe Néel (ASN) phases appear. In the right phase diagram, the ‘triplet dimer’-‘singlet dimer’ (TD-SD), Néel (N), Haldane (H) and triplet dimer (TD) phases appear. See the text for more details.

these results, we may conclude that the phase transition between the Néel phase and one of the other three phases are of the first-order, although, strictly speaking, it is difficult to come to a right and final conclusion from the finite-size calculations. The dot-dashed lines are the first-order phase boundary lines. On the other hand, the solid line is the second-order (Gaussian) phase boundary line; this line is determined by Kitazawa’s level spectroscopy analysis [6], which has very recently been modified to some extent [1,7].

This work has been done in collaboration with K. Okamoto, T. Hikihara, T. Sakai, J. Morishige and K. Nomura. Performing the ED calculations, we have used the fortran program package KOBEPACK [8], which is very well vectorized for the NEC SX-9 system.

- [1] T. Tonegawa, K. Okamoto, T. Hikihara, T. Sakai, J. Morishige and K. Nomura: in preparation.
- [2] W. Chen, K. Hida and B. C. Sanctuary: Phys. Rev. B **67** (2003) 104401.
- [3] S. R. White: Phys. Rev. Lett. **69** (1992) 2863.
- [4] K. Okamoto and Y. Ichikawa: J. Phys. Chem. Solids **63** (2002) 1575.
- [5] M. P. Nightingale: Physica A **83** 561 (1976).
- [6] A. Kitazawa: J. Phys. A **30** (1997) L285.
- [7] K. Nomura, J. Morishige, T. Tonegawa, K. Okamoto, T. Hikihara, T. Sakai: in preparation.
- [8] M. Kaburagi, T. Tonegawa and T. Nishino: *Computational Approaches in Condensed Matter Physics*, Springer Proc. Phys., ed. S. Miyashita, M. Imada and T. Takayama (Springer, Berlin, 1992) p.179.

# Phonon Effects and Frustration in Quantum Spin Systems

Chitoshi YASUDA

*Department of Physics and Earth Sciences, Faculty of Science, University of the Ryukyus, Nishihara, Okinawa 903-0213, Japan*

In frustrated quantum spin systems with competing interactions (frustration systems), novel spin states are often formed due to the strong quantum effects and have attracted considerable attention. In this project, we derived effective Hamiltonians of coupled systems of spins and phonons (phonon systems) by performing a unitary transformation [1]. Since the effective Hamiltonians describe the frustrated quantum spin systems, we can investigate relations between the phonon and frustration systems. For one-dimensional quantum Heisenberg-like models with a spin-phonon interaction, we consider a next-nearest-neighbor spin interaction in addition to a nearest-neighbor interaction and a spin-phonon interaction with a parameter to control a change of a geometric structure. In order to perform a unitary transformation for phonon systems, we use the computational software program ‘Mathematica’ and also check the results by hand calculation whenever it is possible. The effective Hamiltonian we obtained is expanded by the strength of the spin interaction  $J$  and that of the spin-phonon interaction  $g$  and can be theoretically derived for all order of the series expansion. If the order becomes large, the source memory we need becomes large. In the present work, we derived the effective Hamiltonian of fourth order in  $g$  and investigate the properties. The Hamiltonian consists of spin interactions up to fifth-nearest-neighbor and four-body interactions. The eigen values of the effective Hamil-

tonian are calculated by the exact diagonalization in the  $\sum_i S_i^z = 0$  and  $k = \pi$  subspace and the Berezinskii-Kosterlitz-Thouless-type phase transition points are evaluated by level-spectroscopy analysis. The agreement between results of system-size  $N = 12$  and 16 suggests that the size dependence is negligible. Furthermore, the results for small  $J$  agree with phase transition points estimated by using  $J_2/J_1 = \alpha$ , where  $J_1$  and  $J_2$  are the strengths of the nearest- and next-nearest-neighbor interactions of the effective Hamiltonian and  $\alpha_c$  is the phase transition point of the  $J_1$ - $J_2$  model. Thus, this phase transition is driven between the spin-liquid and spin-gapped phases. We can control the ground state for  $g = 0$  by changing the strength of the next-nearest-neighbor spin interaction. In the system where the ground state is in the spin-liquid phase for  $g = 0$ , the spin-phonon interaction causes the usual phase transition to the spin-gapped phase. In the system where the ground state is in the spin-gapped phase for  $g = 0$ , on the other hand, the spin-phonon interaction causes the novel phase transition to the spin-liquid phase for some geometric structures. This work is done in collaboration with Satoru Akiyama (Wakayama National College of Technology).

## References

- [1] S. Akiyama and C. Yasuda: J. Phys. Soc. Jpn. **80** (2011) 104709.

# Characterization of thermal transport at nanostructure interface

Junichiro SHIOMI

*Department of Mechanical Engineering,*

*The University of Tokyo, 7-3-1, Hongo, Bunkyo-ku, Tokyo, 113-8656*

Since interfacial thermal transport determines heat exchange, dissipation, thermoelectric efficiency and so on, it is a key property for the development of thermal management. Recently the non-equilibrium Green's function (NEGF) method with non-empirical force fields[1] has been applied to the silicon-germanium solid-solid interface, and microscopic and quantitative calculations of interfacial phonon transport were reported[2]. Although NEGF tells us the mode-dependent interfacial phonon transport, it cannot cover the effect of inelastic scattering process on thermal boundary conductance ( $G_{TBC}$ ) since it is based on harmonic theory. For the comprehensive understanding and quantitative evaluation of the interfacial thermal transport in terms of phonons, the contribution of the inelastic scattering process to  $G_{TBC}$  needs be investigated.

In this work, considering the lead-telluride and lead-sulfide (PbTe-PbS) system exhibiting high thermoelectric efficiency, we calculated the phonon transmission function[3] by means of equilibrium molecular dynamics (EMD) simulation with a non-empirical force field[4].

Figure 1 shows the frequency dependence of the calculated phonon transmission function,  $\Theta(\omega)$ , at the PbTe-PbS interface and 300 K. Contributions of phonons below the cutoff frequency of PbTe ( $\omega=3.45$  THz) to  $G_{TBC}$  are dominant, whereas it can be seen that phonons ( $\omega>3.45$  THz) also contribute to  $G_{TBC}$ . Note that the latter contribution is caused by inelastic scattering at the interface and is not included in the NEGF calculation.

$G_{TBC}$  can be calculated by simply integrating  $\Theta(\omega)$  over frequency space. The calculated  $G_{TBC}$  is  $0.34 \text{ GWm}^{-2}\text{K}^{-1}$ , which is in excellent agreement with the result of non-equilibrium MD simulation that we also

performed ( $0.33 \text{ GWm}^{-2}\text{K}^{-1}$ ). As shown in Fig.1, the inelastic contribution to  $G_{TBC}$  is around 10% and is not negligible.

To summarize, we calculated the phonon transmission function at PbTe-PbS solid-solid interface by performing EMD simulations. Phonons with a frequency above the cutoff frequency of PbTe transport across the interface and contribute to the  $G_{TBC}$  through inelastic scattering at the interface. We found that the inelastic contribution to  $G_{TBC}$  is around 10%, and thus cannot be neglected in the calculation of  $G_{TBC}$ .

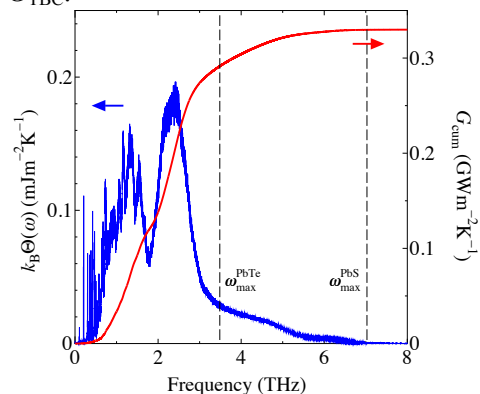


Fig. 1 Frequency dependence of phonon transmission function,  $\Theta(\omega)$ , at PbTe-PbS interface at 300 K. Vertical lines denote the maximum frequencies of PbTe and PbS crystals (3.45 and 7.06 THz), respectively. The solid line is the cumulative of  $k_B\Theta(\omega)$ .

## References

- [1] W. Zhang, T. S. Fisher, and N. Mingo, *Numerical Heat Transfer*, **51**, 333 (2007).
- [2] Z. Tian, K. Esfarjani, and G. Chen, *Phys. Rev. B* **86**, 235304 (2012).
- [3] Y. Chalopin, and S. Volz, *Appl. Phys. Lett.* **103**, 051602 (2013).
- [4] T. Murakami, *et al.*, *Eurphysics Lett.* **102**, 46002 (2013)

# Numerical analysis of field theory with non-trivial topological structure

Michikazu Kobayashi

*Department of Physics and Astronomy, Graduate School of Science, Kyoto University  
Oiwakecho, Sakyo-ku, Kyoto 606-8502*

As a non-trivial topological structure, I have picked up the “knotted structure” of the field theory in the project. Knotted structures broadly appear in physics such as fluid mechanics, superfluid helium, Bose-Einstein condensates, non-equilibrium systems, soft matter, quantum chromodynamics, and so on. One of the most famous field theory for knot is the Hopf map  $\pi_3(S^2) \simeq \mathbb{Z}$  which is the continuous map from  $S^2$  to  $S^3$  spaces. Because  $S^3$  can be expressed as the fiber bundle  $S^3 \simeq S^2 \times S^1$  with the base space  $S^2$  and the fiber  $S^1$ , one  $S^2$  point is mapped to a knotted or unknotted loop in the  $S^3$  space under the Hopf map. The simplest knot structure is the torus knot characterized by the number of string twists  $P$  along the torus and the number of strings  $Q$ , and the relation between the Hopf charge  $C$  for the Hopf map and the torus knot is  $C = PQ$ . The well known classical field model giving stable structure with  $C \geq 1$  is the Faddeev-Skyrme model:

$$\begin{aligned} \mathcal{L}_{\text{FS}} &= \frac{1}{2} \partial_\mu \mathbf{n} \cdot \partial^\mu \mathbf{n} - \kappa F^{\mu\nu} F_{\mu\nu}, \\ \mathbf{n} \cdot \mathbf{n} &= 1, \quad F_{\mu\nu} = \mathbf{n} \cdot (\partial_\mu \mathbf{n} \times \partial_\nu \mathbf{n}). \end{aligned} \quad (1)$$

The stable structure in the Faddeev-Skyrme model, however, cannot be classified as the torus knot because the structure is determined only for  $C$ . In particular, the stable struc-

ture is trivial unknotted one for  $1 \leq C \leq 6$ , and non-trivial knotted structure appears for  $C \geq 7$  in the Faddeev Skyrme model. In this work, I have explicitly constructed stable structure classified  $(P, Q)$  rather than  $C$  [1]. Here I have considered the following extended Faddeev-Skyrme model:

$$\begin{aligned} \mathcal{L}_{\text{TN}} &= \mathcal{L}_{\text{FS}} - m^2(1 - n_3^2) + \beta^2 n_1 \\ m &\gg \beta > 0. \end{aligned} \quad (2)$$

The second and third terms in the right-hand-side make  $n_3 = \pm 1$  and  $n_1 = 1$  states favorable respectively. Under these terms, I expect the toroidal shape of the domain wall interpolating  $n_3 = \pm 1$  states, and  $n_1 = -1$  appears as a soliton string winding on the toroidal domain wall. As a consequence, I can obtain the torus knot of the  $n_1 = -1$  state.

I numerically obtain the stable structure for the  $\mathcal{L}_{\text{TN}}$  in the 3-dimensional semi infinite space. For the time, the steepest descent method is used for finding the stable state. The condition  $\mathbf{n} \cdot \mathbf{n} = 1$  is satisfied by introducing the Lagrange multiplier. For the space, to approximately treat the infinite space, I use the following scaling transformation:

$$\begin{aligned} x_a &= L \tan^{-1} X_a, \quad a = 1, 2, 3, \\ (x_1, x_2, x_3) &= (x, y, z), \end{aligned} \quad (3)$$

for  $-1 < X_a < 1$ , and consider the dependence of  $n_i$  on  $X_a$  instead of  $x_a$ , where  $L$  is the scaling parameter. I use the cubic with the  $(N + 1)^3$  grid points with  $N = 1024$ . On the  $l$ -th point in the  $x_a$ -direction, the value of  $n_i(\{(l)_a\})$  is defined as

$$n_i(\{(l)_a\}) = n_i(\{(\cos(l\pi/N))_a\}), \quad (4)$$

where  $n_i(\{X_a\})$  is the value of  $n_i$  at  $\{X_a\} = (X_1, X_2, X_3)$ . For  $l = 0$  or  $N$ , which corresponds to infinity, the value of  $n_i$  is fixed to the ground state:

$$n_1 = n_2 = 0, \quad n_3 = 1. \quad (5)$$

To calculate the spatial derivative of  $n_i$ , I use the spectral collocation method. Under the discrete forward cosine transformation of  $n_i$ , I obtain the coefficients for the Chebyshev spectrum, and can easily calculate the first and second spatial derivatives of  $n_i$  through the forward and backward cosine transformations..

For the actual numerical procedure, I parallelize the task along the one direction to 128 core with 32 nodes through the standard MPI parallelization in the system B. The discrete cosine transformation for the Chebyshev spectrum is done with the FFT routine included provided by the Intel Math Kernel Library.

Figure 1 shows different stable solution of Eq. (2) for  $C \leq 6$ :  $(P, Q) = (1, 1), (2, 1), (3, 1), (4, 1), (5, 1), (6, 1), (1, 2), (3, 2), (1, 3), (1, 4), (1, 5)$ , and  $(1, 6)$ . Although there is no stable solution for  $(P, Q) = (2, 2)$  or  $(2, 3)$ , I find configurations with different sets of  $(P, Q)$  for torus knots are topologically distinct even then they have the same Hopf charge  $C$  being different from the original Faddeev-Skyrme model. Especially, the state with  $(P, Q) = (3, 2)$  is non-trivial trefoil knot showing that knotted state appears even for  $C = 6$ .

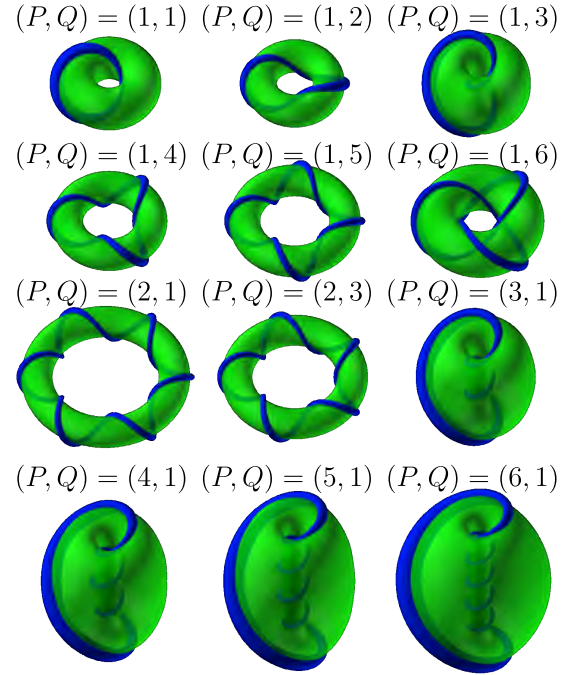


Figure 1: Toroidal domain wall (transparent green surface) and soliton string for  $n_1 = -1$  (blue string). I fix  $\beta^2/m^2 = 0.01$ , and  $\kappa m^2 = 1 \times 10^{-6}$ .

## 参考文献

- [1] M. Kobayashi and M. Nitta, Phys. Lett. B **728** (2014) 314.

# Numerical Study of One Dimensional Frustrated Quantum Spin Systems

Kazuo HIDA

*Division of Material Science, Graduate School of Science and Engineering  
Saitama, Saitama 338-8570*

## 1 Anisotropic Mixed Diamond Chains with Spins 1 and 1/2

Effects of single-site and exchange anisotropies on the ground state of the mixed diamond chain with spins 1 and 1/2 are investigated. The Hamiltonian is given by

$$\mathcal{H} = \sum_{l=1}^L \left[ J(\mathbf{S}_l + \mathbf{S}_{l+1}) \cdot (\boldsymbol{\tau}_l^{(1)} + \boldsymbol{\tau}_l^{(2)}) + DS_l^{z2} + \lambda \left\{ \Delta \tau_l^{z(1)} \tau_l^{z(2)} + \tau_l^{(1)x} \tau_l^{(2)x} + \tau_l^{(1)y} \tau_l^{(2)y} \right\} \right] \quad (1)$$

where  $\mathbf{S}_l$  is the spin-1 operator, and  $\boldsymbol{\tau}_l^{(1)}$  and  $\boldsymbol{\tau}_l^{(2)}$  are the spin-1/2 operators in the  $l$ th unit cell. The total number of unit cells is denoted by  $L$ . As in the case of  $\lambda = 1$ [1, 2], this model can be treated exactly by virtue of a series of conservation laws:  $\forall l, [\mathbf{T}_l^2, \mathcal{H}] = 0$ , where  $\mathbf{T}_l \equiv \boldsymbol{\tau}_l^{(1)} + \boldsymbol{\tau}_l^{(2)}$ . Therefore, each eigenstate has a definite set of  $\{T_l\}$ .

The ground state consists of an array of clusters called cluster- $n$  each containing  $n$  successive bonds with  $T_l = 1$  separated by singlet dimers with  $T_l = 0$ . We call this state DC $n$  (dimer-cluster- $n$ ) state. A cluster- $n$  is equivalent to a spin-1 chain with length  $2n + 1$  and alternating single-site anisotropy.

For  $1 \leq n < \infty$ , DC $n$  phase has  $n + 1$ -fold spontaneous translational symmetry breakdown. The ground state is nonmagnetic or paramagnetic depending on the magnitude of two types of anisotropies[3].

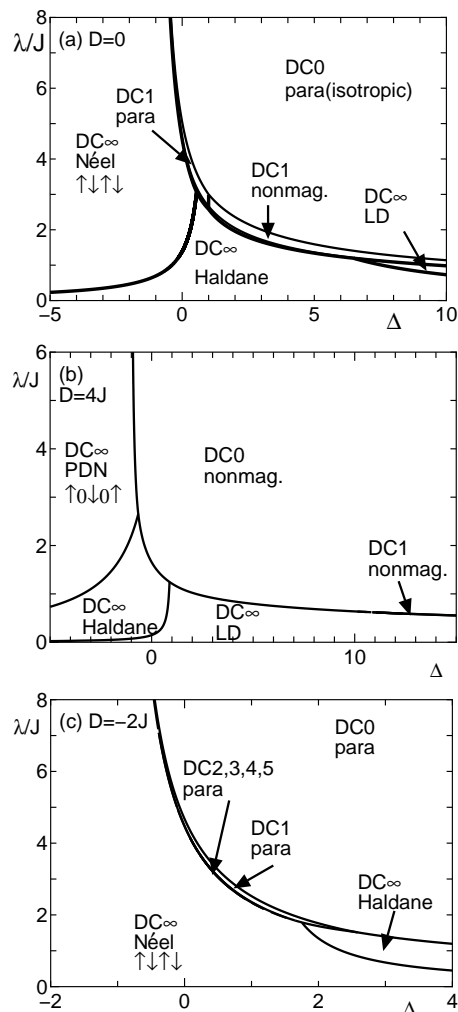


Figure 1: Ground-state phase diagram of the Hamiltonian (1) with (a)  $D = 0$ , (b)  $D = 4J$ , and (c)  $D = -2J$ .

For  $n \rightarrow \infty$ , the translational symmetry is recovered. The DC $\infty$  phase is realized for small  $\lambda$ . Actually, this phase consists of four different phases; Néel, period-

doubled Néel(PDN), Haldane, and large- $D$ (LD) phases. The ground state energy of the DC $n$  phase is calculated by numerical exact diagonalization (NED) of a cluster- $n$ . For the DC $\infty$  phase, the ground state energy is calculated by the infinite size DMRG method. The phase boundaries shown in Fig. 1 are determined by comparing the ground state energy of each phase.

## 2 Antiferromagnetic Heisenberg Chains with Uniform and Alternating Single-site Anisotropies

The ground-state phase diagram of  $S = 2$  antiferromagnetic Heisenberg chains with co-existing uniform and alternating single-site anisotropies described by the Hamiltonian

$$\begin{aligned} \mathcal{H} = & \sum_{l=1}^N JS_l S_{l+1} + (D_0 + \delta D) \sum_{l=1}^{N/2} S_{2l-1}^z S_{2l}^z \\ & + (D_0 - \delta D) \sum_{l=1}^{N/2} S_{2l}^z S_{2l+1}^z, \end{aligned} \quad (2)$$

is investigated[4]. Here  $\mathbf{S}_i$  is the  $S = 2$  spin operator on the  $i$ -th site. We consider the antiferromagnetic case  $J > 0$ . The case of  $D_0 = 0$  has been investigated in [5]. We also take  $\delta D > 0$  without the loss of generality. We investigate this model using NED and DMRG methods.

As shown in Fig. 2, we find the Haldane, LD, Néel, PDN, gapless spin fluid (SF), quantized ferrimagnetic(QF), and partial ferrimagnetic I and II (PFI and PFII) phases. In contrast to the case of  $S = 1$ [3], the Haldane phase is limited to the close neighborhood of the isotropic point. Within the numerical accuracy, the transition from the SF phase to the PDN phase is a direct transition. Nevertheless, the presence of a narrow spin-gap phase between these two phases is suggested on the basis of the low-energy effective theory. The ferrimagnetic ground state is present in a wide parameter range.

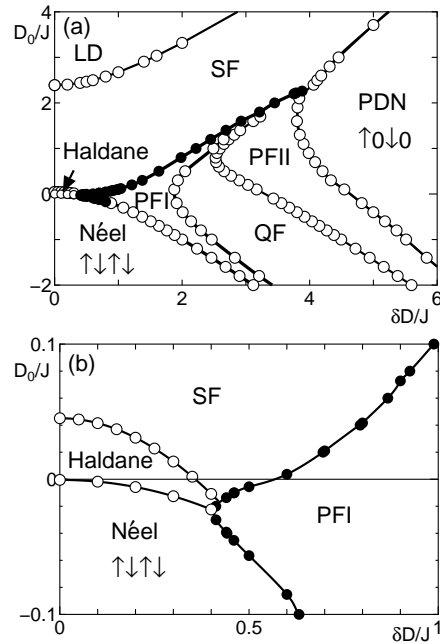


Figure 2: Ground-state phase diagram of the Hamiltonian (2). Open symbols are determined by extrapolation from the NED data for  $4 \leq N \leq 12$ . Filled symbols are determined from DMRG data with  $N = 60$ . (a) Overall phase diagram. (b) Enlarged phase diagram around  $(D_0, \delta D) \sim (0, 0)$ .

This work is supported by KAKENHI (C) (Nos. 25400389 and 21540379) from JSPS. The numerical diagonalization program is based on TITPACK ver.2 coded by H. Nishimori.

## References

- [1] K. Takano, H. Suzuki and K. Hida : *Phy. Rev.* **B80**, 104410 (2009).
- [2] K. Hida and K. Takano : *J. Phys. Soc. Jpn.* **80**, 104710 (2011).
- [3] K. Hida and W. Chen : *J. Phys. Soc. Jpn.* **74**, 2090 (2005).
- [4] K. Hida: *J. Phys. Soc. Jpn.* **83**, 034707 (2014).
- [5] K. Hida : *J. Phys. Soc. Jpn.* **76**, 024714 (2007).

# Robustness of Scale-free Networks against Cascading Overload Failures

KOUSUKE YAKUBO

*Department of Applied Physics, Hokkaido University*

*Sapporo 060-8628, Japan*

Availability of functional networks is supported by the global connectivity of the network. The robustness of complex networks against damages is then a significant issue from a practical viewpoint. The network robustness has been extensively studied in context of the percolation problem. One of the most important node removal processes in actual network failures is cascading overload failures. In this work, we study the resilience of scale-free networks to cascading overload failures.

In our model, temporally fluctuating loads on a network are modeled by random walkers on the network. In order to estimate the percolation transition point in the node removal process by overload failures, we must determine the relation between the overload probability and network topology. Considering that the probability to find a random walker at the node  $i$  in the steady state is proportional to the degree of the node  $i$ , the overload probability of the degree- $k$  node is given by the regularized incomplete beta function [1]. The cascading process based on the random-walk model is treated as follows.

1. Calculate the overload probability for the initial total load  $W_0$  and remove nodes with this probability.
2. For the reduced-size network with  $N_t$  nodes, the total load  $W_t$  is updated. Under the new total load  $W_t$ , the overload probability is recalculated and nodes are further removed from the reduced network with this overload probability.
3. Repeat the above procedure until the expectation number of newly removed nodes becomes less than unity.

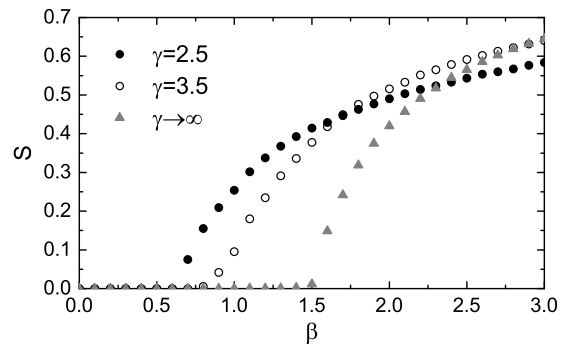


Figure 1: Relative size of the giant component in the final network as a function of the load renewal parameter  $\beta$ .

Figure 1 shows the relative size  $S$  of the giant component in the finally survived network as a function of the load renewal parameter  $\beta$  which characterizes the relation between  $W_t$  and  $N_t$ , for scale-free networks with different values of  $\gamma$ . It is clear that there exist the critical value  $\beta_c$  below which overload failures induce the global breakdown of the network. It should be noticed that the value of  $\beta_c$  for smaller  $\gamma$  is lower than that for larger  $\gamma$ . This implies that scale-free networks are robust against cascading overload failures modeled by random walkers, which is opposed to previous results based on the betweenness centrality [2].

## References

- [1] V. Kishore, M. S. Santhanam, and R. E. Amritkar, Phys. Rev. Lett. **106**, 188701 (2011).
- [2] S. Boccaletti, V. Latora, Y. Moreno, M. Chavez, and D.-U. Hwang, Phys. Rep. **424**, 175 (2006).

# Conformations of polymer chains in nematic liquid crystals

Takayuki UCHIDA and Takeaki ARAKI  
*Department of Physics, Kyoto University*  
*Kitashirakawa-oiwake-cho, Sakyo, Kyoto 606-8502*

The conformation of polymer chains dissolved in a simple solvent has been studied intensively. With changing the solvent quality, or  $\chi$  parameter, a coil-globule transition is induced [1]. It is also interesting to study the conformation of polymers in an anisotropic liquid. It was reported that the conformation of polymers can be anisotropic in a nematic liquid crystal in experiments [2,3]. A mean-field theory on the conformation of semiflexible polymers in the vicinity of the nematic-isotropic (NI) phase transition point is also proposed [4]. Nevertheless, it is poorly understood what microscopic conformation is preferred in nematic liquid crystals. In this work, we studied the conformation of a polymer chain in a nematogenic liquid by means of Monte Carlo simulations. We adopt a spring-beads model to describe a polymer chain (Kremer-Grest and Weeks-Chandler-Andersen potentials) [5] and Gay-Berne potential for monomer-mesogen and mesogen-mesogen interactions [6]. The rigidity of the semi-flexible polymer is controlled with changing the bending modulus for angles between neighbour bonds. We employ NVT ensemble and control the temperature in order to change the phases of the background liquid.

If the chain is flexible, the conformation becomes anisotropic in nematic environment (see Fig. 1). However, the chain is not completely stretched there. If the polymer chain is semiflexible, on the other hand, the globule-stretched transition of the chain is observed in vicinity of the NI transition temperature. As the rigidity of polymer is enlarged, the globule-stretched transition point is increased far above the NI transition temperature. Here

the solvent remains isotropic and the pretransitional nematic layer is formed around the stretched chain.

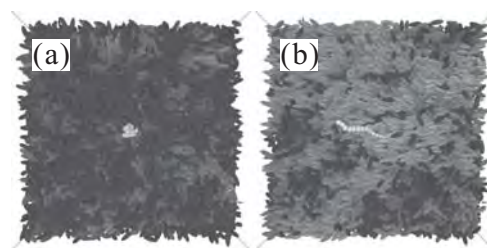


Figure 1: Snapshots of the polymer chain (a) far above and (b) in the vicinity of the NI transition temperature. The white chain represents the polymer. The ellipsoids are the nematogenic molecules and their brightness represent the local nematic order.

## References

- [1] P. G. de Gennes, *Scaling Concepts in Polymer Physics*, (Cornell Univ. Press., New York, 1979).
- [2] J. F. D'Allest *et al.*, Phys. Rev. Lett. 61, 2562 (1988).
- [3] Z. Dogic *et al.*, Phys. Rev. Lett. 92, 125503 (2004).
- [4] A. Matsuyama, Phys. Rev. E 67, 042701 (2003).
- [5] K. Kremer and G. S. Grest, J. Chem. Phys. 92, 5057 (1990).
- [6] J. G. Gay and B. J. Berne, J. Chem. Phys. 74, 3316 (1981).

# Collective Dynamics of Active Particles

Takaaki KAWAGUCHI

*Department of Physics, School of Medicine, Toho University  
5-21-16 Omorinishi, Ota-ku, Tokyo 143-8540, Japan*

We investigate the directed motion of a one-dimensional particle array on a symmetric periodic potential by introducing spatiotemporally periodic modulation of the natural length between particles. Under certain conditions the particle array moves unidirectionally with finite velocity and shows directed motion for any finite value of the potential amplitude. Novel collective dynamics of the directed motion are observed.

The model considered here is an extended version of the one-dimensional Frenkel-Kontorova model, which consists of an array of particles interacting with each other via a linear spring on a periodic substrate. No directed external force works on the particles and no spatial asymmetry exists. We introduce spatiotemporally periodic modulation of the natural length between adjacent particles. The natural length between  $i$ -th and  $(i+1)$ -th particles is given by  $c_{i,i+1}$ . We assume sinusoidal modulation with an amplitude  $\alpha$ , a time period  $T$  and a wave length  $\lambda$ .

The equation of motion of the  $i$ -th particle in the array is given by

$$\ddot{u}_i + \gamma \dot{u}_i = u_{i+1} - 2u_i + u_{i-1} - c_{i,i+1} + c_{i-1,i} - U \sin(2\pi u_i / c_b),$$

where  $u_i$  is the one-dimensional coordinate of the  $i$ -th particle. The equations of motion are solved under the periodic boundary condition by assuming overdamped motion of particles.

Figure 1 shows the time-evolution of the coordinates of the particles  $u_i(t)$  for a certain condition. There appears spatiotemporally correlated motion of the particles. Each particle repeats oscillatory motion with different phases and as a whole moves forward. The motion resembles that of measuring worms, that is, the system repeats extension and con-

traction of its body part by part and moves forward as a whole.

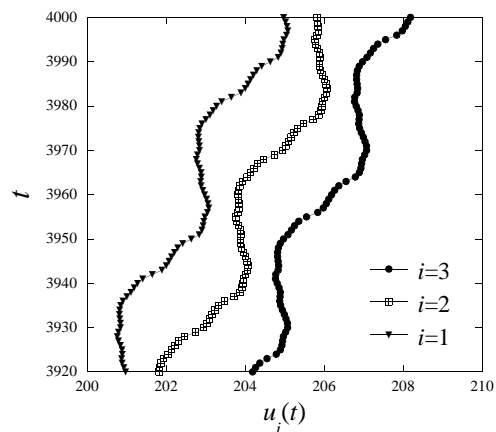


Figure 1: Time evolution of the coordinate of each particle.

The directed motion shows interesting behaviors against the change in the parameters of the modulation. In fig. 2 we show a reversal phenomenon of the direction, i.e., current reversal, against the change in the modulation amplitude  $\alpha$ . The velocity  $v$  is normalized with  $v_0 = c_b/T$ . For  $0.05 < \alpha/c_0 \leq 0.46$  the particle array moves in the positive direction with  $v/v_0 = 1$ . As  $\alpha/c_0$  is increased, reversal of motion appears twice. The first reversal occurs at  $\alpha/c_0 \approx 0.47$  from  $v/v_0 = 1$  to  $v/v_0 = -2$ , and the second one does at  $\alpha/c_0 \approx 0.71$  and the value of  $v/v_0$  returns to the same with that for  $\alpha/c_0 \leq 0.46$ . This may be called the dynamical reentrance of the directed motion. It is characteristic of the directed motion in this system that the strengthening of the modulation amplitude does not increase velocity, but causes the reversal of motion.

We investigate the changes of the system against increasing  $U$  for a suitable constant value of  $T$ . Figure 3 shows a diagram of the dy-

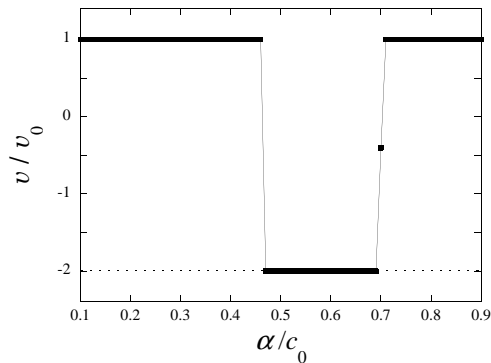


Figure 2: Modulation amplitude dependence of the normalized velocity of the particle array.

namical states for  $T = 40$  in the  $v/v_0 - U$  plane where the normalized velocity  $v/v_0$  is plotted against  $U$  for  $\alpha/c_0 = 0.5$  and  $\lambda/L = 0.25$ . The absolute magnitude of  $v/v_0$  vanishes at

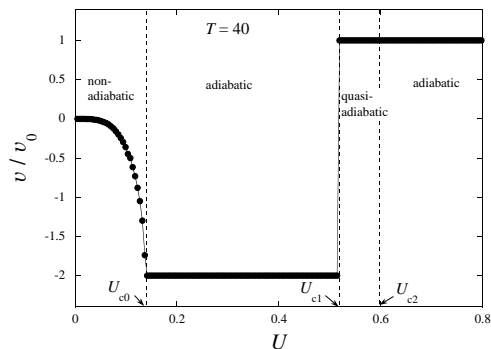


Figure 3: Diagram of dynamical states plotted in the  $v/v_0 - U$  plane.

$U = 0$ , i.e., no barrier cause no directed motion, and increases with  $U$ . The substrate potential yields barrier and frictional force for each particle. The directed motion observed in the present model is, hence, a sort of barrier-assisted and friction-induced motion. The velocity is locked to  $v/v_0 = -2$  when  $U$  is larger than  $U_{c0} \simeq 0.14$ , where  $U_{c0}$  is the critical strength of  $U$  for the occurrence of the velocity locking. For  $0 < U < U_{c0}$  the motion of the system is out of the range of the adiabatic motion. In this regime, hence, the motion is nonadiabatic and the velocity is not locked.

There exist another two critical strengths of  $U$  between the adiabatic and quasi-adiabatic regimes, which are denoted by  $U_{c1}$  and  $U_{c2}$ . In the range  $U_{c0} < U < U_{c1}$  the motion becomes adiabatic and the velocity locking at

certain value appears. In  $U_{c1} < U < U_{c2}$  the new state appears as a quasi-adiabatic state. The velocity locking still occurs, that is “quasi-adiabatic locking”, but the locked value is different from that for  $U_{c0} < U < U_{c1}$ . When we increase  $T$ , the transition from a quasi-adiabatic state with  $v/v_0 = 1$  to an adiabatic one with  $v/v_0 = -2$  occurs at a critical value of  $T$  in  $U_{c1} < U < U_{c2}$ . For  $U \geq U_{c2}$  an adiabatic state with  $v/v_0 = -2$  appears. In the adiabatic regime the velocity locking is stable for  $T \rightarrow \infty$ .

We investigated novel dynamical phenomena of directed motion in a particle array on a periodic substrate potential with no spatial asymmetry and no direct external driving force. The directional motion appears by introducing the spatiotemporally periodic modulation of the natural length between particles. The magnitude of the velocity is locked to multiple values of a unit velocity. The velocity locking behavior appears for adiabatic motion, and furthermore there appears a quasi-adiabatic locking behavior in a nonadiabatic regime.

## References

- [1] T. Kawaguchi and H. Matsukawa: *AIP Conf. Proc.*, **1518**, 737 (2013);
- [2] T. Kawaguchi and H. Matsukawa: *JPS Conf. Proc.*, **1**, 012059 (2014);

## Hydrodynamic effect on phase ordering

Ryotaro Shimizu, Hajime Tanaka

*Institute of Industrial Science, University of Tokyo*

*Komaba 4-6-1, Meguro-ku, Tokyo, Japan*

After shaking a salad dressing, we can see the collisions of oil droplets in vinegar. This coarse graining process is known as phase separation. In past decades researchers the kinetic process of phase separation phenomena have been intensively studied from both scientific and applications viewpoints, since this process is one of the most fundamental physical process of pattern formation[1].

For a binary liquid mixture, the relevant domain coarsening mechanism depends solely on the volume fraction of the minority phase. (1) For a small volume fraction, the evaporation-condensation mechanism is responsible for droplet coarsening. (2) Near a symmetric composition, the tube hydrodynamic instability proposed by Siggia[2] leads to rapid hydrodynamic coarsening. (3) For intermediate volume fraction, it has been believed that the Brownian-coagulation mechanism is responsible for the domain coarsening [2]. In this mechanism droplets grow by accidental collisions between droplets undergoing random Brownian motion.

Some time ago, we found in our microscopy observation of a droplet coarsening process that droplets are moving deterministically) rather than randomly [3,4]. Following trajectories of droplets, we noticed that droplets sometimes move directionally with a speed much faster than the expectation from random Brownian motion. We suggested that this may be due to a non-trivial coupling between composition and velocity fields. Droplets move around by thermal fluctuations while exchanging solutes with neighboring droplets via the surrounding matrix phase. The composition correlation between a pair

of neighboring droplets should develop before an accidental collision between them by Brownian motion takes place. We speculated that this composition correlation may be an origin of rather deterministic motions of droplets.

This time we studied how this complex coupling leads to deterministic motions of droplets and efficient droplet coarsening, by numerically solving a fluid model (known as model H) for phase separation with and without thermal composition and force noises.

Figure 1 shows the snapshot of a binary fluid mixture undergoing droplet spinodal decomposition, which is simulated with thermal fluctuations. The interface of droplets is rough due to thermal fluctuation effects. We note that, to the best of our knowledge, this is the first example of model H simulation in three dimensions including full thermal noises. In the early stage, many small droplets are formed by fragmentations. We observed the growth of droplets by collisions with neighboring droplets in the late stage. We analysed the time evolution of average droplet size during the coarsening process. As the result, we found that the coarsening proceeds faster than the prediction by Brownian-coagulation (BC) theory, even though the coarsening exponent was close to  $1/3$ , which is consistent with the BC theory.

To seek a cause of the faster coarsening mechanism, we analysed the displacements of droplets during the interval of two successive collisions. We found that the droplets move directionally towards a neighboring droplet. We consider that it is this fast directional motion that leads to the fast

coarsening process.

From the result of coarsening process without thermal noises, we can study about the composition correlation between droplets during the phase separation process, without suffering from noises that smear out all the details. We found that the interfacial profile of each droplet is not spherical symmetric but rather anisotropic, reflecting configuration of the neighboring droplets, even though the shape of droplets is almost perfectly spherical because of the action of the Laplace pressure. We also found that the deterministic flow field is induced at each droplet, reflecting the asymmetric interfacial profile of each droplet. This asymmetric interfacial profile leads to the intradroplet gradient of the interfacial tension and this gradient generates hydrodynamic motion of droplets.

In summary, we studied the coarsening process of droplet dispersions. We found that the coupling between diffusion and flow field plays a very important role for the phase separation process of asymmetric binary mixtures.

## References

- [1] J.D.Gunton, M.San Miguel, and P.Sahni:  
in Phase Separation and Critical  
Phenomena, edited by C.Domb and  
J.H.Lebowitz, (Academic, London,  
1983),Vol.8(1976)
- [2] E.D.Siggia, Phys.Rev.A 20,595(1979)
- [3] H.Tanaka, J.Chem.Phys. 103, 2361(1995)
- [4] H.Tanaka, J.Chem.Phys. 107,3734(1997)

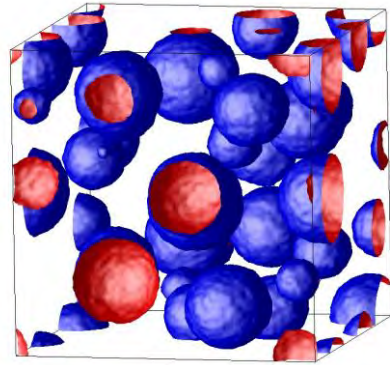


Figure 1: A snapshot during phase separation

# High precision computation of Feigenbaum constant.

Masanori SHIRO

*HTRI, National Institute of Advanced Industrial Science and Technology*

*Umezono1-1-1 Central 2, Tsukuba, Ibaraki 305-8568*

A purposes of our project is calculating the second Feigenbaum constant with high precision.

Properties of critical exponents between many type of phase transitions are not necessarily revealed, although the transitions are found in many solid-state materials. We think that phase transitions are able to treat as chaotic transitions. Feigenbaum constant is an universal value between simple chaotic models and fractals. A series expansion for the constant is not known yet. It is just found in almost two thousands digits in Briggs' thesis[1].

The most important signification of our project is to find a precise value of Feigenbaum constant for the phase-transition studies. In future, the value should be expanded in a series. Many digits provide more correct information whether the values is rational or not, transcendental or not, and so on.

Our project stated at the second half season in 2013. An universal function  $g(x)$  which is required for calculation of the constant, has following properties,

1.  $g(x)$  is an even function.
2.  $g(\alpha x)/\alpha = g(g(x))$
3.  $\alpha = 1/g(1)$
4.  $g(0) = 1$

We did basis expansion of  $g(x)$  and its coefficients as a vector and divided  $x_i \in [0, 1]$  are constructed to a matrix.

Although required libraries as Eigen are not installed, we wrote a prototype in C++ and checked its workings, computational effort and required memory[2]. We found that a realistic digits is till later thousands order in our available resources.

Fortunately, our work will run on the next year. Required libraries such as Eigen and Mpreal will be modified for our computers, installed by the center staff and we want to do our task completely.

## 参考文献

- [1] Doctor thesis: K. Briggs (1997)
- [2] JPS abstracts in 2014 spring: 29pAD11, M. Shiro (2014)

# Symmetry protection of disordered phases and phase transitions in spin chains

Yohei FUJI, Frank POLLMANN<sup>a</sup>, and Masaki OSHIKAWA*Institute for Solid State Physics, University of Tokyo, Kashiwa, Chiba 277-8581*<sup>a</sup>*Max-Planck-Institut für Physik komplexer Systeme, D-01187 Dresden, Germany*

In recent decades, the study of topological phases is one of central interests in condensed matter physics. A special class of the topological phases is called “symmetry-protected topological (SPT)” phases [1], which are distinct only in the existence of certain symmetries. SPT phases are characterized by non-trivial entanglement structures. On the other hand, when the ground state is adiabatically connected to a direct product of local states, it is considered to be in a trivial phase. It appears that there is just one trivial phase. However, in the presence of certain symmetries, there can be distinct trivial phases.

In this work, we show such a symmetry-protected distinction between trivial phases in 1D spin systems in the presence of the symmetry with respect to the combined operation of the site-centered inversion and the  $\pi$ -rotation about one spin axis. [2] To illustrate this, we consider the spin-1 chain with a staggered magnetic field,

$$H = \sum_j \left[ \vec{S}_j \cdot \vec{S}_{j+1} + D_z (S_j^z)^2 + D_x (S_j^x)^2 + h_z (-1)^j S_j^z \right],$$

which possesses the desired symmetry.

We numerically investigate its ground-state properties by the infinite density-matrix renormalization group (iDMRG) method [3], which provides an accurate variational ground-state wavefunction in the matrix-product representation with  $\chi \times \chi$  matrices. We use Fortran90 on the ISSP Supercomputer with OpenMP

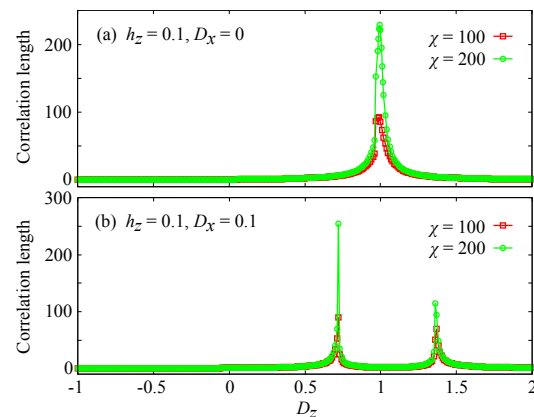


Figure 1: Correlation lengths are plotted against  $D_z$ .

parallelization in order to accelerate the contractions of tensors. In Fig. , we show the correlation length as a function of  $D_z$  for two sets of the parameters. Divergent behaviors of the correlation lengths as increasing  $\chi$  correspond to phase transitions. These phase transitions indicate that two trivial phases are distinguished under the above symmetry.

## References

- [1] Z.-C. Gu and X.-G. Wen, Phys. Rev **80**, 155131 (2009); F. Pollmann, A. M. Turner, E. Berg, and M. Oshikawa, Phys. Rev. B **81**, 064439 (2010).
- [2] Y. Fuji, F. Pollmann, and M. Oshikawa, in preparation.
- [3] I. P. McCulloch, arXiv:0804.2509 (unpublished).

# Fixed Scale Factor Finite-Size Scaling Analysis for Two-Dimensional Spin Systems

Yusuke TOMITA

*Shibaura Institute of Technology*

*307 Fukasaku, Minuma-ku, Saitama-City, Saitama 337-8570*

Critical phenomena in continuous spin systems on two-dimensional (2D) lattices have long been fertile soils for deep understanding of statistical physics. In particular, the Mermin-Wagner-Hohenberg theorem and the theory of the Berezinskii-Kosterlitz-Thouless (BKT) transition play roles of principal guides for investigating critical phenomena in 2D systems. Though the preceding studies are quite helpful to judge whether a system shows critical phenomena or not, a little number of systems yet annoy researchers by showing obscure *critical* behaviors. The obscurity hinders grasp of physics, and sometimes it may lead us to a misunderstanding of critical phenomena. A suitable example of such an obscurity is the 2D ferromagnetic Heisenberg model. The Heisenberg model exhibits exponentially large correlation lengths at low temperatures, and conventional finite-size scaling (FSS) analyses often lead to an erroneous conclusion that the model has the BKT phase.

To improve accuracy of FSS analyses, I proposed a FSS analysis using a fixed scale factor[1]. A procedure of the FSS analysis is like as follows: (1) Calculate two two-point correlation functions,  $G(\beta, L/2)$  and  $G(\beta, L/4)$ . The Correlation ratio  $\mathcal{C}(\beta, L)$  is defined by  $G(\beta, L/2)/G(\beta, L/4)$ . (2) Calculate the ratio of the correlation ratio  $F_C(\xi(\beta, L)/L) = \mathcal{C}(\beta, sL)/\mathcal{C}(\beta, L)$ . Here,  $s$  is a parameter named the fixed scale factor. Since the correlation ratio is a dimensionless quantity, the function  $F_C$  is equal to unity at the critical point. With usual procedure, a location of a critical point is estimated by a crossing point of a dimensionless FSS function, but the estimation of the crossing point is usually difficult

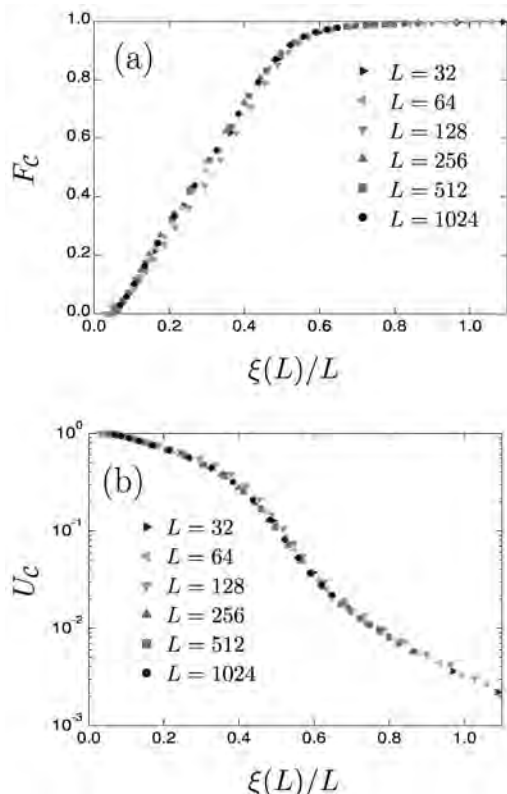


Figure 1: (a) An FSF-FSS plot of the correlation ratio for the 2D Heisenberg model. (b) A semi-logarithmic plot of an FSF-FSS function for the 2D Heisenberg model.

task for systems under discussion. The conciseness in estimating a critical point ( $F_C = 1$ ) is a main advantage of the new FSS analysis. Even though the improved FSS analysis gives the concise measure, we need a further improvement to estimate criticalities of systems whose correlation lengths are exponentially large. The improvement is accomplished by introducing the form of the two-point correlation function in the critical region,

$G(\beta, r) \sim e^{-\kappa r}/r^{d-2+\eta}$ . The parameter  $\kappa$  is proportional to the inverse of the correlation length; that is  $G(\beta, r)$  gives the power law decaying correlation function at the critical point ( $\kappa = 0$ ). Using the expression, the distance from unity [ $U_C (= 1 - F_C)$ ] is approximately estimated as  $(s - 1)\kappa L/4$  in the critical region.

Figure 1 shows the FSS function  $F_C$  and the logarithm of the distance from unity for the 2D Heisenberg model. Since the correlation length of the model exponentially develops as lowering temperature,  $F_C$  is almost unity at low temperatures. However, the logarithmic plot of the function  $U_C$  manifestly shows the distance is finite at finite temperatures. Therefore, the correlation length of the 2D Heisenberg model never diverges at finite temperature.

I also applied the FSS analysis to the 2D XY and  $RP^2$  models, and the results proved the analysis is quite helpful to judge whether a system exhibits a phase transition or not. The method can be applied to other systems straightforwardly. The applications will give firm evidences of existence or absence of the systems' criticalities.

## References

- [1] Y. Tomita, in preparation.

# Large scale hard sphere molecular dynamics simulation in the nonequilibrium transport phenomena

Masaharu ISOBE

*Nagoya Institute of Technology*

*Gokiso-cho, Showa-ku, Nagoya, 466-8555*

In this project, we investigated several non-equilibrium phenomena in the simple model system by using event-driven molecular dynamics (EDMD) algorithm in hard core system [1] and other alternative methods.

(i) *Cluster Impact and Shock Wave Propagation in Freely Evolving Granular Gas*: Granular gas without any external force evolves from the initial homogeneous state to the inhomogeneous clustering state, at which the energy decay deviate from Haff's law. The asymptotic behavior of energy decay after the clustering regime have been predicted by two theories, which are based on mode coupling theory or extension of inelastic hard rods gas. In our study, we investigated this system especially in the clustering regime of freely evolving granular gas by a large-scale molecular dynamics simulation up to 16.7 million particles. We found novel regime regarding on collisions between "clusters" appearing after clustering regime spontaneously, which can be clearly identified more than a few million particles system. The volumetric dilatation patterns of semicircular shape originated from density shock propagation characterize the "cluster impact" during the aggregation process of clusters. The theories don't agree with our numerical results because of cluster collision. Our novel findings indicate that the freely cooling granular gas in quasi-elastic and thermodynamic limit is strongly related to Navier-Stokes incompressible turbulence (shearing regime),

however, it eventually behaves as a compressible fluid (shock wave) after clustering regime (cluster collision regime) [2].

(ii) *Hard Disks Equation of State: First-Order Liquid-Hexatic Transition in Two Dimensions with Three Different Simulation Methods* [3]: Large-scale molecular simulations of the two dimensional hard disk system around the melting point are investigated with three different methods (i.e., event-chain Monte Carlo, a massively parallel Monte Carlo and EDMD). We reproduce the equation of state up to one million particles system. The relative performance of these methods is analyzed and the first-order melting transition in hard disks is confirmed, which were previously obtained using event-chain Monte Carlo method. Furthermore, the analyses of positional order confirms the existence of the hexatic phase in the one-million hard disk system.

## References

- [1] M. Isobe: *Int. J. Mod. Phys. C* **10** (1999) 1281.
- [2] M. Isobe, *Phys. Rev. E* **68** (2003) 040301(R); *Int. J. Mod. Phys. C* **23** (2012) 1250032; *J. Phys: Conf. Ser.* **402** (2012) 012041; (2014) in preparation.
- [3] M. Engel, J. A. Anderson, S. C. Glotzer, M. Isobe, E.P. Bernard and W. Krauth: *Phys. Rev. E* **87** (2013) 042134.

# Study of the effect of the short-range interaction on critical phenomena driven by elastic interactions

Masamichi Nishino

*Computational Materials Science Center, National Institute for Materials Science  
Tsukuba, Ibaraki, Japan*

Domain wall (interface) propagation is frequently seen in growth of a new ordered state. The structure of the interface has been studied extensively and the following scaling relation has been established:  $W(L, t) \sim L^\alpha f(\frac{t}{L^z})$ , where  $L$  is the system size parallel to the interface,  $t$  is time, and  $f(x)$  is a scaling function. The critical exponents are established as  $\alpha = 1/2$ ,  $z = 3/2$  in KPZ universality class for one-dimensional interface, i.e., in two-dimensional systems. Various kinds of growth models such as Ising model, BD model, RSOS model, etc, are in this class. In the steady state of interface growth, i.e., when  $\frac{t}{L^z} \gg 1$ , the interface width is scaled as  $W(L, t) \sim L^\alpha$ .

Spin crossover (SC) materials show a wide variety of phase transitions and have attracted much attention in applicability to devices [1]. The SC system has bistable states, i.e., low spin (LS) state and high (HS) state and the size of each molecule depends on the states. The elastic interaction caused by the lattice distortion due to difference of the molecular sizes is important for the cooperative interaction. We modeled the cooperative interaction by constructing an elastic-interaction model, in which the changeable volume of the molecular unit is taken into consideration.

In this work we investigated domain wall propagation between HS and LS phases and the scaling property of the interface [2]. There exist two kinds of interfaces in SC systems. One is the interface of the spin states of molecules and the other is the interface of the lattice structure. The nature of the lattice interface width does not depend on the dynamics of the lattice and spin, and the shape is of macroscopic structure due to long-range nature of the elastic interaction. In contrast, the nature of the spin interface width changes depending on the dynamics of the lattice and

spin. When the change of the spin state is fast and the lattice relaxation does not follow it sufficiently, the roughness exponent has the value  $\alpha = 1/2$ , which is commonly found in models of short-range interactions. In contrast, when the lattice relaxes well, the spin dynamics is influenced by the lattice dynamics, which leads to  $\alpha = 1$  of the roughness exponent. In this case the macroscopic nature of the elastic interaction affects the spin interface.



Figure 1: Snapshot of interface growth in the SC system. Blue and red parts denote LS and HS phases, respectively.

## References

- [1] “Theoretical Descriptions of Spin-Transitions in Bulk Lattice”, C. Enachescu, M. Nishino, S. Miyashita in “Spin-crossover materials - properties and applications” M.A. Halcrow (ed) John Wiley & Sons, Chichester, UK, 2013, 455-474.
- [2] “Crossover of the roughness exponent for interface growth in systems with long-range interactions due to lattice distortion”, M. Nishino, T. Nakada, C. Enachescu, K. Boukheddaden and S. Miyashita, Phys. Rev. B 88, 094303 (2013).

# Fracture dynamics and pattern formation

Satoshi YUKAWA and Shin-ichi ITO

*Department of Earth and Space Science, Osaka University  
Machikaneyama, Toyonaka, Osaka 560-0043*

A fracture pattern of a thin layer is seen in everyday life. It is essentially caused by shrinkage of the paste; The fracture pattern of the dried mud is also caused by stress increment during the desiccation process of the paste. There are lots of interesting phenomena which have not been understood yet. Over the last few years, we have studied the fracture dynamics in a drying thin layer of the paste numerically and analytically.[1] The main result of this study is that the dynamical scaling law of the fragment size distribution is found; The bare distribution of the fragment size  $S$  at time  $t$ ,  $P(S, t)$ , can be scaled by its average,  $P(S, t) \sim \tilde{P}(S/\langle S \rangle_t)$ . This result resembles the Vicsek-Family scaling for the aggregation process,[2] but the direction of time is opposite.

In this year, in order to understand the dynamical scaling property, we study the stochastic model based on the Gibrat process,[3] which is called the modified Gibrat process. Original Gibrat process is a discrete-time dividing stochastic process with the multiplicative noise. For the modified Gibrat process, we introduce the concept of the lifetime of the fragments. Thus the discrete-time stochastic process becomes continuous-time one. The lifetime is a function of the area of the fragments, which is analytically evaluated by equations of motion for elastic continuum.

In the last year, we found that the modified Gibrat process obeyed the dynamical scaling law in the case that the lifetime is a power-law function on the area. In this year, on the ISSP super computers, we performed numeri-

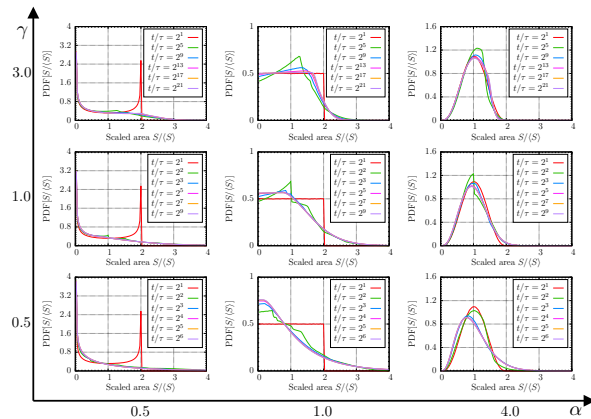


Figure 1: Scaled distributions for several parameters. Shapes of the final scaled distributions are different, but all distributions are scaled.

cal simulations with parameter parallelization to survey the large parameter space. In Fig. 1, several scaled distributions are shown. In addition, we analyzed the Markovianized stochastic model of the modified Gibrat process. Further theoretical and experimental investigation are now in progress.

## References

- [1] S. Ito and S. Yukawa: arXiv:1209.6114.
- [2] T. Vicsek and F. Family, Phys. Rev. Lett., **52**, b 1669, (1984).
- [3] E. W. Crow and K. Shimizu ed, “Log-normal distributions: theory and applications” (Marcel Dekker, New York, 1988).

# Multifractality near a Point Defect at Topological Phase Transitions

Hideaki OBUSE

*Department of Applied Physics, Hokkaido University  
Sapporo 060-8628, Japan*

Multifractality at Anderson transitions, which reflects non-trivial self-similar structures of wave functions due to the absence of characteristic lengths, has attracted much attentions for its importance to understand the phase transitions[1]. Multifractality also exposes interesting natures when a topological insulator with disorder undergoes a phase transition into a metal or a topological insulator with the different topological number[2, 3]. On one hand, multifractality in the bulk region is determined by only symmetries and the spatial dimension of the system even for topological phase transitions. Thereby, bulk multifractality observed at topological phase transition is identical with bulk multifractality of one of the conventional Anderson transitions. On the other hand, multifractality near (straight) boundaries, called boundary multifractality, of the topological phase transition depends on the topological number of the adjacent topological insulating phase together with symmetries and the spatial dimension. Therefore, boundary multifractality of the topological phase transition is different from that of the conventional Anderson transitions. In this work, we study multifractality near a point like topological defect.

We focus on the two-dimensional square lattice with random hoppings. We note that there is no on-site disorder so that the system retains chiral symmetry. A vacancy, in other words, a point defect in this system is a topological defect and generates a zero energy state. We have

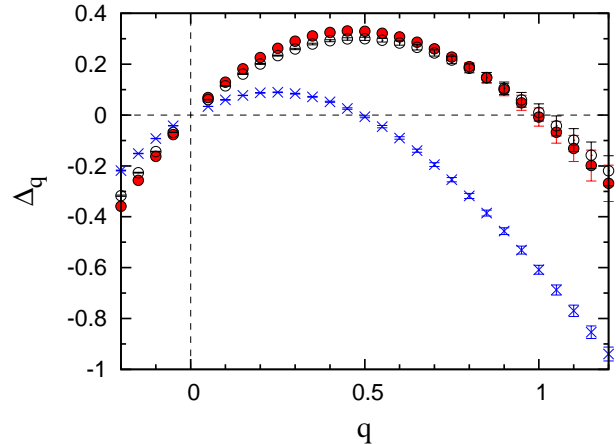


Figure 1: The  $q$  dependence of anomalous dimensions  $\Delta_q$ . The blue crosses and red filled circles represent anomalous dimensions calculated from wave function amplitudes near and far from the defect, respectively. For comparison, the anomalous dimension for systems with no point defects is shown by the black open circles.

numerically calculated the wave function  $\psi(\mathbf{r})$  at the zero energy of the system with the linear size  $L$  for many disorder realizations. The system size  $L$  is changed from 40 to 1000 and the number of disorder realizations is  $10^6$  for each  $L$ . Then, multifractality is quantitatively calculated from the size  $L$  dependence of the relation,  $L^{2q} \overline{|\psi(\mathbf{r})|^{2q}} \propto L^{-\Delta_q}$ , where  $\Delta_q$  is an anomalous dimension and the overline represents the ensemble averaging. We have calculated  $\Delta_q$  from the wave function amplitudes far from and close to the point defect.

Figure 1 shows  $\Delta_q$  in case the position of wave function amplitude  $\boldsymbol{r}$  is close to or far from the point defect. We have confirmed that  $\Delta_q$  from wave function amplitude far from the point defect is the same with  $\Delta_q$  calculated from a system with no point defect. We have also found that  $\Delta_q$  from wave function amplitudes close to the point defect exhibits new multifractality which is different from  $\Delta_q$  in the bulk.

## References

- [1] F. Evers and A. D. Mirlin: Rev. Mod. Phys. **80** (2007) 1355.
- [2] H. Obuse, A. Furusaki, S. Ryu, and C. Mudry: Phys. Rev. B **78** (2008) 115301.
- [3] R. Bondesan, I. A. Gruzberg, J. L. Jacobsen, H. Obuse, and H. Saleur: Phys. Rev. Lett. **108** (2012) 126801.

# Molecular Simulation Study of Supramolecular Structure Formation by Amphiphilic Molecules

Susumu FUJIWARA

*Graduate School of Science and Technology, Kyoto Institute of Technology*

*Matsugasaki, Sakyo-ku, Kyoto 606-8585*

Amphiphilic molecules such as lipids and surfactants are composed of hydrophilic and hydrophobic parts. In aqueous solutions, amphiphilic molecules spontaneously self-assemble into various structures such as micelles, vesicles, and bicontinuous structures [1-3]. Although numerous computer simulation studies have so far been done on structure formation of amphiphilic molecules, each of which consists of a hydrophilic head group and a hydrophobic tail group, there have been few theoretical and simulation studies on structure formation of bolaamphiphilic molecules, each of which contains a hydrophobic stalk and two hydrophilic ends. The purpose of this study is to clarify the effect of hydrophilicity on the phase behavior of bolaamphiphilic solutions. With a view to investigating the phase behavior of bolaamphiphilic solutions at the molecular level, we perform the molecular dynamics (MD) simulations of coarse-grained bolaamphiphilic molecules with explicit solvent molecules and systematically analyze the formation processes of micelles and mesophases.

A bolaamphiphilic molecule is modeled as a

semiflexible chain which consists of a hydrophobic stalk with three particles and two hydrophilic ends (H1 and H2), each of which contains one particle. The solvent molecules are modeled as hydrophilic particles. As bonded potentials, we consider the bond-stretching potential and the bond-bending potential. The interaction between hydrophilic and hydrophobic particles is modeled by the repulsive soft core potential and all other interactions are modeled by the Lennard-Jones (LJ) potential. Note that the LJ interaction parameter  $\epsilon_{hs2}^*$  between a hydrophilic end particle (H2) and a solvent particle can be varied whereas the LJ interaction parameter  $\epsilon_{hs1}^*$  between a hydrophilic end particle (H1) and a solvent particle is fixed constant.

The numerical integrations of the equations of motion for all particles are carried out using the velocity Verlet algorithm at constant temperature with a time step of 0.0005. We apply the periodic boundary conditions and the number density is set at 0.75. Initially, we prepare homogeneous bolaamphiphilic solutions at high temperature ( $T^* = 10$ ) for various values of the amphiphilic

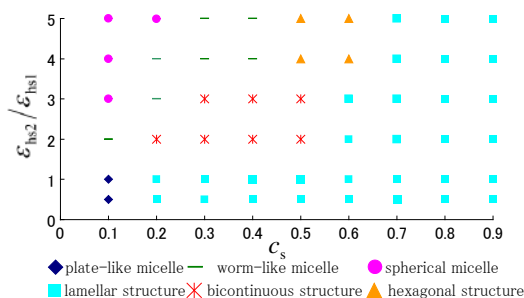


Fig. 1:  $\epsilon_{hs2}^*/\epsilon_{hs1}$  vs  $c_s$  “phase diagram”.

concentrations  $c_s$  and the LJ interaction parameters  $\epsilon_{hs2}^*$ . The system is then quenched to  $T^* = 1.3$  and MD simulations of  $5.0 \times 10^7$  time steps are performed for each simulation run.

Our simulations show that various kinds of higher-order structures such as worm-like micelles, hexagonal structures and bicontinuous structures are obtained (Fig.1). We also clarified that, at low amphiphilic concentrations ( $c_s = 0.1$ ), a plate-like micelle changes to

worm-like micelles, and then to spherical micelles as the interaction parameter  $\epsilon_{hs2}^*$  increases. At intermediate amphiphilic concentrations ( $c_s = 0.5$ ), on the other hand, it is ascertained that the lamellar structure changes to the bicontinuous structure, and then to the worm-like or hexagonal structures as the interaction parameter  $\epsilon_{hs2}^*$  increases.

## References

- [1] J. N. Israelachvili: *Intermolecular and Surface Forces*, 2nd ed. (Academic Press, London, 1992).
- [2] *Micelles, Membranes, Microemulsions, and Monolayers*, edited by W. M. Gelbart, A. Ben-Shaul and D. Roux (Springer-Verlag, New York, 1994), pp. 1-104.
- [3] I. W. Hamley: *Introduction to Soft Matter*, Rev. ed. (J. Wiley, Chichester, 2007).

## Phase Diagram of the Spin-1/2 Heisenberg Antiferromagnets on the Cairo-Pentagon Lattice

Makoto ISODA<sup>1</sup>, Hiroki NAKANO<sup>2</sup>, and Tōru SAKAI<sup>2,3</sup>

<sup>1</sup>*Department of Science Education, Faculty of Education, Kagawa University  
Takamatsu 760-8522*

<sup>2</sup>*Graduate School of Material Science, University of Hyogo, 3-2-1 Kouto, Kamigori-cho, Akou-gun,  
Hyogo 678-1297, Japan*

<sup>3</sup>*Japan Atomic Energy Agency, SPring-8, Sayo 679-5148, Japan*

Two-dimensional frustrated spin-1/2 Heisenberg antiferromagnet on the Cairo-pentagon lattice<sup>1,2</sup> is investigated by the numerical diagonalization method on the finite-size clusters up to 36 sites<sup>3</sup> with the periodic boundary condition. The lattice is constituted with the three-coordinated A-sites and the four-coordinated B-sites in the occupation ratio of 2 to 1. Hence the Heisenberg-type Hamiltonian requires two-types of nearest neighbor interactions, such as  $J = J_{AA}$  and  $J' = J_{AB}$ , at least.

The magnetization under the magnetic field has been calculated. The so-called 1/3-plateau is observed for every value of  $x \equiv J/J'$ , with the exceptional narrow region around  $x \sim 0.8$ , where the plateau may vanish or survive with a narrow width in the thermodynamic limit. The magnetization jumps accompanying the change of the total spin  $\Delta S_t \geq 2$  are observed at the upper-field edge of the 1/3-plateau for  $0 < x < 0.8$  and at the lower-field edge of the 1/3-plateau for  $0.8 < x < 2.0$ . Such jump in the isotropic spin system is peculiar and has been found in some spin frustrated systems. The mechanism is attributed to the spin flop transition under the isotropic spin system<sup>3</sup> and is confirmed by the drastic change in the correlation function as a function of  $x$  or the total magnetization  $m$ .

From the results of the magnetization process and the nn correlation functions for the longitudinal ( $z$ -axis) and the transverse components, the magnetic phase diagram was derived in the plane of  $x - h/J$ , where  $h$  is the magnetic field applied along the  $z$ -axis. The phase diagram is shown in Fig.1. The phase I is the disordered state, which emerges between the orthogonal dimer state at  $x \gtrsim 0$  and the ferrimagnetic ordered state for  $x \gtrsim 2.0$ , under the absence of the magnetic field. The phases II and III are the 1/3-plateau states,

which states are continued to each state at  $x \sim 0$  and  $x \gtrsim 2.0$ , respectively. In the former phase, the 1/3-magnetization at  $h = 0$  is attributed to the free 1/3 spins and in the latter phase, it is to the resultant ferrimagnetic magnetization.

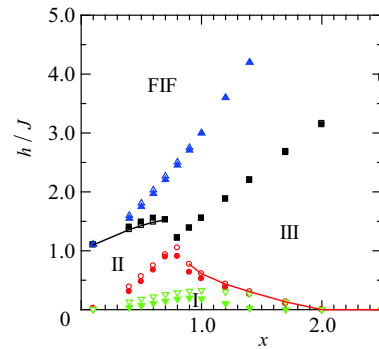


Fig. 1 The phase diagram under the magnetic field  $h$ . Reverse triangle, circle, square, and triangle denote the level-crossing field between the lowest energy state within the multiplet of  $S_t = 0$  and  $S_t = 1$  for the total spin  $S_t$ , the lower-field-edge (LFE) of the 1/3-plateau, the higher-field-edge (HFE) of the plateau, and the full polarization field, respectively. The solid and the vacant ones in those symbols denote data for the system sizes  $N = 30$  and  $N = 24$  systems, respectively. The phase FIF designates the field-induced ferromagnetic phases. The solid curves at the HFE of the phase II and the LFE of the phase III denote the regime of  $x$  where the magnetization jump of  $\Delta S_t^z \geq 2$  emerges in the magnetization process, for the case of  $N = 24$  as an example.

### References

- 1) E. Ressouche et al.: Phys. Rev. Lett. **103** (2009) 267204.
- 2) I. Rousochatzakis et al.: Phys. Rev. B **85** (2012) 104415.
- 3) H. Nakano, M. Isoda, and T. Sakai: J. Phys. Soc. Jpn. **83** (2014) 053702.